Movement Control and Guidance of an Automated Underwater Vehicle

by

Simon James Pauck

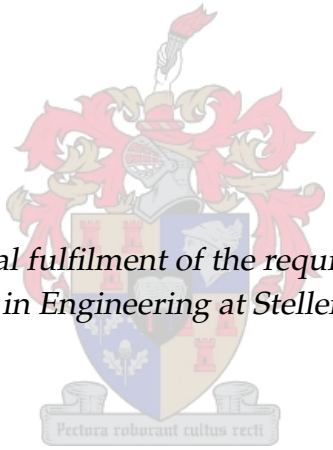

Thesis presented in partial fulfilment of the requirements for the degree of Master of Science in Engineering at Stellenbosch University

Supervisor: Dr Iain Peddle

Department of Electrical and Electronic Engineering

March 2010

Declaration

By submitting this thesis electronically, I declare that the entirety of the work contained therein is my own, original work, that I am the owner of the copyright thereof (unless to the extent otherwise explicitly stated), and that I have not previously in its entirety or in part submitted it for obtaining any qualification.

March 2010

Abstract

This thesis presents the design process of the movement control and guidance systems for an automated underwater vehicle (AUV) constructed by the Institute of Maritime Technology in Simon's Town. The full non-linear mathematical model and simulation environment for the AUV were previously developed in [1]. The design process in this thesis covers an analysis of existing test data and the performance of the current systems in place on the AUV, derivation and analysis of the linear model for the AUV, design of upgraded control and guidance systems, analysis of the new designs including simulation results, practical implementation of the new designs and the results thereof. Over the course of this project a number of flaws were identified in the original control designs and other aspects of the AUV. Most notably, the capability of the AUV is limited owing to its construction, and the current control and guidance methods result in poor movement characteristics. The new control designs are executed through multiple SISO feedback loops, with the most complicated controllers consisting of proportional and integral control. A completely new guidance method was designed which grants the AUV the ability to track both straight line and circular path segments with no steady state error. These designs were tested in simulation, with results showing good tracking performance, even in the presence of output disturbances. The new designs were implemented on the physical AUV, but testing was limited, with poor results being obtained. The poor test results were caused primarily by the construction of the AUV.

Uittreksel

Hierdie tesis stel die ontwerpsproses voor vir die bewegingsbeheer- en navigasiestelsels vir 'n outonome duikboot wat gebou is deur die Instituut vir Maritieme Tegnologie in Simonstad. Die volle nie-lineêre wiskundige model en simulasieomgewing vir die duikboot is voorheen ontwikkel in [1]. Die ontwerpsproses in hierdie tesis behels 'n analise van bestaande toetsdata en van die werksverrigting van die stelsels wat tans op die duikboot geïnstalleer is, die afleiding en analise van 'n lineêre model vir die duikboot, die ontwerp van verbeterde beheer- en navigasiestelsels, die analise van die nuwe ontwerpe, wat simulasieresultate insluit, die praktiese implementering van die nuwe ontwerpe, en die resultate daarvan. Deur die loop van die projek is 'n aantal tekortkominge geïdentifiseer in die oorspronklike beheerstelselontwerpe en ander aspekte van die duikboot. Die mees beduidende tekortkominge is dat die vermoë van die duikboot beperk word deur die konstruksie daarvan, en dat die huidige beheer- en navigasietegnieke swak bewegingseienskappe lewer. Die nuwe beheerstelselontwerpe is uitgevoer deur 'n aantal enkelintree, enkeluittree terugvoerlusse, waar die mees komplekse beheerders bestaan uit proporsionele en integraalbeheer. 'n Heeltemal nuwe navigasiemetode is ontwerp, wat die duikboot in staat stel om beide reguit lyne en sirkulêre padsegmente te volg sonder 'n stasionêre volgfout. Hierdie ontwerpe is getoets in simulasie, waar die resultate goeie volging getoon het, selfs in die teenwoordigheid van uittreeversteurings. Die nuwe ontwerpe is geïmplementeer op die fisiese duikboot, maar beperkte toetse is gedoen, en het swak resultate gelewer. Die swak toetsresultate was hoofsaaklik as gevolg van die konstruksie van die duikboot.

Acknowledgements

My gratitude goes out to the following people and organisations for the part each of them played in bringing this Master's to fruition.

- Jesus Christ, for His saving grace and without Whom my entire life would have no purpose.
- Dr Iain K. Peddle, for your wisdom and guidance as my supervisor.
- IMT, for funding this project.
- University of Stellenbosch and the ESL, for providing an amazing work environment.
- Mr Regardt Busch, for his prior work on the AUV model and simulation environment.
- Mr Chris Jaquet, for never failing to drop what he was doing to help me with my petty requests and questions.
- Mr Marcus Collins, for his excellent proof reading.
- Everyone else in the ESL, for pub lunches, late night working sessions, distractions and friendship.
- My family, both in blood and in spirit, for your support in all areas of my life.

Contents

List of Figures

List of Tables

Nomenclature

Capital Letters

$\mathbf{F}$	Force vector
$\mathbf{I}$	AUV inertial tensor
I_x	Moment of inertia about the roll axis
I_y	Moment of inertia about the pitch axis
I_z	Moment of inertia about the yaw axis
I_{xy}	Roll and pitch product of inertia
I_{xz}	Roll and yaw product of inertia
I_{yz}	Pitch and yaw product of inertia
$\mathbf{M}$	Moment vector
K	Roll moment
M	Pitch moment
N	Yaw moment
P	Roll rate
Q	Pitch rate
R	Yaw rate
$\mathbf{V}$	Velocity vector
$\bar{V}$	Velocity magnitude
U	Axial velocity
V	Lateral velocity
W	Normal velocity
X	Axial force
Y	Lateral force
Z	Normal force

Small Letters

g	Gravitational acceleration
m	mass

Greek Letters

α	Angle of attack
β	Angle of sideslip
Φ	Roll attitude angle
Θ	Pitch attitude angle
Ψ	Yaw attitude angle
ω	Angular velocity vector
ρ	Fluid density

Subscripts

0	Trim condition
B	Buoyancy-related variables
C	Control-related variables
G	Gravitational-related variables
H	Hydrodynamic-related variables
T	Thruster-related variables

Superscripts

B	Body axis
E	Inertial axis

Abbreviations

AUV	Autonomous Underwater Vehicle
COB	Centre of Buoyancy
COM	Centre of Mass
DLL	Dynamic Link Library
HIL	Hardware In the Loop
IMT	Institute for Marine Technology
SLC	Successive Loop Closure
UAV	Unmanned Air Vehicle
UUV	Unmanned Underwater Vehicle

Miscellaneous

$G_c(s)$	General controller transfer function
$G_g(s)$	General guidance transfer function
$G_p(s)$	General plant transfer function

Chapter 1

Introduction and Project Background

1.1 Introduction

Interest in research regarding underwater vehicles has increased dramatically in recent years. Apart from outer space, the Earth's oceans are the most unexplored location in the natural world. There are thus a number of research groups around the world working on various unmanned underwater vehicles. Unmanned vehicles are important for furthering knowledge about the ocean, considering how inhospitable this environment is to human beings. Currently, the general class of unmanned underwater vehicles (UUVs) is split into a number of sub-classes, namely remotely operated vehicles (ROVs), automated underwater vehicles (AUVs) and underwater gliders. ROVs are usually tethered somehow and receive control inputs from a human director through an umbilical link. By design these vehicles are usually very stable and have precise but restrictive movement capabilities, since they are usually used for complicated tasks involving the use of robotic manipulators. AUVs on the other hand are not tethered and do not receive commands from a human operator. They tend to resemble conventional manned submarines in their construction and movement characteristics. This is the type of vehicle that has been created by the Institute of Maritime Technology (IMT). Underwater gliders are essentially a sub-class of AUV which relies on wings and slow, subtle changes in vehicle characteristics to achieve very energy-efficient movement below the water surface. As such, the intention of their design is usually focused on long-distance travel and long mission periods.

Some potential uses for UUVs are listed below, [4; 5; 6]. Examples of AUVs similar in construction and size to the IMT AUV can be found in [7; 8; 9]. More information and publications on numerous AUVs can be found at [10].

- Surveying and mapping
- Search and rescue
- Environmental monitoring and data collection, [11; 12]
- Transport
- Maintenance and repair
- Equipment testbed
- Military uses such as interception, defencive countermeasures, mine detection and harbour patrol
- Hazard detection and warning
- Scientific missions
- Investigation into novel control and movement techniques, [13]

The IMT AUV has been developed primarily for use as a testbed for underwater equipment such as video cameras and sonar scanners. It also forms part of research aimed at investigating underwater movement systems. The aim of this Master's project is to analyse, evaluate and upgrade the current control and guidance system employed on the AUV to provide a more reliable testbed AUV and to increase insight into underwater movement control. Many AUVs, such as "Urashima" in [9], use forms of buoyancy control to perform what is known as static diving. The IMT AUV, however, has only fin control surfaces with which to control its movement. Adding a form of buoyancy control to the IMT AUV is investigated in **Chapter 6**.

1.2 The IMT AUV

Basic hardware

A picture of the IMT AUV in the water is shown in **Figure 1.1**. CAD drawings with some dimensioned geometric data of the outer shell of the AUV can be viewed in [1, Appendix A.2]. The AUV is about 3m long, 1.5m wide and 0.6m high. Excluding the thrusters and the protrusions visible on top, the main body of the AUV is 1m wide and 0.3m high. Its structural strength is provided by a metal frame, which is enclosed in fibreglass panels that can be easily removed for access to the inner workings of the AUV. These panels have open vents, visible in the figure, to allow the body of the AUV to flood. The electronics for the AUV are housed in

sealed cylindrical containers. The AUV is powered by batteries; consequently, the actuators and thrusters on the AUV are DC electronic actuators and motors. The centre of mass of the dry AUV is situated near the winch point, also visible in the picture. The dry mass of the AUV is approximately 350kg. When fully submerged, the combined mass of the AUV and the water it contains is about 840kg. The AUV has antennae located on top of the protrusion near its stern. These provide wireless communication with the ground-station when the AUV is floating on the ocean surface. The heart of the AUV avionics is an Intel Pentium 166 MMX on a 128MB Kontron board, which runs Microsoft Windows 98 operating system. All interfacing with the communication devices, actuators and other external components is done through a serial card attached to the board. The AUV software is coded in Delphi, which runs in the standard Microsoft Windows 98 operating environment.

Figure 1.1: Photo of the AUV in its natural habitat

Actuators

The AUV is controlled by a number of fins which can be deflected 25° either side of their centre points. The locations of these control surfaces are highlighted in **Figure 1.2**. There is a pair of horizontal fins near the front of the AUV and a horizontal elevator at the back. The front fins can be commanded independently and can therefore be used in both *common mode* and *differential mode* to *pitch* and *roll* the AUV respectively. The elevator is used to pitch the AUV. There is a pair of vertical rudders near the back of the AUV that are used to yaw the AUV. The two rudder fins are mechanically connected and cannot be moved independently. Each rudder

is positioned in the outlet flow of one of the two thrusters. The increased fluid flow speed over the rudders makes them the most effective of the control surfaces.

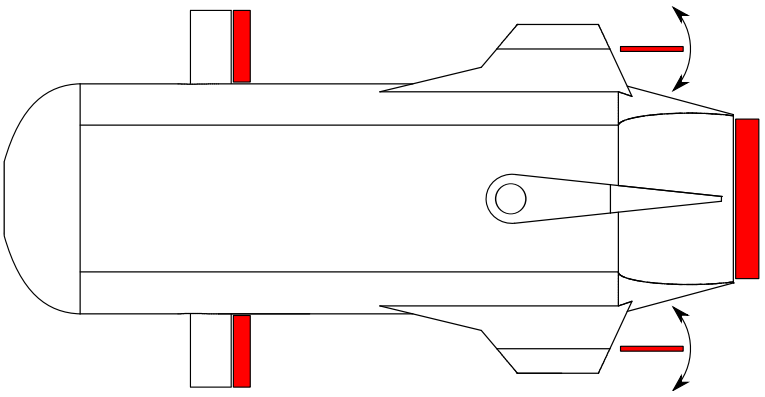

Figure 1.2: AUV control surfaces (Top view of the AUV)

Sensors

The AUV utilises an advanced inertial measurement unit made by IXSea, called PHINS (PHotonic Inertial Navigation System). It is a sealed unit, containing accelerometers and gyroscopes, which it integrates to propagate a measurement of its inertial position and attitude as it travels underwater. The inertial position is updated with GPS data when the AUV is surfaced. The PHINS unit also uses DVL (Doppler Velocity Log) measurements to bound the propagated measurements. A pressure sensor is incorporated to aid depth sensing. The PHINS Unit has a built-in Kalman filter. With its current setup, the unit measures the data shown in **Table 1.1**, with the given accuracies.

Table 1.1: PHINS measurements and accuracies [3]

Measurement	Accuracy
Heading (Yaw) angle	0.02° secant latitude
Pitch/Roll angle	0.01°
Latitude/Longitude	0.1% of travelled distance
Depth	0.05m
Roll/Pitch/Yaw rate	0.001°/sec
North/East/Down velocity	0.0015m.s^{-1}

1.3 Prior work on the AUV

The AUV has working control systems on board that were designed by IMT. These control systems consist of attitude angle feedback based proportional controllers. The reference commands for these controllers are generated by guidance controllers, which seek to control the AUV depth and heading angle. The guidance is based on waypoints, which are described only as points in three-dimensional Cartesian space. An analysis of this implementation of control and guidance is carried out in **Chapter 5**. Some undersea trials have been performed by IMT, for which data was recorded. This data is analysed in **Chapter 2**.

The mathematical model for the AUV was derived in [1] as part of a Master's project. The basics of the mathematical model are covered in **Chapter 3** and analysed in **Chapter 4** to gain insight into the behaviour of the AUV. Included in [1] was the development of a simulation environment for the AUV. The simulation environment is a full non-linear six degrees of freedom simulation that includes all the modelled AUV dynamics and non-linearities. The mathematical aspects of the simulation are handled in SIMULINK, which interfaces with a graphical front end to provide an intuitive display of the simulation results. The simulation environment and simulation results are discussed in **Chapter 8**, following the design of the new control and guidance systems in **Chapter 6** and **Chapter 7**.

Chapter 2

Analysis of Existing Test Data

Although the AUV model was derived in [1], analysis of IMT test data may prove useful in refining the model and gaining insight into the model. This analysis was performed with knowledge of the mathematical model; therefore only the relevant points will be discussed below. A few sets of test data were obtained from IMT, which they gathered from undersea trials with the AUV in 2008. The plots are derived from the longest set of trial data available, which provided the most insight into the AUV's behaviour.

A top view of the AUV travel path is shown in **Figure 2.1**. This plot is used to determine the turning circle of the AUV. Although it is not entirely clear how sharp the AUV can turn, since in some cases it appears to have been aided by underwater currents, a conservative estimate for the diameter of its turning circle is around 20 m. This represents the maximum turning rate of the AUV with its rudder deflection saturated. This is effectively an uncontrolled response and can be used to adjust parameters in the mathematical model such that in simulation the AUV displays the same turning characteristics. This plot also shows tracking characteristics of the AUV. It appears that there was a constant ocean current flowing in a westerly direction, which is evidenced by the curved travel path of the AUV. This poor tracking performance is one of the main issues that will be addressed in the controller designs presented in this thesis.

The instances of the sharp turns made by the AUV in **Figure 2.1** are clear from the rudder deflection and change in heading shown in **Figure 2.2**. These plots show dramatic coupling from the AUV's yaw action into its roll. This highlights the need for a roll controller, which the current control implementation on the AUV does not have. The AUV does, however, return to its trim roll angle quite quickly. The roll angle plot reveals that the trim roll angle of the AUV is not zero. This offset in the roll angle could be due to the AUV thrusters, which are not counter-rotating and thus apply a constant moment about the AUV roll axis. This offset is not very

large, however, and can most likely be eliminated with a roll controller. Since the roll response is uncontrolled, this data can be used to gain insight into the physical system. The roll response appears to have regular oscillations with a frequency of 0.42rad.s^{-1}. In the mathematical model of the AUV there exists a number of free variables, parameters that need to be estimated. The model parameters were therefore adjusted so that the roll poles of the model correlate with this observation in the test data. This is covered in **Section 3.3**.

Figure 2.3 displays some data pertaining to the longitudinal motion of the AUV. From these plots one can see how the AUV depth in the water also changes as it turns sharply, but this is expected to be regulated by improved controller designs. The trim value of the elevator is of great concern and is highlighted in the elevator angle plot of **Figure 2.3**. The average angular position of the elevator is about $-20°$, which is almost at its lower limit of $-25°$. This severely limits the achievable performance of the AUV when attempting to pitch the AUV upwards. This will also impact the robustness of the AUV to disturbances. This problem can be solved only by changing the AUV physically, either by changing the weight distribution within the AUV or by adding trim tabs so that the elevator can trim near its centre point.

Figure 2.4 shows the speed of the AUV as it moves through the water, which varies by about 15%. This speed appears to drop briefly through each turn, but not too dramatically. The differences in speed of the AUV during separate sections of the trial are most likely due to the AUV travelling with or against the ocean currents. Its actual speed through the water is probably more consistent than the plot suggests. Based on this plot, a trim value of 1.3m.s^{-1} was selected for forward speed of the AUV in the model.

Another problem that was identified with the current AUV setup was a very unstable measurement sample time. A plot of the time difference between each successive sample is shown in **Figure 2.5**. Although the originally specified sample time of the AUV was 0.5 seconds, this plot reveals that it was on average 0.3 seconds, which is in any case better. But the sample time is very erratic between samples, with some samples taking a number of seconds to complete. This is obviously not desirable and will heavily affect the performance of the control system, especially one that does not consist of proportional terms only. Fortunately a solution to this problem was found and is presented in **Section 9.1**.

2.1 Chapter summary

The primary goals of the analysis in this chapter were to gather data to refine the mathematical model on the AUV and to establish which aspects of the AUV

performance need to be upgraded and can be improved with new control designs. The analysis results will allow for a more refined roll model for the AUV and minor adjustments to other model parameters. The primary control problems discovered in this chapter are the poor guidance performance, trim conditions and sample rate consistency of the AUV.

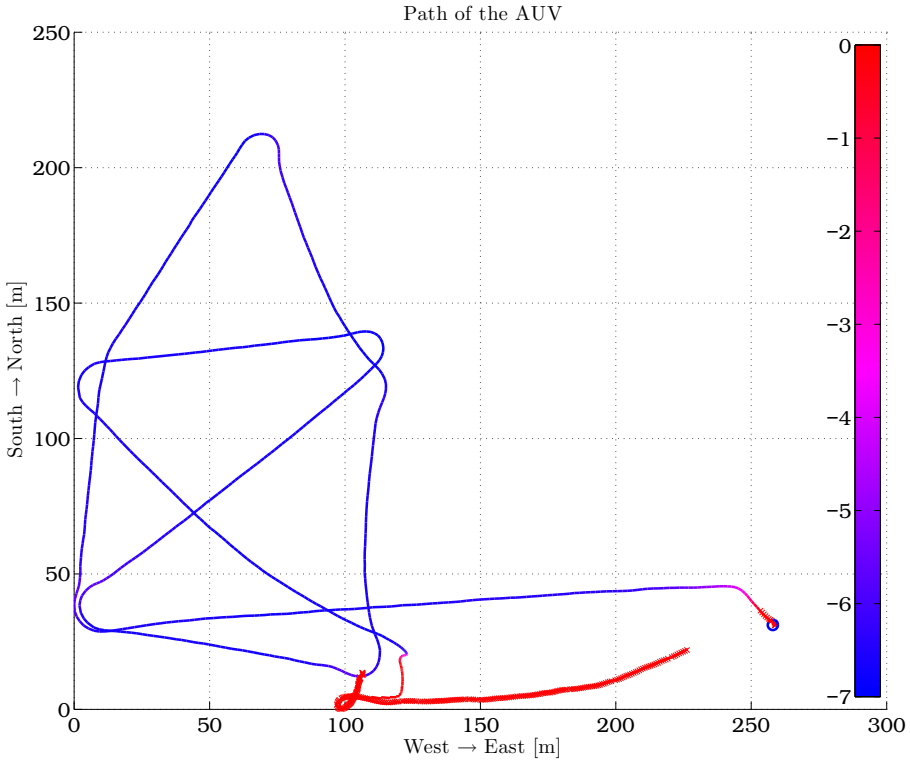

Figure 2.1: Top-down view of the AUV travel path. GPS updates are shown with '×' markers. The AUV depth is shown with path colour, according to the bar on the right of the figure.

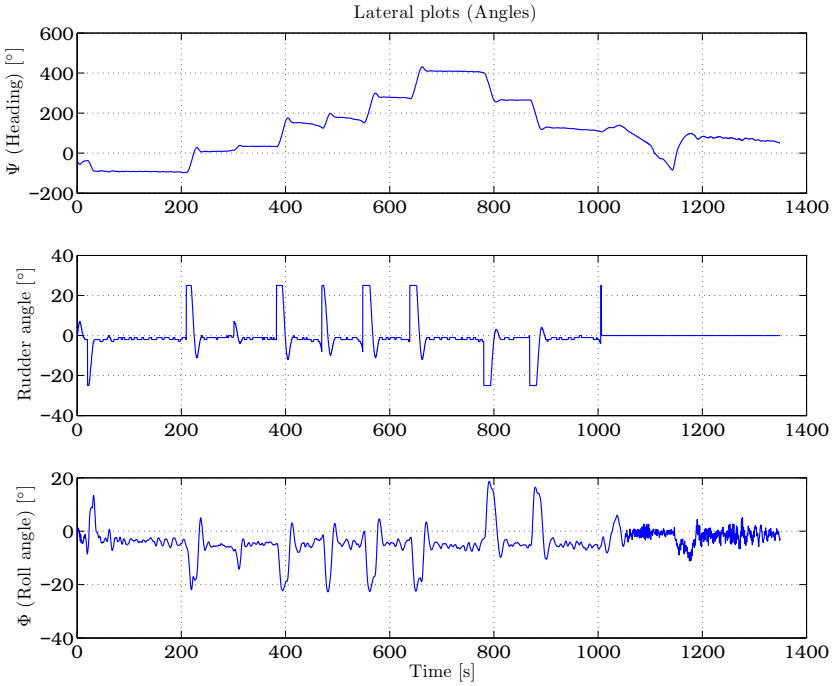

Figure 2.2: Relevant lateral data plots

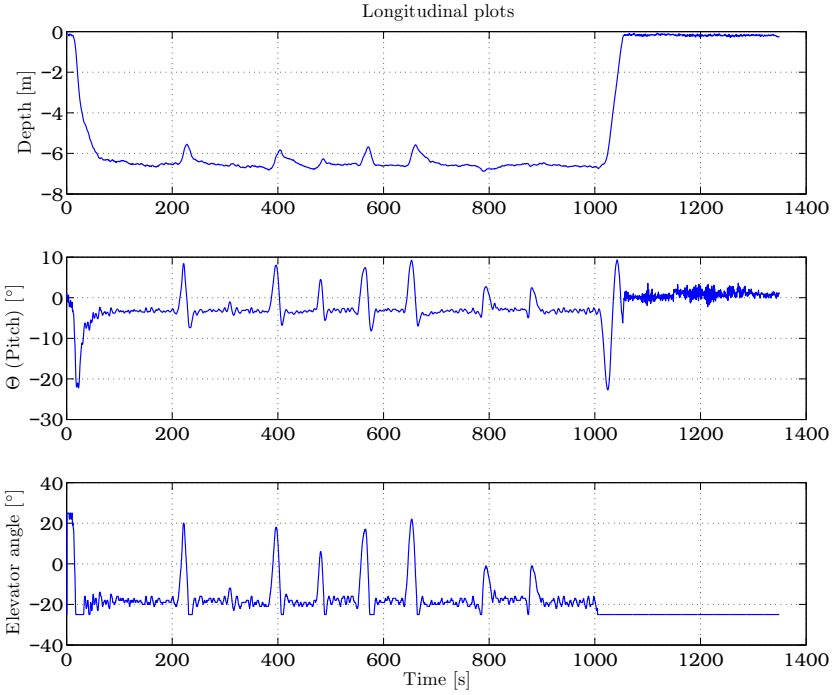

Figure 2.3: Relevant longitudinal data plots

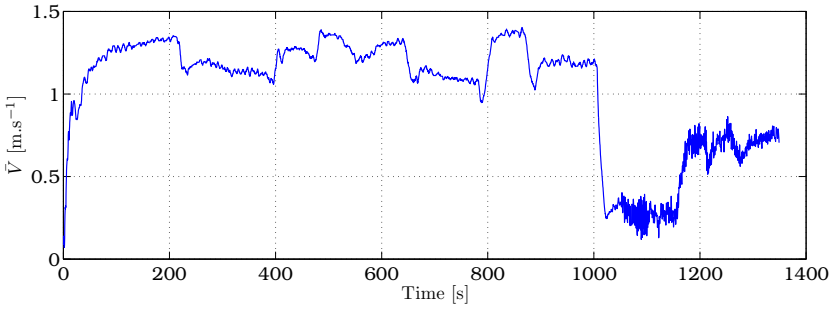

Figure 2.4: Velocity magnitude plot

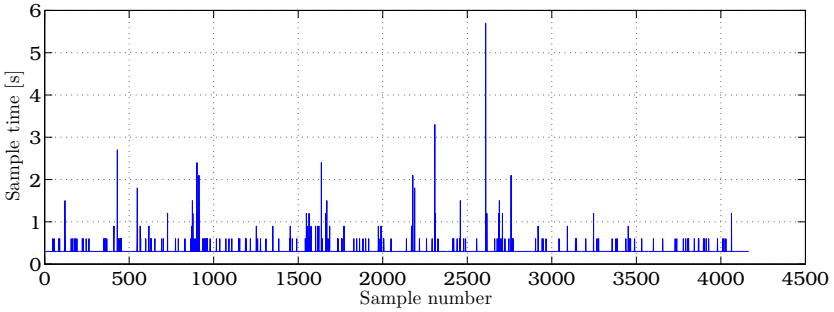

Figure 2.5: Sample time plot, showing inconsistencies

Chapter 3

Mathematical Model

The mathematical model used to describe the motion of the AUV for the purposes of control design is derived in this chapter. This follows directly from the work presented in [1]; however some of the model parameters and trim conditions have been adjusted to suit the needs of this project. Since the focus of this thesis is on the control design, the linear model is of greatest importance here. The non-linear model is useful for examining the effects of various model parameters on the final model. For this reason, each section of the model is linearised as early as possible, with relevant non-linearities being dealt with as they appear.

3.1 Mathematical definitions and conventions

Axis systems

Since the AUV moves through three-dimensional space, axis systems need to be defined in which the AUV's movement can described. Only two different axis systems are required in this thesis, both of which are right-handed orthogonal axis systems. All positive rotations about specific axes obey the right-hand rule.

Local NED axes - X^E, Y^E, Z^E

The origin for this axis system is arbitrary and is chosen to be at some convenient point, usually close to the starting point of the AUV. The axes are referred to as local NED (North, East, Down) axes, since the X-axis points North, the Y-axis points East and the Z-axis points Down. This axis system is the reference system for the AUV's movement. Since the model for the AUV was derived using Newton's equations of motion [1, Chapter 3], it requires an inertial axis system for the equations to hold. Since the Earth's rotational rate is very small when compared to the AUV's

rotational rates, and the curvature of the Earth is negligible for the operating area of the AUV, this axis system is considered to be inertial.

Body axes - X^B, Y^B, Z^B

This axis system is fixed to the AUV body, with the origin at the centre of mass (COM) of the AUV. Since the model is intended to describe the behaviour of the AUV during operation, the centre of mass referred to is the centre of mass of the flooded AUV. The X^B-axis points to the front of the AUV, the Y^B-axis to the right and the Z^B-axis to the bottom, as shown in **Figure 3.1**.

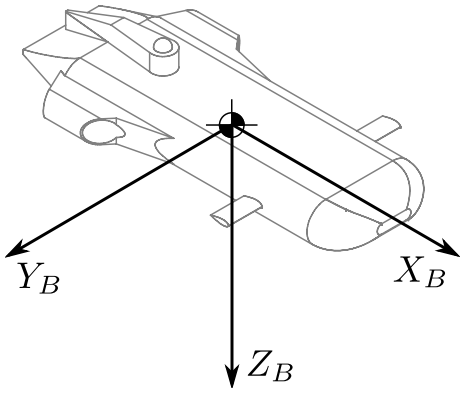

Figure 3.1: Body axis system with its origin on the AUV centre of mass

State variables

The mathematical model for the AUV follows the form of a typical aerodynamic state space model often used to describe the behaviour of aeroplanes [14]. The model is given in terms of state space matrices with the states listed in **Table 3.1**. This choice of state variables is essentially the same as that found in [1], with modification to the velocity states, which are replaced by the polar coordinate velocity variables. The equations relating the polar velocity coordinates to the Cartesian velocity coordinates are given in **(3.1)** to **(3.3)**. In these equations, U, V and W are the X^B, Y^B and Z^B components of the AUV's velocity vector. The angle of attack, α, is the angle measured between the X^B-axis and the projection of the AUV's velocity vector onto the X^BZ^B-plane. The angle of sideslip, β, is the absolute angle measured between the X^BZ^B-plane and the AUV's velocity vector. The roll, pitch and yaw rate variables refer to the various coordinates of the AUV's angular velocity vector about the X^B, Y^B and Z^B axes respectively. The Euler attitude angles, Φ, Θ and Ψ, are those obtained from the 321 Euler sequence, as given in [14], and relate the orientation of the AUV's body axis system to the local NED axis system.

Table 3.1: States used to describe the AUV

Variable	Description
$\bar{V}$	Velocity magnitude
α	Angle of attack
β	Angle of sideslip
P	Roll rate
Q	Pitch rate
R	Yaw rate
Φ	Roll angle
Θ	Pitch angle
Ψ	Yaw angle

$$\bar{V} = \sqrt{U^2 + V^2 + W^2} \tag{3.1}$$

$$\alpha = \tan^{-1}\left(\frac{W}{U}\right) \tag{3.2}$$

$$\beta = \sin^{-1}\left(\frac{V}{\bar{V}}\right) \tag{3.3}$$

3.2 Derivation of model

The derivation of the full mathematical model is complicated and is given in full in [1]. For the purposes of this thesis a simple derivation, covering only the necessary details, will be given. The final model is a linear perturbation state space model. The states thus represent the values of perturbations from the trim conditions around which the model is linearised. The perturbation state variables are represented by lowercase letters to distinguish them from the actual state variables. The trim conditions for the AUV in steady state are all assumed to be zero, excepting the forward velocity. This means the AUV should be travelling straight and level, with no angular rates. The heading direction, Ψ, does not influence any of the other state variables in any way and so it can be set to any value. This will therefore be set to an initial value of zero for most derivations to simplify the mathematics. In the original derivation of the AUV model [1, p. 95], the trim conditions included a non-zero value for the angle of attack of the AUV which changed the values of some of the other model parameters. However, since that value was calculated to be small and the uncertainty of the derivation of the hydrodynamic parameters was not known (but probably large [1, p. 34]), it is safe to set this to zero in order to further simplify calculations. To cater for this uncertainty, the controller designs are expected to incorporate integrating action, which should account for all the trim conditions in practice, including the actuator trim values, which are also set to zero.

Six degrees of freedom equations of motion

To begin with, the following assumptions are made. The AUV is symmetrical about the X^BZ^B-plane. This sets the inertial products, I_{xy} and I_{yz}, of the inertial tensor to zero. The AUV is relatively symmetrical about the X^BY^B-plane as well, which implies that the final product of inertia, I_{zx}, is most likely negligibly small. In this way, all the products of inertia are removed from Newton's equations of motion.

The AUV's general motion in the inertial axis system can now be described using the simplified Newton's equations of motion, which relate the components of the forces on the AUV in the inertial axis system to the accelerations and angular velocities of the AUV components in the body-axis, as given in **(3.4)** to **(3.9)**. These equations can be simplified even further by assuming the products of the angular rates are much smaller than the other terms, giving way to equations **(3.10)** and **(3.11)**, which are essentially linearised and thus described using the perturbation variables.

Forces:

$$X = m(\dot{U} + QW + RV) \tag{3.4}$$

$$Y = m(\dot{V} + RU - PW) \tag{3.5}$$

$$Z = m(\dot{W} + PV - QU) \tag{3.6}$$

Moments:

$$K = I_{xx}\dot{P} + (I_{zz} - I_{yy})QR \tag{3.7}$$

$$M = I_{yy}\dot{Q} + (I_{xx} - I_{zz})RP \tag{3.8}$$

$$N = I_{zz}\dot{R} + (I_{yy} - I_{xx})PQ \tag{3.9}$$

Forces:

$$\left[\mathbf{F}\right] = m\begin{bmatrix} \dot{u} \\ \dot{v} + U_0 r \\ \dot{w} - U_0 q \end{bmatrix} \tag{3.10}$$

Moments:

$$\left[\mathbf{M}\right] = \begin{bmatrix} I_{xx} & 0 & 0 \\ 0 & I_{yy} & 0 \\ 0 & 0 & I_{zz} \end{bmatrix}\begin{bmatrix} \dot{p} \\ \dot{q} \\ \dot{r} \end{bmatrix} \tag{3.11}$$

All the modelled forces and moments on the AUV will come from the effects of gravity, buoyancy, hydrodynamics, and the AUV's control surfaces and thrusters, resulting in equations **(3.12)** and **(3.13)**. Here, the subscripts G, B, H, C and T correspond with the various components mentioned above, respectively.

Forces:

$$[\mathbf{F}] = [\mathbf{F}_G] + [\mathbf{F}_B] + [\mathbf{F}_H] + [\mathbf{F}_C] + [\mathbf{F}_T] \tag{3.12}$$

Moments:

$$[\mathbf{M}] = [\mathbf{M}_G] + [\mathbf{M}_B] + [\mathbf{M}_H] + [\mathbf{M}_C] + [\mathbf{M}_T] \tag{3.13}$$

Gravity

The gravitational force on the AUV has a constant magnitude and always acts parallel to the Z^E-axis, at the centre of gravity of the AUV. The magnitude of the force is given by **(3.14)**, where m is the AUV's mass when flooded and g is the gravitational acceleration experienced by the AUV, which is assumed to be constant at $9.81 m.s^{-1}$. The gravitational force on the AUV is thus given by **(3.15)**, which approximates to the linear perturbation force about the trim conditions in **(3.16)**. The gravitational field around the AUV is assumed to be uniform; thus the centre of gravity coincides with the centre of mass of the flooded AUV, and the moments caused by gravity are all zero.

$$W_G = mg \tag{3.14}$$

$$\begin{bmatrix} X_G \\ Y_G \\ Z_G \end{bmatrix} = W_G \begin{bmatrix} -\sin\Theta \\ \cos\Theta \sin\Phi \\ \cos\Theta \cos\Phi \end{bmatrix} \tag{3.15}$$

$$\begin{bmatrix} \mathbf{F}_G \end{bmatrix} \approx W_G \begin{bmatrix} -\theta \\ \phi \\ 0 \end{bmatrix} \tag{3.16}$$

Buoyancy

The buoyancy forces are similar in nature to gravitational forces on the AUV. Essentially, the AUV will experience a force that acts parallel to the Z^E-axis in the upwards (negative) direction, equal in magnitude to the gravitational force that would be experienced by the mass of water it displaces. The magnitude of this force is given by **(3.17)**, where m_B is the mass of water displaced by the volume of the AUV. In the same way as shown above for the gravitational forces, the linear perturbation buoyancy forces are derived and given by **(3.18)**.

$$B = m_B g \tag{3.17}$$

$$\begin{bmatrix} \mathbf{F}_B \end{bmatrix} \approx -B \begin{bmatrix} -\theta \\ \phi \\ 0 \end{bmatrix} \tag{3.18}$$

The buoyancy force acts at the centre of buoyancy (COB) of the AUV, which, unlike the centre of gravity, does not coincide with the AUV's centre of mass. The centre of buoyancy of the AUV is determined solely by its geometry and would coincide with the centre of mass if the AUV had a uniform density across its entire volume. That is, it is the same as the centre of mass of the theoretical volume of water displaced by the AUV. Due to the displacement of the COB from the COM of the AUV, the buoyancy force has a pendulum effect on AUV. The force creates restoring moments

about the AUV's centre of mass that always act to align the centre of mass and centre of buoyancy parallel to the Z^E-axis, with the centre of buoyancy being above the centre of mass. Just as with a pendulum, this will cause oscillatory motions in the AUV. For the two-dimensional case shown in **Figure 3.2**, the restoring moment is given by **(3.19)**, where I is the moment of inertia of the AUV about that specific axis of rotation. This results in oscillations at the frequency given in **(3.20)**. Since the force, $\mathbf{F}_B$, is very large and approximately equal to the gravitational force on the AUV, even very small displacements of the COB from the COM (on the order of millimetres) will generate large restoring moments. It will be seen later that this pendulum effect dominates the roll response of the AUV. The vertical displacement of the COB from the COM can therefore be adjusted to control the placement of the model poles for the rolling action of the AUV. As the displacement is increased the AUV becomes more stable, but also less responsive to control. A large displacement also results in poor damping, since the buoyancy-created moments overwhelm the roll damping of the AUV. This effect was visible in [1], where the chosen value for the COB displacement was clearly too large, resulting poor damping and frequency response which was much higher than that evidenced by the test results in **Chapter 2**.

$$\mathbf{M}_B = d\mathbf{F}_B \sin(\vartheta) \tag{3.19}$$

$$\omega_B = \sqrt{\frac{d\mathbf{F}_B}{I}} \tag{3.20}$$

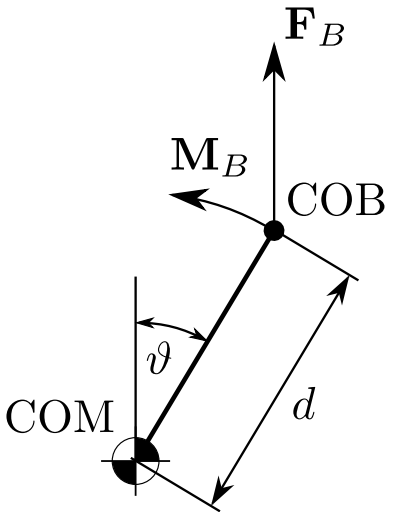

Figure 3.2: Buoyancy force and moment acting mechanism

If the centre of buoyancy is displaced from the centre of mass along each of the body axes by values $\begin{bmatrix} x_{COB} & y_{COB} & z_{COB} \end{bmatrix}^T$, the moments developed by the buoyancy force

will then be given by **(3.21)**. However, as stated previously, the AUV is assumed to be symmetrical about the X^BZ^B-plane, which implies that $y_{COB} = 0$. This, combined with the trim conditions, leaves the linearised equation for the moments created by the AUV as **(3.22)**. The AUV is expected to travel through the water straight and level, which suggests that the largest and most significant displacement of the centre of buoyancy lies along its Z^B-axis. Following this, x_{COB} is also set to zero for simplicity, which allows **(3.22)** to be approximated to **(3.23)**. Any error in this assumption would influence the trim conditions of the AUV. As stated before, this is catered for by including integrators in the controller designs.

$$\begin{bmatrix} K_B \\ M_B \\ N_B \end{bmatrix} = B \begin{bmatrix} -y_{COB}\cos(\Theta)\cos(\Phi) + z_{COB}\cos(\Theta)\sin(\Phi) \\ x_{COB}\cos(\Theta)\cos(\Phi) + z_{COB}\sin(\Theta) \\ -x_{COB}cos(\Theta)sin(\Phi) - y_{COB}sin(\Theta) \end{bmatrix} \tag{3.21}$$

$$\begin{bmatrix} K_B \\ M_B \\ N_B \end{bmatrix} \approx B \begin{bmatrix} z_{COB}\phi \\ x_{COB} + z_{COB}\theta \\ -x_{COB}\phi \end{bmatrix} \tag{3.22}$$

$$\begin{bmatrix} \mathbf{M}_B \end{bmatrix} = B \begin{bmatrix} z_{\mathrm{COB}}\phi \\ z_{\mathrm{COB}}\theta \\ 0 \end{bmatrix} \tag{3.23}$$

Thrusters

Although a complicated derivation of the effects of the thrusters on the AUV exists in [1], similar results can be arrived at intuitively by making a small number of assumptions. This approach was used in early work in [1] and produced similar results to the full derivation. No speed control is performed on the AUV since the thrusters are not very powerful and are always run at full throttle. The following assumptions have been made when modelling the thrusters.

- Thrust force generated is linearly proportional to the input power delivered to the thrusters by the constant ratio c_T.
- The thrusters lie in the X^BY^B-plane and the force they generate is parallel to the X^B-axis.
- The thrusters are displaced by the same amount on opposite sides of the X^BZ^B-plane, by a constant y_T.
- The thrusters are counter-rotating and therefore generate no rolling moments on the AUV.

The first assumption is reasonably accurate and is based on the graph shown in **Figure 3.3**. The second assumption should also be quite accurate, however, if this

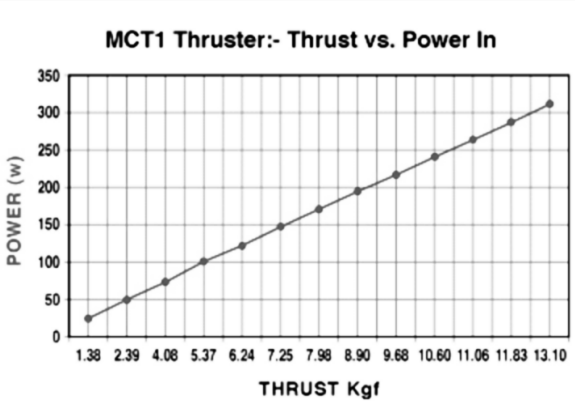

Figure 3.3: Seaeye MCT1 thruster force vs input power [2]

is not the case and the thrusters have some offset placement or inclination, then a constant pitching moment will be generated on the AUV. The third assumption is similar in nature and any imbalance in the placement of the thrusters would result in a constant yaw moment on the AUV. Both of these errors would affect the trim of the AUV and will be handled the same way as other trim offsets, by including integral action in the AUV control systems. The same effects on the AUV trim will be created by differences in the thruster forces. The fourth assumption is in fact not true and both thrusters rotate in the same direction. As was seen in **Chapter** 2 this does not seem to have a profound effect on the AUV and should be easily eliminated with a roll controller. It is therefore not worth incorporating it into the model and will rather be treated as a disturbance. The AUV roll is also not as important as roll in an aeroplane. The lift vector of an aeroplane is used to change the heading of an aeroplane by rolling the aeroplane. The AUV does not experience this effect, since it is almost neutrally buoyant. Rolling an AUV, therefore, for the most part simply changes its roll angle. There may be some coupling into the pitch and yaw aspects of its motion, but these are expected to be minimal.

Control inputs δT_l and δT_r are defined for the left and right thrusters respectively, each ranging from -1 to 1 (full reverse thrust to full forward thrust). Equations describing the forces and moments generated by each thruster on the AUV are now

defined in **(3.24)** to **(3.27)**.

$$\begin{bmatrix} X_{T_l} \\ Y_{T_l} \\ Z_{T_l} \end{bmatrix} = \begin{bmatrix} c_T \delta T_l \\ 0 \\ 0 \end{bmatrix} \tag{3.24}$$

$$\begin{bmatrix} K_{T_l} \\ M_{T_l} \\ N_{T_l} \end{bmatrix} = \begin{bmatrix} 0 \\ 0 \\ y_T c_T \delta T_l \end{bmatrix} \tag{3.25}$$

$$\begin{bmatrix} X_{T_r} \\ Y_{T_r} \\ Z_{T_r} \end{bmatrix} = \begin{bmatrix} c_T \delta T_r \\ 0 \\ 0 \end{bmatrix} \tag{3.26}$$

$$\begin{bmatrix} K_{T_r} \\ M_{T_r} \\ N_{T_r} \end{bmatrix} = \begin{bmatrix} 0 \\ 0 \\ -y_T c_T \delta T_r \end{bmatrix} \tag{3.27}$$

This model can be simplified and made more useful for control purposes, in a similar way to the front fins, by defining common mode thrust, δT_c, in **(3.28)** and differential mode thrust, δT_d, in **(3.29)**. These control inputs are defined to have the same range as the individual thrust inputs (that is -1 to 1). The thrust forces and moments can now be written more generally and in terms of the new thrust control inputs, as in **(3.32)** and **(3.33)**. The inputs to each of the individual thrusters must now be calculated from the new control inputs, using equations **(3.30)** and **(3.31)**.

$$\delta T_c = \frac{1}{2}(\delta T_l + \delta T_r) \tag{3.28}$$

$$\delta T_d = \frac{1}{2}(\delta T_l - \delta T_r) \tag{3.29}$$

$$\delta T_l = \delta T_c + \delta T_d \tag{3.30}$$

$$\delta T_d = \delta T_c - \delta T_d \tag{3.31}$$

$$\begin{bmatrix} \mathbf{F}_T \end{bmatrix} = \begin{bmatrix} 2c_T \delta T_c \\ 0 \\ 0 \end{bmatrix} \tag{3.32}$$

$$\begin{bmatrix} \mathbf{M}_T \end{bmatrix} = \begin{bmatrix} 0 \\ 0 \\ 2y_T c_T \delta T_d \end{bmatrix} \tag{3.33}$$

Hydrodynamics

The full derivation of the hydrodynamic model is covered in [1]. The basic equations will be given in this section to aid understanding of the model and show where

the significant simplifications have been made. Each of the forces and moments are defined in terms of non-dimensional hydrodynamic derivatives. The variable $\bar{q}$ is known as the kinetic pressure and is given by **(3.34)**, where ρ is the density of the fluid through which the AUV is travelling and $\bar{V}$ is the magnitude of the AUV's velocity as stated before. Each of these non-dimensional hydrodynamic terms then consists of a number of linearised partial derivative terms multiplied by each of the AUV states. However, the equations for each specific non-dimensional term only make use of a select few partial derivative terms, since all cross-coupling hydrodynamic derivatives are excluded and many others are zero, either by assumption or calculation. The specifics of this are discussed in **Section 3.3**, where the values for individual terms are given.

Due to the origins of these equations in the aerodynamics field, the X_H and Z_H derivatives are expressed in terms of *drag* and *lift* coefficients respectively. When linearised about the trim conditions, the lift and drag forces act in the opposite direction to the X^B and Z^B axes respectively, which results in the negative signs present in equations **(3.35)** and **(3.37)**.

$$\bar{q} = \frac{1}{2}\rho\bar{V}^2 \tag{3.34}$$
$$X_H = -\bar{q}l^2C_D \tag{3.35}$$
$$Y_H = \bar{q}l^2C_Y \tag{3.36}$$
$$Z_H = -\bar{q}l^2C_L \tag{3.37}$$
$$K_H = \bar{q}l^3C_K \tag{3.38}$$
$$M_H = \bar{q}l^3C_M \tag{3.39}$$
$$N_H = \bar{q}l^3C_N \tag{3.40}$$

After applying trim conditions, the equations for each of the dimensionless hydrodynamic forces and moments are given by **(3.41)** to **(3.42)**. Here the rate variables are replaced with the normalised rate variables given in **(3.47)** to **(3.49)**.

$$C_D = C_{D_0} \tag{3.41}$$
$$C_Y = C_{Y_\beta}\beta + C_{Y_p}\hat{p} \tag{3.42}$$
$$C_L = C_{L_\alpha}\alpha + C_{L_q}\hat{q} \tag{3.43}$$
$$C_K = C_{K_p}\hat{p} \tag{3.44}$$
$$C_M = C_{M_\alpha}\alpha + C_{M_q}\hat{q} \tag{3.45}$$
$$C_N = C_{N_\beta}\beta + C_{N_r}\hat{r} \tag{3.46}$$

$$\hat{p} = \frac{l}{2V}p \tag{3.47}$$

$$\hat{q} = \frac{l}{2V}q \tag{3.48}$$

$$\hat{r} = \frac{l}{2V}r \tag{3.49}$$

Combining equations (3.35) to (3.40) with equations (3.41) to (3.46), and substituting in equations (3.34), (3.47), (3.48) and (3.49), as well as using the nominal AUV velocity, $\bar{V}_0$, the following equations for the hydrodynamic forces and moments on the AUV are obtained in (3.50) to (3.55).

$$X_H = -\left\{\frac{1}{2}\rho l^2 \bar{V}^2 C_{D_0}\right\} \tag{3.50}$$

$$Y_H = \left\{\frac{1}{2}\rho l^2 \bar{V}_0^2 C_{Y_\beta}\right\}\beta + \left\{\frac{1}{4}\rho l^3 \bar{V}_0 C_{Y_p}\right\}p \tag{3.51}$$

$$Z_H = -\left\{\frac{1}{2}\rho l^2 \bar{V}_0^2 C_{L_\alpha}\right\}\alpha - \left\{\frac{1}{4}\rho l^3 \bar{V}_0 C_{L_q}\right\}q \tag{3.52}$$

$$K_H = \left\{\frac{1}{4}\rho l^4 \bar{V}_0 C_{K_p}\right\}p \tag{3.53}$$

$$M_H = \left\{\frac{1}{2}\rho l^3 \bar{V}_0^2 C_{M_\alpha}\right\}\alpha + \left\{\frac{1}{4}\rho l^4 \bar{V}_0 C_{M_q}\right\}q \tag{3.54}$$

$$N_H = \left\{\frac{1}{2}\rho l^3 \bar{V}_0^2 C_{N_\beta}\right\}\beta + \left\{\frac{1}{4}\rho l^4 \bar{V}_0 C_{N_r}\right\}r \tag{3.55}$$

Only a lumped drag coefficient, C_{D_0}, was available to calculate drag. This is used to derive an equation for X_H based on the state variable $\bar{V}$. The drag coefficient term in (3.50) is differentiated by $\bar{V}$ to generate the final X_H equation for the perturbation about $\bar{V}_0$, which is given below in (3.56)

$$X_H = -\left\{\rho l^2 \bar{V}_0 C_{D_0}\right\}\bar{v} \tag{3.56}$$

These equations can be written more concisely as:

$$\begin{aligned}
X_H &= -\{D_{\bar{v}}\}\bar{v} \\
Y_H &= \left\{Y_\beta\right\}\beta + \left\{Y_p\right\}p \\
Z_H &= -\{L_\alpha\}\alpha - \left\{L_q\right\}q \\
K_H &= \left\{K_p\right\}p \\
M_H &= \{M_\alpha\}\alpha + \left\{M_q\right\}q \\
N_H &= \left\{N_\beta\right\}\beta + \{N_r\}r
\end{aligned}$$

Control

The forces and moments produced by fin deflections are also part of hydrodynamics of the AUV. The equations describing these forces and moments have the same form

Table 3.2: AUV control inputs

Symbol	Description
δE	Elevator deflection
δA_l	Left front fin deflection
δA_r	Right front fin deflection
δR	Rudder deflection

as the hydrodynamic equations above. The variables tabulated in **Table 3.2** are used to describe the control inputs for AUV fin positions.

All deflections are measured in degrees, with the conventions such that positive deflections of the fins result in negative moments on the AUV. To clarify:

- A positive deflection of the elevator moves the fin down, producing a negative pitching moment.
- A positive deflection of both front fins simultaneously moves those fin up, producing a negative pitching moment.
- A positive deflection of the rudders moves both fins to the left, producing a negative yawing moment. Since the two rudder fins are mechanically connected they are treated as one control input to the model.

These conventions are defined here for consistency in the mathematical model. They may not be the same as the physical conventions on the AUV, but this will be catered for simply by inverting the control signals where necessary.

Since the front fins can be operated independently of each other, their operation can be combined in different ways to provide more intuitive control inputs. When both are deflected with equal magnitude in the same direction, in *common mode*, the AUV experiences a pitching moment. When they are deflected with equal magnitude in opposite directions, in *differential mode*, the AUV experiences a rolling moment. New control inputs are thus defined for each of the virtual control inputs respectively, in **(3.57)** and **(3.58)**. Since the model will be linearised and the actual response is quite linear for individual fin deflections as large as 15°, the control inputs are merely added or subtracted as necessary. The new control inputs are defined such that the convention of positive control signals yielding negative moments still applies, with positive δA_c producing a negative pitching moment and positive δA_d producing a negative rolling moment on the AUV. The definitions maintain the same saturation limits on the new control inputs (that is ±25°).

$$\text{Common mode:} \quad \delta A_c = \frac{1}{2}(\delta A_l + \delta A_r) \tag{3.57}$$

$$\text{Differential mode:} \quad \delta A_d = \frac{1}{2}(\delta A_l - \delta A_r) \tag{3.58}$$

The individual fin deflections must now be commanded in terms of the new control inputs according to **(3.59)** and **(3.60)**.

$$\delta A_l = \delta A_c + \delta A_d \tag{3.59}$$

$$\delta A_r = \delta A_c - \delta A_d \tag{3.60}$$

Proceeding as before with the hydrodynamic equations, linearised equations incorporating the control inputs into the model are arrived at below, where V_f is the flow velocity over each individual fin:

$$\begin{aligned}
Y_C &= \left\{\frac{1}{2}\rho l^2 \bar{V}_f^2 C_{Y_{\delta R}}\right\}\delta R \\
Z_C &= -\left\{\frac{1}{2}\rho l^2 \bar{V}_f^2 C_{L_{\delta E}}\right\}\delta E - \left\{\frac{1}{2}\rho l^2 \bar{V}_f^2 C_{L_{\delta A_l}}\right\}\delta A_l - \left\{\frac{1}{2}\rho l^2 \bar{V}_f^2 C_{L_{\delta A_r}}\right\}\delta A_r \\
K_C &= \left\{\frac{1}{2}\rho l^3 \bar{V}_f^2 C_{K_{\delta A_l}}\right\}\delta A_l + \left\{\frac{1}{2}\rho l^3 \bar{V}_f^2 C_{K_{\delta A_r}}\right\}\delta A_r \\
M_C &= \left\{\frac{1}{2}\rho l^3 \bar{V}_f^2 C_{M_{\delta E}}\right\}\delta E + \left\{\frac{1}{2}\rho l^3 \bar{V}_f^2 C_{M_{\delta A_l}}\right\}\delta A_l + \left\{\frac{1}{2}\rho l^3 \bar{V}_f^2 C_{M_{\delta A_r}}\right\}\delta A_r \\
N_C &= \left\{\frac{1}{2}\rho l^3 \bar{V}_f^2 C_{N_{\delta R}}\right\}\delta R
\end{aligned}$$

For the front fins and elevator, the flow velocity is expected to be the same as AUV's forward velocity. The rudder fins, however, are located in the outlet flow of the thrusters. The flow velocity of the fluid over these fins is therefore approximately equal to the outlet velocity of the thrusters. This information can now be substituted into the above equations, where the variable V_{T_0} represents the nominal thruster outlet velocity of the fluid. Also, noting the relationships in equations **(3.61)** to **(3.63)**, the equations can be modified to be in terms of the control inputs A_c and A_d. The final expressions for the forces and moments produced by the control fins on the AUV are now given in **(3.64)** to **(3.68)**. Here the switch to perturbation variables is also made, although these are equivalent to the actual control inputs, since the trim values for all the control fins have been set at 0°.

$$C_{L_{\delta A_l}} = C_{L_{\delta A_r}} \tag{3.61}$$

$$C_{M_{\delta A_l}} = C_{M_{\delta A_r}} \tag{3.62}$$

$$C_{K_{\delta A_l}} = -C_{K_{\delta A_r}} \tag{3.63}$$

$$Y_C = \left\{\frac{1}{2}\rho l^2 \bar{V}_{T_0}^2 C_{Y_{\delta R}}\right\}\delta r \tag{3.64}$$

$$Z_C = -\left\{\frac{1}{2}\rho l^2 \bar{V}_0^2 C_{L_{\delta E}}\right\}\delta e - \left\{\frac{1}{2}\rho l^2 \bar{V}_0^2 \left(2C_{L_{\delta A_l}}\right)\right\}\delta a_c \tag{3.65}$$

$$K_C = \left\{\frac{1}{2}\rho l^3 \bar{V}_0^2 \left(2C_{K_{\delta A_l}}\right)\right\}\delta a_d \tag{3.66}$$

$$M_C = \left\{\frac{1}{2}\rho l^3 \bar{V}_0^2 C_{M_{\delta E}}\right\}\delta e + \left\{\frac{1}{2}\rho l^3 \bar{V}_0^2 \left(2C_{M_{\delta A_l}}\right)\right\}\delta a_c \tag{3.67}$$

$$N_C = \left\{\frac{1}{2}\rho l^3 \bar{V}_{T_0}^2 C_{N_{\delta R}}\right\}\delta r \tag{3.68}$$

These equations can now be written more concisely as:

$$Y_C = \{Y_{\delta r}\}\,\delta r \tag{3.69}$$
$$Z_C = -\{L_{\delta e}\}\,\delta e - \{L_{\delta a_c}\}\,\delta a_c \tag{3.70}$$
$$K_C = \left\{K_{\delta a_d}\right\}\delta a_d \tag{3.71}$$
$$M_C = \{M_{\delta e}\}\,\delta e + \{M_{\delta a_c}\}\,\delta a_c \tag{3.72}$$
$$N_C = \{N_{\delta r}\}\,\delta r \tag{3.73}$$

Added Mass Terms

There are some other hydrodynamic derivatives that have not yet been mentioned, which depend on derivatives of the AUV velocity (U, V, W) and angular rate (P, Q, R) variables. These terms ($X_{\dot{u}}$, $Y_{\dot{v}}$, $Z_{\dot{w}}$, $K_{\dot{p}}$, $M_{\dot{q}}$, $N_{\dot{r}}$), however, have the same mathematical form as mass when introduced into the model, and are thus called *added mass* terms. They are included in the model simply by adding them to the mass and inertia matrices in equations **(3.10)** and **(3.11)**, yielding equations **(3.74)** and **(3.75)**. A more thorough explanation of these terms is available in [1, p. 40].

$$\left[\mathbf{F}\right] = \begin{bmatrix} m + X_{\dot{u}} & 0 & 0 \\ 0 & m + Y_{\dot{v}} & 0 \\ 0 & 0 & m + Z_{\dot{w}} \end{bmatrix} \begin{bmatrix} \dot{u} \\ \dot{v} + U_0 r \\ \dot{w} - U_0 q \end{bmatrix} \tag{3.74}$$

$$\left[\mathbf{M}\right] = \begin{bmatrix} I_{xx} + K_{\dot{p}} & 0 & 0 \\ 0 & I_{yy} + M_{\dot{q}} & 0 \\ 0 & 0 & I_{zz} + N_{\dot{r}} \end{bmatrix} \begin{bmatrix} \dot{p} \\ \dot{q} \\ \dot{r} \end{bmatrix} \tag{3.75}$$

These will be simplified to **(3.76)** and **(3.77)** in the rest of this thesis for the sake of brevity.

$$\left[\mathbf{F}\right] = \begin{bmatrix} m_x & 0 & 0 \\ 0 & m_y & 0 \\ 0 & 0 & m_z \end{bmatrix} \begin{bmatrix} \dot{u} \\ \dot{v} + U_0 r \\ \dot{w} - U_0 q \end{bmatrix} \tag{3.76}$$

$$\left[\mathbf{M}\right] = \begin{bmatrix} I_x & 0 & 0 \\ 0 & I_y & 0 \\ 0 & 0 & I_z \end{bmatrix} \begin{bmatrix} \dot{p} \\ \dot{q} \\ \dot{r} \end{bmatrix} \tag{3.77}$$

The Complete State Space Model

The various equations mentioned up to this point can now be combined to give the final state space model of the AUV. These equations require some manipulation so that the state space model can be obtained, remembering that the model must be

described in terms of state variables. Equations **(3.76)** and **(3.77)** are manipulated and combined to give **(3.78)** below.

$$\begin{bmatrix} \dot{u} \\ \dot{v} \\ \dot{w} \\ \dot{p} \\ \dot{q} \\ \dot{r} \end{bmatrix} = \begin{bmatrix} m_x & 0 & 0 & 0 & 0 & 0 \\ 0 & m_y & 0 & 0 & 0 & 0 \\ 0 & 0 & m_z & 0 & 0 & 0 \\ 0 & 0 & 0 & I_x & 0 & 0 \\ 0 & 0 & 0 & 0 & I_y & 0 \\ 0 & 0 & 0 & 0 & 0 & I_z \end{bmatrix}^{-1} \begin{bmatrix} X \\ Y \\ Z \\ K \\ M \\ N \end{bmatrix} + \begin{bmatrix} 0 \\ U_0 r \\ -U_0 q \\ 0 \\ 0 \\ 0 \end{bmatrix} \tag{3.78}$$

The following linearisations about $\alpha = 0°$ and $\beta = 0°$ are used to transform the velocity related states:

$$\begin{aligned} \bar{v} &\approx u \\ U_0 &\approx \bar{V}_0 \\ \alpha &\approx \frac{w}{\bar{V}_0} \\ \beta &\approx \frac{v}{\bar{V}_0} \end{aligned}$$

These are then substituted into equation **(3.78)** to give **(3.79)**

$$\begin{bmatrix} \dot{\bar{v}} \\ \dot{\beta} \\ \dot{\alpha} \\ \dot{p} \\ \dot{q} \\ \dot{r} \end{bmatrix} = \begin{bmatrix} \frac{1}{m_x} & 0 & 0 & 0 & 0 & 0 \\ 0 & \frac{1}{m_y \bar{V}_0} & 0 & 0 & 0 & 0 \\ 0 & 0 & \frac{1}{m_z \bar{V}_0} & 0 & 0 & 0 \\ 0 & 0 & 0 & \frac{1}{I_x} & 0 & 0 \\ 0 & 0 & 0 & 0 & \frac{1}{I_y} & 0 \\ 0 & 0 & 0 & 0 & 0 & \frac{1}{I_z} \end{bmatrix} \begin{bmatrix} X \\ Y \\ Z \\ K \\ M \\ N \end{bmatrix} + \begin{bmatrix} 0 \\ r \\ -q \\ 0 \\ 0 \\ 0 \end{bmatrix} \tag{3.79}$$

The various forces and moments from the model can now be substituted in as follows in **(3.80)**. The zero-valued components of each of the forces and moments have been excluded from the equation.

$$\begin{bmatrix} X \\ Y \\ Z \\ K \\ M \\ N \end{bmatrix} = \begin{bmatrix} X_G + X_B + X_H + X_T \\ Y_G + Y_B + Y_H + Y_C \\ Z_G + Z_B + Z_H + Z_C \\ K_B + K_H + K_C \\ M_B + M_H + M_C \\ N_B + N_H + N_C + N_T \end{bmatrix} \tag{3.80}$$

Before substitutions are made, and with knowledge of the final model, **(3.79)** is first decoupled to aid clarity of the substitutions. The model is decoupled into a *longitudinal* and *lateral* model, as given below in **(3.81)** and **(3.82)**.

Longitudinal model:

$$\begin{bmatrix} \dot{\bar{v}} \\ \dot{\alpha} \\ \dot{q} \end{bmatrix} = \begin{bmatrix} \frac{1}{m_x} & 0 & 0 \\ 0 & \frac{1}{m_z \bar{V}_0} & 0 \\ 0 & 0 & \frac{1}{I_y} \end{bmatrix} \begin{bmatrix} X \\ Z \\ M \end{bmatrix} + \begin{bmatrix} 0 \\ -q \\ 0 \end{bmatrix} \tag{3.81}$$

Lateral model:

$$\begin{bmatrix} \dot{\beta} \\ \dot{p} \\ \dot{r} \end{bmatrix} = \begin{bmatrix} \frac{1}{m_y \bar{V}_0} & 0 & 0 \\ 0 & \frac{1}{I_x} & 0 \\ 0 & 0 & \frac{1}{I_z} \end{bmatrix} \begin{bmatrix} X \\ Z \\ M \end{bmatrix} + \begin{bmatrix} r \\ 0 \\ 0 \end{bmatrix} \tag{3.82}$$

The various forces and moments are now substituted into **(3.81)** and **(3.82)**, to give the final longitudinal and lateral state space models in **(3.83)** and **(3.84)** respectively. Note also that the state vectors in each model are appended with the Euler orientation variables, Φ and Θ, which are needed for the inclusion of the gravity and buoyancy forces and moments. The Euler yaw angle, Ψ, is included to bring completeness to later analysis of the model, but is otherwise not necessary in the model as it does not couple into any of the other state variables. For brevity, the diagonal inertia matrices are represented by column vectors with a subscript D.

Final linear longitudinal state space model:

$$\begin{aligned} \begin{bmatrix} \dot{\bar{v}} \\ \dot{\alpha} \\ \dot{q} \\ \dot{\theta} \end{bmatrix} = & \begin{bmatrix} \frac{1}{m_x} \\ \frac{1}{m_z \bar{V}_0} \\ \frac{1}{I_y} \\ 1 \end{bmatrix}_D \begin{bmatrix} -D_{\bar{v}} & 0 & 0 & (B - W_G) \\ 0 & -L_\alpha & -L_q - m_z U_0 & 0 \\ 0 & M_\alpha & M_q & z_{\text{COB}} B \\ 0 & 0 & 1 & 0 \end{bmatrix} \begin{bmatrix} \bar{v} \\ \alpha \\ q \\ \theta \end{bmatrix} \\ & + \begin{bmatrix} \frac{1}{m_x} \\ \frac{1}{m_z \bar{V}_0} \\ \frac{1}{I_y} \\ 1 \end{bmatrix}_D \begin{bmatrix} 2c_T & 0 & 0 \\ 0 & -L_{\delta a_c} & -L_{\delta e} \\ 0 & M_{\delta a_c} & M_{\delta e} \\ 0 & 0 & 0 \end{bmatrix} \begin{bmatrix} \delta t_c \\ \delta a_c \\ \delta e \end{bmatrix} \end{aligned} \tag{3.83}$$

Final linear lateral state space model:

$$\begin{aligned} \begin{bmatrix} \dot{\beta} \\ \dot{p} \\ \dot{r} \\ \dot{\phi} \\ \dot{\psi} \end{bmatrix} = & \begin{bmatrix} \frac{1}{m_y \bar{V}_0} \\ \frac{1}{I_x} \\ \frac{1}{I_z} \\ 1 \\ 1 \end{bmatrix}_D \begin{bmatrix} Y_\beta & Y_p & -m_y U_0 & (W_G - B) & 0 \\ 0 & K_p & 0 & z_{\text{COB}} B & 0 \\ N_\beta & 0 & N_r & 0 & 0 \\ 0 & 1 & 0 & 0 & 0 \\ 0 & 0 & 1 & 0 & 0 \end{bmatrix} \begin{bmatrix} \beta \\ p \\ r \\ \phi \\ \psi \end{bmatrix} \\ & + \begin{bmatrix} \frac{1}{m_y \bar{V}_0} \\ \frac{1}{I_x} \\ \frac{1}{I_z} \\ 1 \\ 1 \end{bmatrix}_D \begin{bmatrix} 0 & 0 & Y_{\delta r} \\ 0 & K_{\delta a_d} & 0 \\ 2y_T c_T & 0 & N_{\delta r} \\ 0 & 0 & 0 \\ 0 & 0 & 0 \end{bmatrix} \begin{bmatrix} \delta t_d \\ \delta a_d \\ \delta r \end{bmatrix} \end{aligned} \tag{3.84}$$

3.3 Model parameters

Acquiring values for the model parameters is usually the most difficult part of mathematical modelling. All the values of the parameters in this model will be given below and are taken at the specific trim condition about which the model was linearised. Almost all the parameters are obtained directly from the results obtained in [1]. Where this is not the case, the determination of their values will be discussed.

Vehicle parameters

The physical parameters associated with the AUV itself are listed in this section. The various mass and inertia parameters were calculated in [1]. The thruster parameters are also listed and are obtained directly from [1]. The added mass terms are included in this section because of how they are included in the model. These values are displayed in **Table 3.3** and result in the values for the lumped parameters displayed in the same table.

The buoyant mass, or mass of water displaced by the AUV, is not known exactly and was estimated based on how the AUV responded in the simulation environment. What is actually important with regards to the buoyant mass is its difference with respect to the actual mass of the AUV. This difference results in the AUV either naturally sinking or floating when in the water. IMT specifically ensure the AUV is positively buoyant so that it will float to the water surface if the system fails. This means the buoyant mass of the AUV is larger than its actual flooded mass. A large difference between actual and buoyant mass would make the AUV difficult to control, since there would be a large force acting to make it float or sink. This difference was estimated to be 5kg. Larger values of buoyant mass made it very difficult to control the AUV since it would tend to float to the surface in simulation.

The centre of buoyancy position, z_{COB}, is also not known and had to be estimated. Analysis of the lateral model revealed that the poles associated with the AUV roll are dominated by the effects of buoyancy. Therefore, using **(3.20)** from **Section 3.2** and results from the analysis of IMT test data in **Chapter 2**, the value of z_{COB} was set to 1.5 millimetres. The calculation is displayed below in **(3.85)** for convenience.

$$\begin{aligned} z_{\text{COB}} &= (\omega_{\text{roll}})^2 \frac{I_x}{B} \\ &= (0.42)^2 \frac{71}{8289} \\ &= 0.0015 \end{aligned} \tag{3.85}$$

Table 3.3: Model parameters relating to the physical AUV

Brief description	Symbol	Value	Units
AUV mass when flooded	m	840	kg
Principle moments of inertia:	I_{xx}	65	kg.m^2
	I_{yy}	497	kg.m^2
	I_{zz}	547	kg.m^2
Added mass terms:	$X_{\dot{u}}$	8	kg
	$Y_{\dot{v}}$	84	kg
	$Z_{\dot{w}}$	658	kg
	$K_{\dot{p}}$	6	kg.m^2
	$M_{\dot{q}}$	259	kg.m^2
	$N_{\dot{r}}$	31	kg.m^2
Buoyant mass	m_B	845	kg
COB displacement	z_{COB}	-0.005	m
Thruster displacement	y_T	0.6	m
Thrust constant	c_T	127	N
lumped parameters:	m_x	848	kg
	m_y	924	kg
	m_z	1498	kg
	I_x	71	kg.m^2
	I_y	756	kg.m^2
	I_z	578	kg.m^2
	W_G	8240	N
	B	8289	N

Hydrodynamic model parameters

The parameters listed in this section are those that pertain to the hydrodynamics of the model, which includes the control derivative parameters for the control fins. The trim velocity of the AUV was set based on results from recorded data analysed in **Section 2**. The thruster outlet velocity, V_{T_0}, was estimated using simulation and adjusted such that in simulation the turning circle of the AUV when the rudders were fully deflected was similar to that observed in recorded data, which was about 20 m in diameter. The length of the AUV is listed here, as it is in fact arbitrary and used only for converting the non-dimensional hydrodynamic derivatives to dimensional values. The parameters used for making the model dimensional are listed below in **Table 3.4**.

The values for the hydrodynamic coefficients were obtained from [1]. The data for these coefficients is plotted in **Figure A.1** to **Figure A.6** in **Appendix A**. All the hydrodynamic coefficients were obtained as functions of α. The linearised, nominal values for each coefficient were obtained simply by taking the values calculated at trim $\alpha_0 = 0°$. The exceptions to this are the α derivative coefficients, C_{L_α} and C_{M_α}.

Table 3.4: Model parameters relating to the hydrodynamic model

Description	symbol	value	units
Length of the AUV	l	3	m
Trim velocity	$\bar{V}_0$	1.3	$m.s^{-1}$
Thruster outlet velocity	V_{T_0}	5.8	$m.s^{-1}$
Fluid density	ρ	1016.8	$kg.m^{-3}$

The linearised values for these were obtained from the gradients of the C_L and C_M data plots respectively, at $\alpha_0 = 0°$. It should be noted that in the state space matrices these coefficients describe each state relation in SI units. The gradients, therefore, must be obtained using α measured in radians. The lumped parameter, C_{D_0}, was used to calculate a value for the dimensional derivative $D_{\bar{v}}$. The non-dimensional hydrodynamic coefficients are listed below in **Table 3.5**, along with the resulting dimensional derivatives.

The parameters that are not included in **Table 3.5** below are accounted for in the following ways. Naturally, all cross-coupling terms between the longitudinal and lateral models are zero. The coefficients C_{Y_p}, C_{K_β}, C_{K_r} and C_{N_p} are zero at the specified trim condition. The coefficients C_L and C_M can also be used to calculate $C_{L_{\bar{v}}}$ and $C_{M_{\bar{v}}}$, which are also zero at trim. The coefficients C_{D_α}, C_{D_q} and C_{Y_r} were not determined in [1]. C_{D_q} and C_{Y_r} represent the same type of effect on the AUV, that is, a force due to an angular rate. Intuitively this does not make much sense. If the AUV were to experience either a pitch or yaw rate, this would affect its angle of attack or angle of side-slip respectively. These would then result in forces on the AUV, but a specific rate itself is not expected to have any direct impact on the forces experienced by the AUV. These terms are neglected from the model on this basis. C_{D_α} could be calculated in much the same way as C_{L_α} and C_{M_α}; however, C_{D_0} is very non-linear with α. Because $C_{L_{\bar{v}}}$ and $C_{M_{\bar{v}}}$ are zero, the $\bar{v}$ state in the model will not couple into any other states, so the calculation of C_{D_α} will affect only this one state. As will be discussed later in **Chapter 6**, speed control is not of great concern in this project. This parameter has therefore been omitted from the model.

The absolute value for C_{K_p} at trim is very small, and increases dramatically outside the chosen trim conditions. The exact value for C_{K_p} at $\alpha_0 = 0°$ was therefore not used in the model but was doubled to provide some extra roll damping in the linear model. This is more likely the case in the physical model, as was shown in the test data analysis in **Chapter 2**. The accuracy of the model is not expected to be very high, because a fair number of parameters have been estimated, no parameter validation was carried out in [1], and there are non-linearities in parameters such as C_{D_0} and C_{K_p} that have not been captured. As such, the coefficient values are given to at most three significant digits.

Table 3.5: Hydrodynamic model parameters

Non-dimensional		Dimensional	
symbol	value	symbol	value
C_{D_0}	0.03	$D_{\bar{v}}$	357
C_{Y_β}	-0.07	Y_β	-541
C_{L_α}	0.166	L_α	1284
C_{L_q}	0.0185	L_q	165
C_{K_p}	-0.0006	K_p	-1.61
C_{M_α}	0.064	M_α	1485
C_{M_q}	-0.11	M_q	-2945
C_{N_β}	0.0155	N_β	360
C_{N_r}	-0.0098	N_r	-262

The control derivative data given in [1] was specified at particular fin deflection values, and not in terms of fin deflections. This data is plotted in **Figure A.8**, **Figure A.7** and **Figure A.9** in **Appendix A**. Thus, similarly to the way the coefficients for C_{L_α} and C_{M_α} were obtained, all the control derivative coefficient values were taken as the gradients of the coefficient data about 0° fin deflections. The fin control inputs in the model are given in terms of degrees of deflection and not in radians as is the case with the other hydrodynamic derivatives. The gradient values can thus be obtained directly from the plots. The drag caused by any of the control fins is very small in comparison to the overall drag caused by the AUV body. The drag coefficients are also quadratically non-linear. These coefficients were therefore omitted from the linear model altogether. All the other control derivatives excluded from the table are intuitively expected to be negligibly small. The right front fin coefficients have been omitted from the table, since in the model they were replaced by the left front fin coefficients. The front fin coefficients are all identical, excepting $C_{K_{\delta a_r}}$, which has the same magnitude, but inverse sign of $C_{K_{\delta a_l}}$. The data given for the rudder coefficients, was calculated for only a single rudder. The values for these coefficients must therefore be double the calculated plot gradient, to take into account the double rudder configuration of the AUV. The non-dimensional and resulting dimensional derivatives are listed below in **Table 3.6**

3.4 Chapter summary

The values for the model parameters are substituted into the state space matrices to give the final mathematical model for the AUV, as in **(3.86)** ans **(3.87)**. The values here are restricted to three significant digits. These linear state space models are used directly for the new control and guidance designs. These models are analysed in the next chapter.

Table 3.6: Control fin model parameters

Non-dimensional		Dimensional	
symbol	value	symbol	value
$C_{M_{\delta e}}$	-0.00025	$M_{\delta e}$	-5.8
$C_{L_{\delta e}}$	0.0002	$L_{\delta e}$	1.55
$C_{M_{\delta a_l}}$	-0.0000088	$M_{\delta a_c}$	-0.408
$C_{L_{\delta a_l}}$	-0.00007	$L_{\delta a_c}$	-1.083
$C_{K_{\delta a_l}}$	-0.000045	$K_{\delta a_d}$	-2.088
$C_{Y_{\delta r}}$	0.000022	$Y_{\delta r}$	2.517
$C_{N_{\delta r}}$	-0.00002	$N_{\delta r}$	-6.864

Final linear longitudinal state space model:

$$\dot{\mathbf{x}}_{\text{long}} = \mathbf{A}_{\text{long}}\mathbf{x}_{\text{long}} + \mathbf{B}_{\text{long}}\mathbf{u}_{\text{long}}$$

$$\begin{bmatrix} \dot{\bar{v}} \\ \dot{\alpha} \\ \dot{q} \\ \dot{\theta} \end{bmatrix} = \begin{bmatrix} -0.421 & 0 & 0 & 0.0579 \\ 0 & -0.659 & 0.915 & 0 \\ 0 & 1.96 & -3.9 & -0.022 \\ 0 & 0 & 1 & 0 \end{bmatrix} \begin{bmatrix} \bar{v} \\ \alpha \\ q \\ \theta \end{bmatrix} + \begin{bmatrix} 0.3 & 0 & 0 \\ 0 & 0.000556 & -0.000794 \\ 0 & -0.00054 & -0.00767 \\ 0 & 0 & 0 \end{bmatrix} \begin{bmatrix} \delta t_c \\ \delta a_c \\ \delta e \end{bmatrix} \tag{3.86}$$

Final linear lateral state space model:

$$\dot{\mathbf{x}}_{\text{lat}} = \mathbf{A}_{\text{lat}}\mathbf{x}_{\text{lat}} + \mathbf{B}_{\text{lat}}\mathbf{u}_{\text{lat}}$$

$$\begin{bmatrix} \dot{\beta} \\ \dot{p} \\ \dot{r} \\ \dot{\phi} \\ \dot{\psi} \end{bmatrix} = \begin{bmatrix} -0.451 & 0 & -1 & -0.0408 & 0 \\ 0 & -0.0227 & 0 & -0.233 & 0 \\ 0.622 & 0 & -0.454 & 0 & 0 \\ 0 & 1 & 0 & 0 & 0 \\ 0 & 0 & 1 & 0 & 0 \end{bmatrix} \begin{bmatrix} \beta \\ p \\ r \\ \phi \\ \psi \end{bmatrix} + \begin{bmatrix} 0 & 0 & 0.0028 \\ 0 & -0.0293 & 0 \\ 0.265 & 0 & -0.016 \\ 0 & 0 & 0 \\ 0 & 0 & 0 \end{bmatrix} \begin{bmatrix} \delta t_d \\ \delta a_d \\ \delta r \end{bmatrix} \tag{3.87}$$

Chapter 4

Model Analysis

This chapter analyses the linear mathematical model to gain insight for the control designs. An initial intuitive analysis shows the decoupled nature of the longitudinal and lateral sub-models. This is followed by a more in depth analysis of the full longitudinal and lateral models, using a technique known as modal analysis. The main purpose of this analysis is to gather information which will aid in selecting input-output feedback pairs and to identify any possible issues that may arise in the controller design process. At the end of this chapter the control fin non-linearities are analysed and modelled such that their effects on the system behaviour can be taken into account during controller designs.

4.1 Initial intuitive analysis

Intuitively, further decoupling of the models is possible by noting that the relative magnitudes of the boxed elements of the matrices shown in **(4.1)** and **(4.4)**, when compared to the other elements in those rows, are about two orders of magnitude lower than those of the other elements. Decoupling on this basis requires the measurement units for the states to be normalised. This is usually performed by scaling the states according to their expected deviations about trim, which requires estimates of these deviations. The boxed elements in this case are multiplied by attitude angle states of the AUV, which are expected to trim near zero and are limited to maximum deviations of about 1 radian at the most and are not likely to exceed 0.5 radians during normal operation. The deviations of the other states in these rows can easily be expected to exceed values of 0.005 (with appropriate units) by some margin. Also, the top boxed units in each of the state space matrices are dependent on the difference between the actual mass and buoyant mass of the AUV. As the buoyant mass tends to the same value as the actual mass, as is usually the case in AUVs, these terms tend to zero. The boxed elements can therefore be

considered negligible and the model further decoupled. Although these further simplified models are not used in the controller design process which follows this chapter, they support the control design philosophy of using simple SISO control in favour of more complicated coupled MIMO controllers, and suggest that each aspect of the AUV's movement can be controlled independently.

By setting the boxed element in the first row of $\mathbf{A}_{\text{long}}$ to zero, the velocity dynamics of the AUV can be decoupled and are given in **(4.2)**. The decoupled dynamics have a first-order response with a time constant of 2.38 seconds. By setting the boxed element in the third row of $\mathbf{A}_{\text{long}}$ to zero, the fast pitch dynamics of the AUV can be decoupled and are given in **(4.3)**. The decoupled system has two stable real poles, with time constants of 0.23 seconds and 5.69 seconds. This leaves only the pitch angle, which is extraneous to the decoupled dynamics.

$$\mathbf{A}_{\text{long}} = \begin{bmatrix} -0.421 & 0 & 0 & \boxed{0.0579} \\ 0 & -0.659 & 0.915 & 0 \\ 0 & 1.96 & -3.9 & \boxed{\text{-0.022}} \\ 0 & 0 & 1 & 0 \end{bmatrix} \tag{4.1}$$

Further decoupled linear longitudinal state space model:

$$\begin{bmatrix} \dot{\bar{v}} \end{bmatrix} = \begin{bmatrix} -0.421 \end{bmatrix} \begin{bmatrix} \bar{v} \end{bmatrix} + \begin{bmatrix} 0.3 \end{bmatrix} \begin{bmatrix} \delta t_c \end{bmatrix} \tag{4.2}$$

$$\begin{bmatrix} \dot{\alpha} \\ \dot{q} \end{bmatrix} = \begin{bmatrix} -0.659 & 0.915 \\ 1.96 & -3.9 \end{bmatrix} \begin{bmatrix} \alpha \\ q \end{bmatrix} + \begin{bmatrix} 0.000556 & -0.000794 \\ -0.00054 & -0.00767 \end{bmatrix} \begin{bmatrix} \delta a_c \\ \delta e \end{bmatrix} \tag{4.3}$$

By setting the boxed element in the first row of $\mathbf{A}_{\text{lat}}$ to zero, the roll and yaw lateral dynamics can be decoupled from one another. The yaw response is given in **(4.5)** and has complex poles with a frequency of 0.91 rad.s^{-1} and damping factor of 0.5. The roll response is given in **(4.6)** and has complex poles with a frequency of 0.42 rad.s^{-1} and damping factor of 0.027. The numerical results for the decoupled models can be compared to the modal responses in the next section to further validate this decoupling.

$$\mathbf{A}_{\text{lat}} = \begin{bmatrix} -0.451 & 0 & -1 & \boxed{\text{-0.0408}} & 0 \\ 0 & -0.0227 & 0 & -0.233 & 0 \\ 0.622 & 0 & -0.454 & 0 & 0 \\ 0 & 1 & 0 & 0 & 0 \\ 0 & 0 & 1 & 0 & 0 \end{bmatrix} \tag{4.4}$$

Further decoupled linear lateral state space model:

$$\begin{bmatrix} \dot{\beta} \\ \dot{r} \end{bmatrix} = \begin{bmatrix} -0.45 & -1 \\ 0.622 & -0.454 \end{bmatrix} \begin{bmatrix} \beta \\ r \end{bmatrix} + \begin{bmatrix} 0 & 0.0021 \\ 0.265 & -0.0119 \end{bmatrix} \begin{bmatrix} \delta t_d \\ \delta r \end{bmatrix} \tag{4.5}$$

$$\begin{bmatrix} \dot{p} \\ \dot{\phi} \end{bmatrix} = \begin{bmatrix} -0.0226 & -0.233 \\ 1 & 0 \end{bmatrix} \begin{bmatrix} p \\ \phi \end{bmatrix} + \begin{bmatrix} -0.0293 \\ 0 \end{bmatrix} \begin{bmatrix} \delta a_d \end{bmatrix} \tag{4.6}$$

4.2 Modal analysis

Modal analysis is a useful tool for gaining insight into a mathematical model. This approach analyses the solutions to the state space system for the case where there is no control input. This solution is given by the eigenvalues of the state space A matrix. Each eigenvalue has associated with it an eigenvector, which gives the relationships between the original states of the system for that mode of motion. The eigenvalue determines the response of the system when excited into a specific mode. The matrix transformation that leads to this solution can then be applied to each control vector. The resulting control vector can be used to assess each original control input's ability to control that particular mode of motion. Since all control fins have the same deflection limits, their effectiveness on each mode can be compared directly. Theoretically, the system states also require normalisation before comparing their contributions to a mode of motion. In this analysis, however, it is clear which aspect of the AUV's motion is dominant in each mode of motion, so the state normalisation is skipped. The relevant vectors and numerical information for each mode are displayed on the response plots themselves.

Longitudinal model

The response of the first mode of motion, shown in **Figure 4.1**, displays the uncontrolled forward velocity dynamics of the system. Any velocity disturbance is expected to decay with a time constant of 2.38 seconds. This corresponds exactly to the time constant of the decoupled velocity dynamics system. As expected, the modal control vector indicates that this mode is best controlled with the thrusters and does not couple into any of the other state variables.

The next two modal responses, shown in **Figure 4.2** and **Figure 4.3**, have time constants similar to those of the decoupled pitch response dynamics. These two separate responses constitute what would usually be identified as the so-called short period mode in aircraft dynamics. The short period mode usually has a complex response and represents the fastest dynamics of the aircraft's natural response. In the case of the AUV, the complex poles have moved onto the real axis and become two different natural modes.

The final modal response is shown in **Figure 4.4**. The characteristics of this response are very similar to those of the slower of the two fast pitch dynamics responses. This is to be expected, since the pitch angle of the AUV is merely the integral of its pitch rate with a small amount of negative feedback to the pitch rate. The similarities between these two modes are observed in the following ways:

- The ratio between the contributions of the pitch angle, θ, and velocity, $\bar{v}$, is similar in both modes

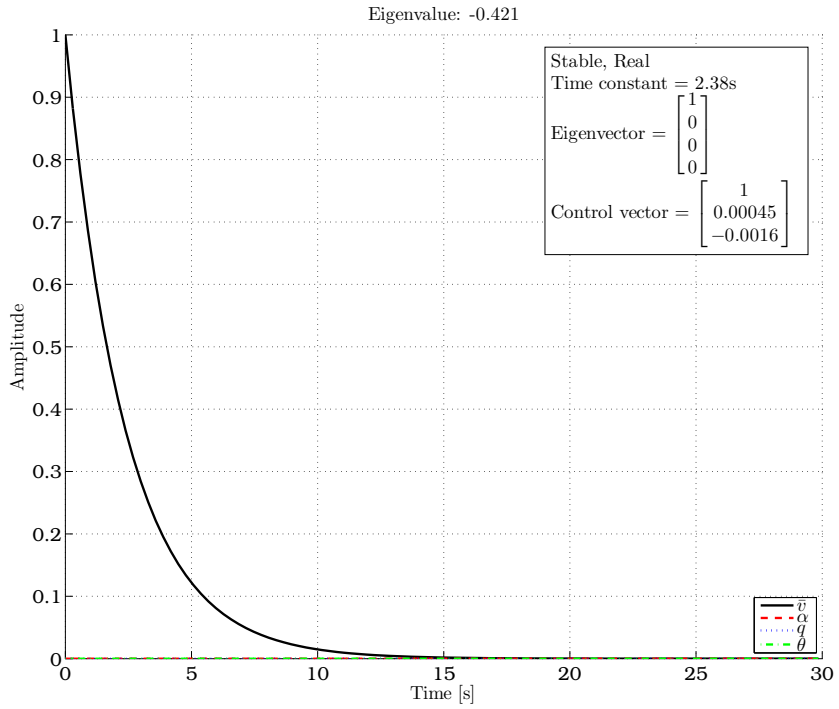

Figure 4.1: Longitudinal modal response: velocity dynamics

- The ratio between the contributions of the pitch rate, q, and angle of attack, α, is similar in both modes
- The relative signs of the various state contributions are the same in both modes.
- The resulting control vectors for each mode are similar.

Judging from the modal control vectors of these responses, the elevator seems to be the most effective control surface for controlling the AUV pitch. This is intuitively correct since the elevator is larger than the two front fins. The close correlation between the decoupled system dynamics and the modal responses suggests that the decoupling is valid and that the pitch and velocity of the AUV can be controlled without interaction occurring between them.

Lateral model

Having five states, the lateral model should naturally have five eigenvalues, giving five natural responses. However, because of the introduction of the extraneous yaw angle state, one of the eigenvalues is zero. This particular eigenvalue gives no information about the model. The other four eigenvalues form two complex

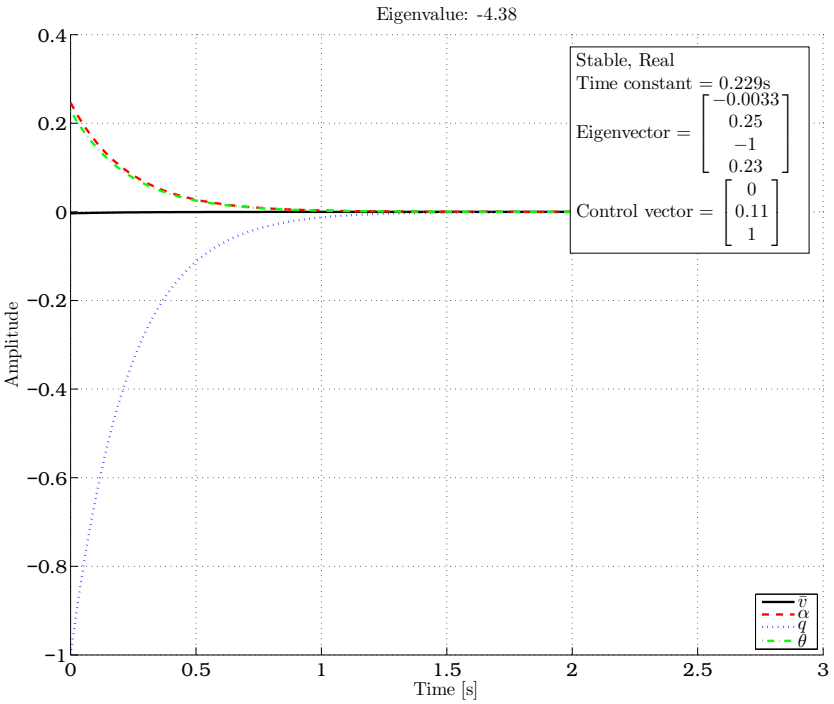

Figure 4.2: Longitudinal modal response: Fast pitching dynamics

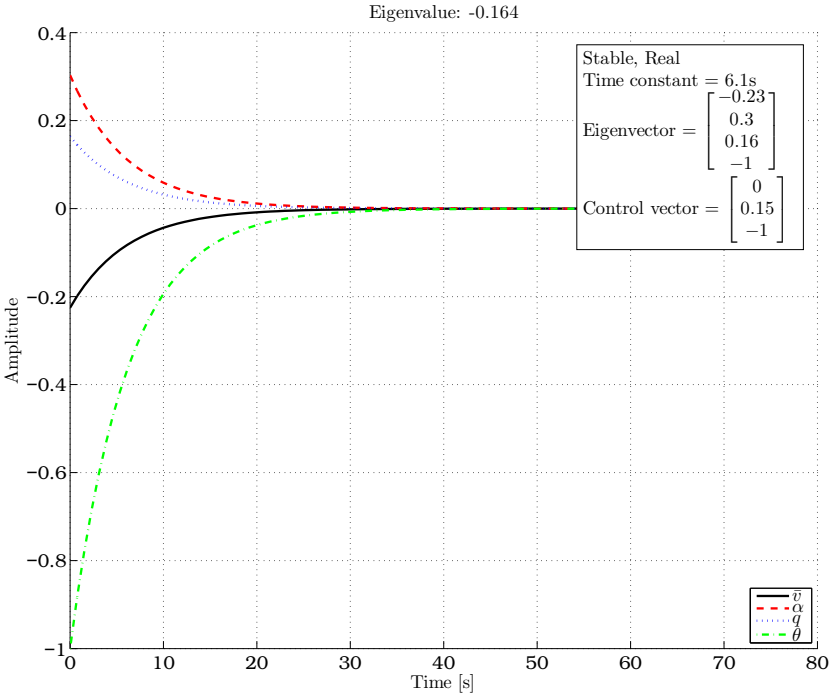

Figure 4.3: Longitudinal modal response: velocity dynamics

conjugate pole pairs, which results in two oscillatory natural responses in the lateral

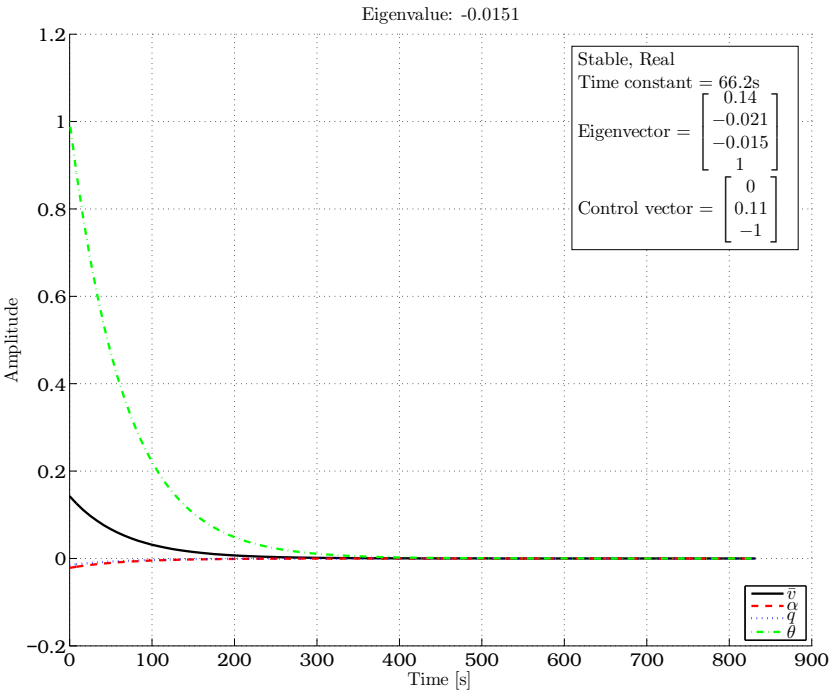

Figure 4.4: Longitudinal modal response: velocity dynamics

model.

The natural response of the first lateral mode of motion is plotted in **Figure 4.5** and is visible predominately as roll angle and roll rate disturbances. Here the pendulum-like behaviour of the buoyancy of the AUV is observed as it accelerates the AUV back towards its equilibrium position, increasing the roll rate of the AUV so that it overshoots the equilibrium position. The roll damping of the model is clearly quite poor, with a damping factor of only 0.027. The differential deflection of the AUV's front fins is the only way to control this rolling action. The 90° phase lag seen in the modal control vector also indicates that this action cannot be controlled by feeding the roll angle, ϕ, back to the front fin input through a simple gain. Rather, the AUV roll rate should be controlled before a reference roll angle is commanded, if the controllers are to remain as simple as possible. Disturbances to the AUV roll do couple into the AUV yaw states as well, but these should be controllable by regulating the yaw independently.

The response of the second mode of motion is plotted in **Figure 4.6**. This response is evident only in the yaw-related states of the AUV, β, R and Ψ. Clearly, the rudder is ten times more effective than the front fins at controlling the yaw of the AUV. Since the front fins couple heavily into the roll of the AUV, they will not be used at all for yaw control. The effectiveness of the rudders compared to differential thrusting is not immediately evident, since the input limits are different for each. Normalising these inputs reveals that the rudders are about 1.125 times as effective as differential

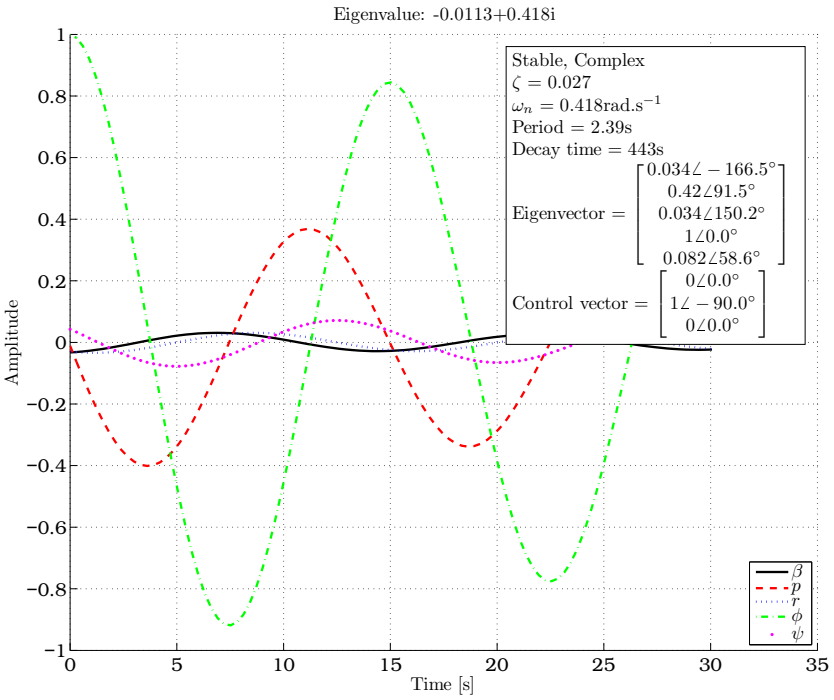

Figure 4.5: Lateral modal response: roll dynamics

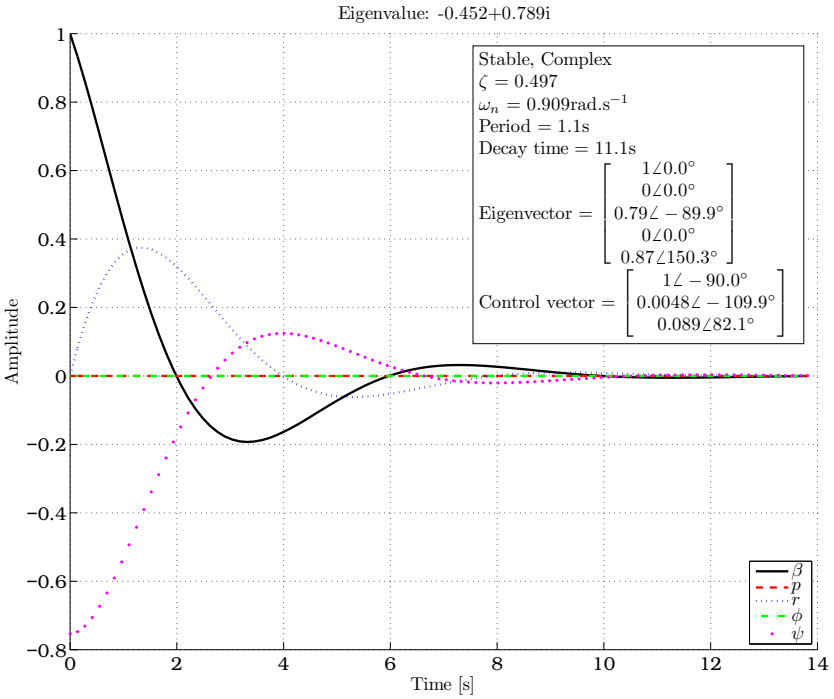

Figure 4.6: Lateral modal response: yaw dynamics

thrusting for controlling the AUV yaw. Both inputs are therefore assumed to be

equally capable of controlling the AUV yaw. As with the roll mode, the influences of both control inputs are essentially in phase with the yaw rate and 90° out of phase with the yaw angle of the AUV, which advocates feeding back yaw rate to control this mode of motion. As was the case with the longitudinal modes of motion, the dynamics of the lateral modes are very similar to those of the decoupled models, which indicates that the decoupling is valid.

4.3 Non-linearities

In order to test the robustness of controller designs, the simulation environment was set up to incorporate all known and modelled non-linearities. These are discussed in the following paragraphs. There are, of course, many physical non-linearities that cannot be accounted for, which are naturally not included in the simulation environment.

Model non-linearities

The full non-linear gravity and buoyancy forces on the AUV are included in the simulation.

The linear thruster model is used in simulation. Although a non-linear model of the thruster behaviour was created in [1], the end results were quite linear. The AUV thrusters are also never varied during operation. This operating condition is not expected to change unless the thruster power of the AUV is increased. For these reasons the much simpler linear thruster model is used in simulation.

In the plots in **Appendix A** it is evident that some of the modelled hydrodynamic parameters are very non-linear. The actual non-linearities of all the parameters are most likely not even captured in these plots. This probably accounts for the largest uncertainty in the model. Unfortunately, not much can be done to incorporate this into the mathematical model, so nominal values were used. The non-linear hydrodynamic parameters were, however, included in the simulation environment to include as much of the model uncertainty as possible.

Physical non-linearities

The only quantifiable physical non-linearities are those pertaining to the control fin actuators. These non-linearities are easy to include in the simulation. Their impact on the AUV performance cannot be ignored, however, as failure to design around these non-linearities could result in instability. Efforts to model the actuator non-linearities are discussed below. There are three known control surface non-linearities, which are listed below.

- Control surface deflection limits (±25°)
- Control surface deflection quantisation (1° steps)
- Control surface slew limit (±14.3° per second)

All fins on the AUV use the same type of actuator, so all bear the same non-linearities. SIMULINK provides simulation blocks to incorporate each one of these non-linearities into the simulation. The first two non-linearities are difficult to model, but the deflection limits can be avoided by keeping controller gains low, and quantisation effects are not expected to cause problems with the AUV in practice since they will effectively be filtered by the effective plant transfer functions. The effect of the slew limit is quite severe, though, as it puts bandwidth limitations on the controllers and affects the stability of the controllers. Fortunately it can be modelled to a certain degree.

Modelling slew limits for design purposes

Two approaches were considered in order to take the control surface slew rate into account. The first is a traditional frequency response approach to taking slew limits into account. If a sinusoidal input signal, $v(t) = A\sin(\omega t)$, is commanded of an actuator, the slew rate of this signal is $\dot{v}(t) = A\omega\cos(\omega t)$, which is maximum when $\cos(\omega t) = 1$. The maximum slew rate is therefore $A\omega$, which must be less than the slew limit, L, to maintain linear operation. This results in the inequality shown below in **(4.7)**. This leads to **(4.8)**, which sets a theoretical limit on the achievable bandwidth of the plant.

$$|A\omega| \leq L \tag{4.7}$$

$$\omega \leq \frac{L}{|A|} \tag{4.8}$$

Thus, using **(4.8)**, it is possible to choose a suitable value for A so that an upper limit for the closed-loop bandwidth of the system can be established. Logically, A would be set to the same value as the maximum possible deflections of the control surfaces. Often, however, full deflection of a control surface is not needed to stabilise or adequately control a system, so it is possible to relax the constraints on the controller by choosing a smaller value for A. In any case, this is merely a guideline and provides insight into the design. Substituting the constraints for the AUV control fins gives the minimum bandwidth limit to use as a guide for designing the AUV controllers. This limitation, shown in **(4.9)**, will be taken into account when designing the various controllers for the AUV. This pole essentially represents the behaviour of the system when the slew limit comes into play. It must therefore not be included in the plant model when designing the controllers, but

rather the final closed-loop plant transfer should be within, or at least near to, the bandwidth of this theoretical pole.

$$\omega \leq 0.57\text{rad.s}^{-1} \tag{4.9}$$

The second approach taken towards the slew limit problem involved controlling actuator velocity rather than position. This is achieved by adding an integrator to the original open-loop plant model and designing around that. The controller commanding the actuator would then require an added integrator at its output. This essentially transforms the slew limit into a clipping limit, which, as mentioned before, can be avoided largely by keeping the controller gains low. This method has some associated advantages and disadvantages.

Advantages:

- No direct feed-through to the actuator position occurs because of the added integrator, so no sudden jumps in the actuator position command are possible.
- A much better handle on slew rate is available, which may present opportunities for some interesting non-linear control solutions.

Disadvantages:

- The controller will tend to be much slower than is perhaps needed to maintain linear operation and still effectively stabilise and control the system. This will be particularly detrimental when the slew limit is indeed encountered with this controller and will have the same effect as integrator wind-up when the controller output needs to move in the opposite direction.
- The added integrators at the outputs of each controller need saturation protection as well.

In initial testing phases, controllers were designed using both of these design methods, with the general conclusion that the velocity control design method yielded slower controllers. In fact, the actuator velocity controllers required derivative action, in the form of lag-lead compensators, to perform well. This makes the controllers unnecessarily complex as well as making them more sensitive to sensor noise, although in the case of the AUV sensor noise is not expected to be a problem. It was therefore decided to design the controllers using only the slew limit approximation given in **(4.7)** as a guide.

4.4 Chapter summary

The model analysis revealed that the AUV is statically stable in every aspect of its motion and that these motions are well decoupled. Controllers for the AUV should therefore be simple to design. The analysis suggests that angular rate feedback control loops should be used for the fundamental control of the AUV. The roll motion of the AUV, which currently is not controlled, is very poorly damped and should be regulated to increase the reliability of the AUV's movement. It is also important that the control surface slew rate limit be taken into account when designing the AUV control systems, to avoid instability and other ill effects that could be caused by encountering the slew rate limit. This is taken into account by keeping all control designs below a certain bandwidth, which should avoid commanding the control surfaces to exceed their slew rate limits.

Chapter 5

Analysis of IMT Control and Guidance

The current controller on board the AUV employs a very simple control and guidance strategy. Only two feedback loops are used for stability control. One loop feeds back the current pitch angle of the AUV, through a proportional controller, to elevator position. The second loop feeds back the current AUV heading, also through a proportional controller, to rudder position. No roll control is currently implemented. Guidance is handled in a similar manner, as follows. The path of the AUV is designated by a set of waypoints, described only as position coordinates. In essence, the AUV travels towards each waypoint until it comes within some threshold distance of the target waypoint. Once it reaches the target waypoint, it changes targets to the next waypoint. The travel trajectory is based on depth and heading. A pitch reference for the AUV is generated based on the depth error between the AUV's current location and the reference depth of the target waypoint. The heading reference for the AUV is set as the direct path from its current position to the waypoint. These two aspects of the AUV's motion are essentially decoupled as the longitudinal and lateral control loops respectively. The respective linearised feedback structures used for the control and guidance are shown in **Figure** 5.1 and **Figure** 5.2. The general symbols used in block diagrams are shown in **Table** 5.1.

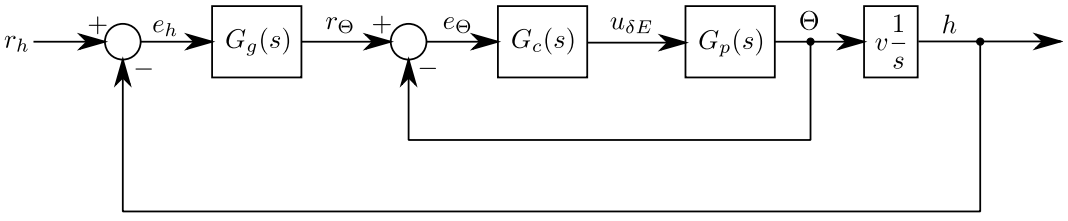

Figure 5.1: Feedback structure of IMT's longitudinal controller

Table 5.1: Block diagram symbols

symbol	description
subscript g	Relates to *guidance*
subscript c	Relates to *controllers*
subscript p	Relates to *plants*
G_x	A general transfer function
r_x	Reference signal for variable x
e_x	Error signal for variable x
u_x	Input to a specific actuator x

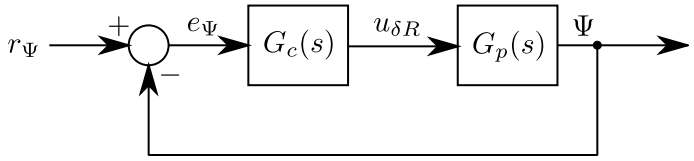

Figure 5.2: Feedback structure of IMT's lateral controller

5.1 Controller analysis

All controllers are based on attitude angle measurements and fin commands in degrees. The controllers on the AUV are currently operated with a measurement sample frequency of 3Hz. The effects of this will be examined in each loop. Although the controllers are only proportional controllers, so there is no emulation error when converting the controllers from continuous domain to digital domain, if the sampling rate is not high enough, it may fail to correctly sample all the dynamics of the AUV, which could easily lead to instability. The controller analyses are based on the existing linear model for the AUV.

Pitch control

For pitch control the AUV pitch angle, Θ, is fed back and subtracted from the pitch reference, r_Θ, supplied by the depth guidance controller. The proportional gain, K_Θ, has two different values, depending on whether the AUV is required to pitch up or down.

$$\begin{aligned} K_{\Theta\text{pitch up}} &= 4 \\ K_{\Theta\text{pitch down}} &= 3 \end{aligned}$$

This controller was analysed by using the higher of the two gains. **Figure 5.3** shows the root locus plot of the inner loop of the longitudinal controller. It is stable, but the dominant poles are poorly damped. The frequency of the closed-loop poles is

also within that of the theoretical slew limit pole. The slew limit is therefore not expected to cause instability, and has not been observed to have done so either.

The closed-loop system has good stability margins, with a 55° phase margin at the gain crossover frequency and theoretically infinite gain margin, as seen on the inverse Nichols chart in **Figure 5.4**. The approximate effect of the digital sampling, according to [15], is also plotted in **Figure 5.4**. This introduces high frequency phase lag, which lowers the stability margins of the system. The gain margin is still large, however, at 20dB, so this is not likely to be a problem.

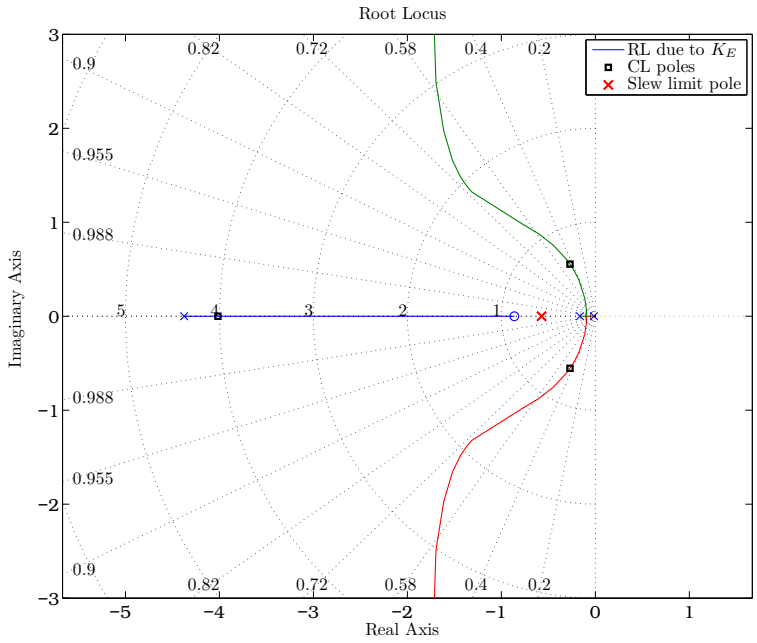

Figure 5.3: Root locus plot of IMT's pitch angle controller

Yaw control

This controller is similar in design to the pitch controller in that it feeds back an attitude angle to a proportional controller. The gain for this controller is fixed at $K_\Psi = 0.5$. This results in the root locus shown in **Figure 5.5**, which has stable poles. The dominant low frequency pole is slower than the slew limit pole and not too close to the low frequency zero either. This controller should therefore not command the rudders beyond the slew limit. The root locus plot suggests that the poles cannot really be placed much better than they already are using only a proportional controller. The digital sampling effect can be seen in **Figure 5.6**. This loop is slightly less robust than the pitch loop, but is still far away from the point of instability. Raising the gain of the controller much more would not be

advisable, since this would further reduce the system gain margins and make it more susceptible to instability if the slew limit were to be encountered.

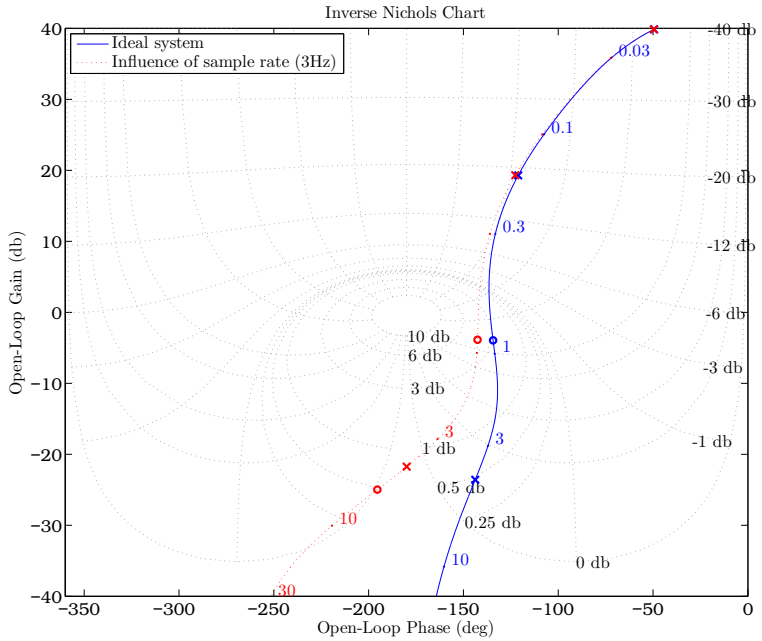

Figure 5.4: Inverse Nichols chart plot of IMT's pitch angle controller

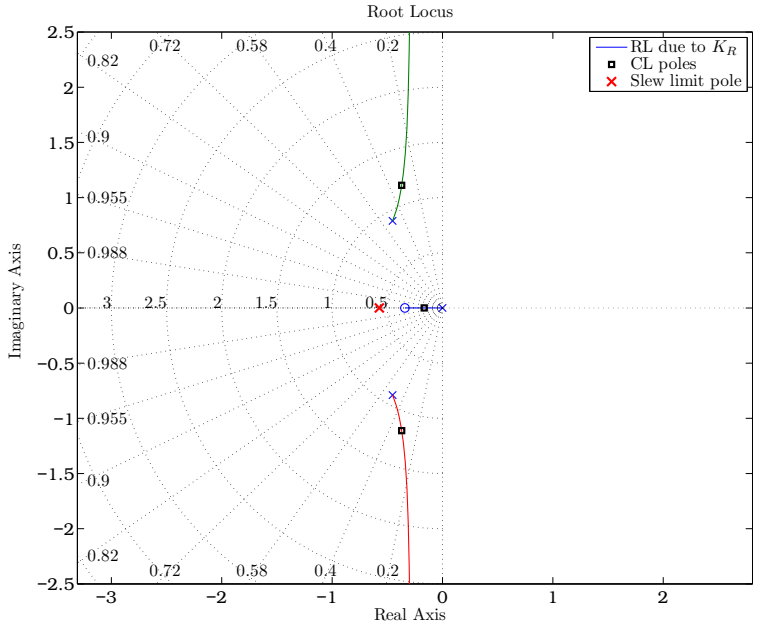

Figure 5.5: Root locus plot of IMT's heading angle controller

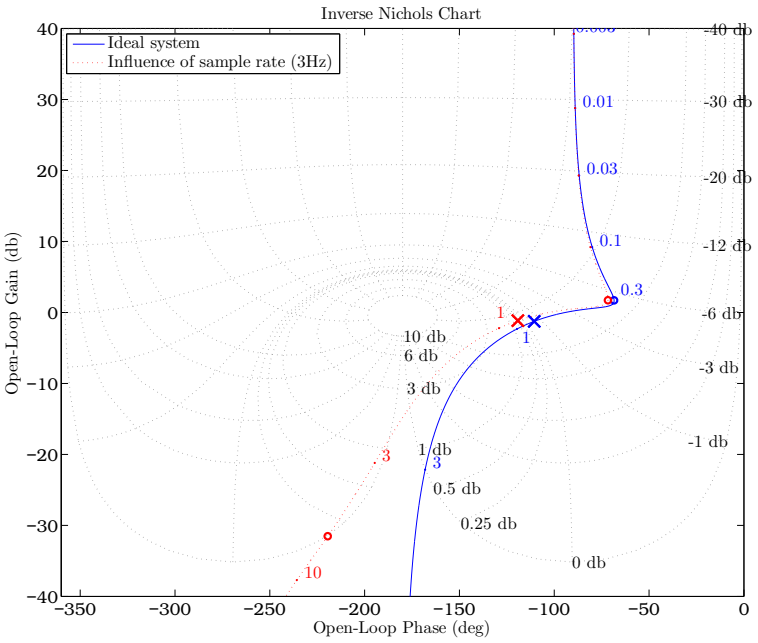

Figure 5.6: Inverse Nichols chart plot of IMT's heading angle controller

Controller conclusions

The main weakness of these controller designs is their susceptibility to offset errors. These offset errors may come in the form of trim condition offsets, physical imbalances in the AUV, disturbances, calibration errors and measurement errors. These errors could manifest in steady state tracking errors of several metres if they accumulate. Adding integral control would make the controllers much more robust to these sorts of offsets. It will be shown at the end of **Chapter 6** that the new controller designs have gains similar to the existing controllers with added integral control and a different feedback structure. They are, however, not that much more complicated than these designs.

5.2 Guidance analysis

Depth guidance

The depth guidance is performed by supplying a reference pitch for the controller which is proportional to the depth error between the AUV's current position and the set reference depth of the target waypoint by a gain, $K_h = 1.8$. This gain relates height in metres to a reference pitch angle in degrees, which is limited to ±30°. The guidance dynamics can be derived as follows. When the AUV depth is close enough to the reference depth such that the height controller is operating in its

linear region, the pitch reference is given by **(5.1)**, where r_Θ is the pitch reference and h is the depth error. If the AUV is assumed to be travelling at a constant speed, v, then from geometry the change in depth error is given by **(5.2)**. Assuming that the AUV follows the desired pitch reference with reasonable accuracy, **(5.1)** can be substituted into **(5.2)** to give **(5.3)**. Since these equations are valid only when $\Theta \approx r_\Theta \leq 30°$, **(5.3)** can be simplified using the small angle approximation for sin, resulting in **(5.4)**, which leads to an expression for the time domain response of the AUV depth error in **(5.5)**.

$$r_\Theta = K_h h \tag{5.1}$$
$$\frac{dh}{dt} = -v\sin(\Theta) \tag{5.2}$$
$$\frac{dh}{dt} = -v\sin(K_h h) \tag{5.3}$$
$$\frac{dh}{dt} \approx -vK_h h \tag{5.4}$$
$$h = e^{-vK_h t} \tag{5.5}$$

The guidance dynamics therefore have the same response as the system, $\frac{1}{s/(vK_h)+1}$. Substituting in (and remembering to convert the gain to relate metres to radians), gives the pole location at about -0.04. This can be used to gauge the overall closed-loop performance of the system and how the guidance and plant dynamics interact. This guidance pole is so slow, when compared to the closed inner loop poles, that it hardly changes the other system dynamics. In light of this, the feedback gain could be increased drastically to improve system performance before it would interact with the inner-loop dynamics. Obviously, if the AUV is far away from the desired depth it will converge to that depth at $\frac{1}{2}v$ m.s^{-1} with a constant pitch angle of $\pm 30°$. In a similar way, the distance dynamics of the AUV can be derived, with the time response given in **(5.6)**, where L is the horizontal distance travelled between waypoints. The depth error of the AUV therefore halves every $\frac{ln2}{K_h}$ metres travelled in the forward direction between two waypoints.

$$h = e^{-K_h L} \tag{5.6}$$

Although this guidance law seems reasonable, it too has no integral action. It is therefore expected that there will be errors in the AUV's steady state travel path. To highlight this problem, a constant current disturbance of 0.2m.s^{-1}, flowing upwards, was simulated to display the poor performance characteristics of the guidance algorithm. The steady state offset in travel depth can be easily calculated by finding the component of the nominal AUV velocity needed to compensate for the ocean current. This angle is given by **(5.7)**. Here, V_C is the current velocity in the up or down direction (current flow components in any other direction are

irrelevant to this controller). This can be substituted into **(5.1)** to give **(5.8)**. Using the small angle approximation for $\sin^{-1}$ results in **(5.9)**. Substituting in for all the constants reveals that the height offset is approximately proportional to the current by a factor of 24, which gives a significant offset error, even for small currents.

$$r_\Theta = \sin^{-1}\left(\frac{V_C}{\bar{V}}\right) \tag{5.7}$$

$$h = \sin^{-1}\left(\frac{V_C}{\bar{V}}\right)\frac{180}{\pi K_h} \tag{5.8}$$

$$h \approx \frac{180 V_C}{\bar{V}\pi K_h} \tag{5.9}$$

Sea currents with some component in the vertical direction are unlikely; however, the same results could be caused by the offset errors mentioned previously in the controller analysis. Because the guidance is essentially just a proportional controller, the constant current causes a constant offset in the AUV's position. This will always be the case with guidance algorithms based on proportional feedback of the current tracking error. Intuitively, this can be fixed by including an integrator in the guidance law, which should offset steady state errors. A good point about this guidance algorithm is that there is no *strange* behaviour as the AUV nears the target waypoint, as will be seen with the lateral guidance. This, however, also has the problem that the offset is maintained, even close to waypoints, so the AUV may miss waypoints altogether unless this is handled in some way.

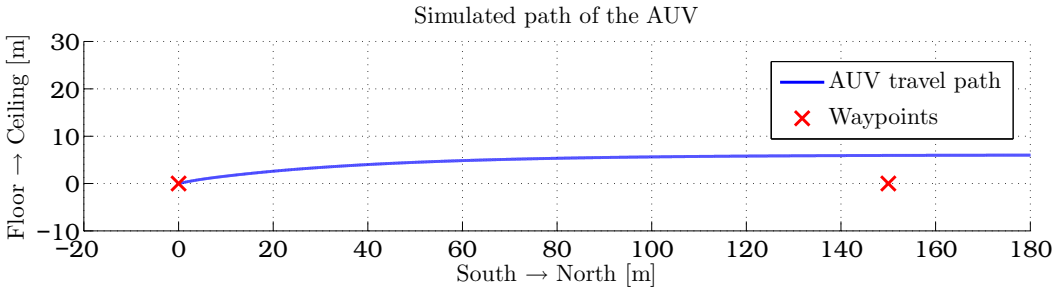

Figure 5.7: IMT longitudinal guidance performance under the influence of a vertical current of 0.2m.s^{-1}

Heading guidance

When evaluating the heading guidance it was assumed that the various waypoints are far enough apart such that as the AUV yaws to align its heading with the target waypoint, the relative heading from the AUV to the waypoint does not change very much. This assumption becomes more valid as the error between the current and desired headings decreases. The heading guidance can therefore be modelled as

a constant heading reference to the yaw control loop, which introduces no extra dynamics into the system under these assumptions. This assumption is, however, not always valid, especially as the AUV nears the target waypoint at an angle. If it is not heading directly towards the waypoint, the heading reference will be changing and the AUV may not be able to follow the reference. In the worst case, the AUV will end up circling the waypoint indefinitely. This would most likely be the case when waypoints are close together or some disturbance is acting on the AUV. This problem is demonstrated in **Figure 5.8**. A constant cross-current in the water flowing at 0.2m.s^{-1} was simulated, with the AUV attempting to travel directly to a waypoint straight ahead of it. Because of the distant aiming point, the AUV is seen to drift out quite significantly and then cut back into the waypoint as it gets closer its target. The further away the waypoint is, the further out the AUV will drift. This behaviour is clearly undesirable, and requires a redesign of the current guidance method. A better approach would be to track to a designated path between waypoints and not simply aim towards the next waypoint.

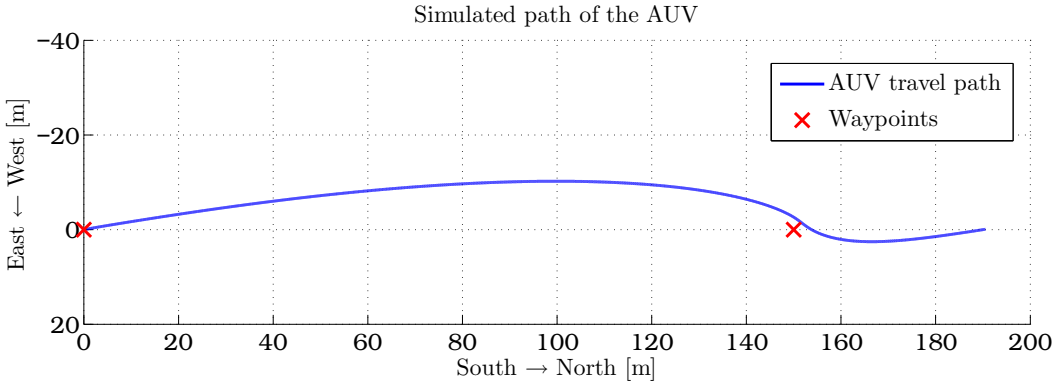

Figure 5.8: IMT lateral guidance performance under the influence of a cross-current of -0.2m.s^{-1}

5.3 Chapter summary

The current controllers and guidance methods on the AUV do not perform well. They are stable, but none of the loops has any integrators, which could result in very bad tracking under the effects of disturbances like ocean currents. The guidance of the AUV is completely oriented about the position of the waypoints only, though, so its ability to stay on-track between waypoints may not be of great concern. However, if reliable consistent AUV behaviour is to be commanded, then the guidance must be re-designed. The weakness of the current guidance methods in this regard has been highlighted. In fact, no matter how well the inner-loop

controllers perform, the poor performance of the system cannot be improved using these guidance methods. The only real advantage of these controllers is simplicity. The sampling frequency of the controllers could be increased, and may need to be in order to improve the system performance, but it does not have an impact on the existing control implementation. New control and guidance designs will focus on improving the steady state tracking ability of the AUV through the introduction of integrators into the control loops and a complete redesign of the AUV guidance.

Chapter 6

Controllers

The design of the complete control of the AUV is separated into two sections. The first section is covered in this chapter and deals with the control of the states of the AUV. The main aim of this section is to ensure that the AUV is stable and that various state references can be tracked. The next section of the control is called guidance. The guidance controllers, which are covered in **Chapter 7**, provide the state references for the controllers designed in this section, so that the AUV can track to waypoints and paths.

6.1 Design considerations

The current controller designs on the AUV show that simple controllers are sufficient to stabilise the AUV. However, analysis thus far suggests that using attitude angle feedback alone is not the best way to design these controllers. Before designing any controllers, various aspects of the AUV influencing the controllers must first be considered.

Sensors

The sensors on board the AUV are very accurate, and provide measurements for the full state vector. These measurements are obtained from an IMU which filters the sensor data and uses an estimator to generate the current measurement data regarding the AUV's position and orientation. This data cannot be improved unless more sensors are added and can therefore be used directly by the controllers. Since the full state vector is available, full state feedback is one possibility for controlling the AUV. However, full-state feedback can be difficult to tune and implement. If the AUV is changed or upgraded, this could present a problem for those maintaining it.

Mathematical model

The accuracy of the mathematical model is poor and not well quantified. Robustness is therefore a priority in the controller designs, which should also be easy to adjust. Complicated controller designs may not necessarily perform well in practice because of the uncertainty of the mathematical model. Theoretically, the motions of the AUV are well decoupled, as was shown in **Chapter 4**. Cascaded SISO feedback loop control design should therefore be a good design approach, since it facilitates easy, intuitive controller design and tuning. The controllers can be designed and adjusted loop by loop, affecting relatively few states in any particular design or tuning stage. This design approach is known as successive loop closure (SLC), in which feedback loops can be designed and tested sequentially, without having to implement the entire system to test each controller.

Hardware constraints

The AUV controller code runs on a Pentium I based computer using the Microsoft Windows 98 operating system. Some basic hardware monitoring was done while the AUV was operating, the results of which indicated that only 10% of CPU's total capacity was being utilised. Implementing more complicated controllers than the current setup should therefore not be a problem. However, the design of controllers should still aim to be computationally efficient, to avoid having to redesign controllers due to CPU performance saturation. Microsoft Windows 98 is not a realtime operating system so it would be safest to keep the calculation load well within the capabilities of the hardware.

Digitisation

The final bandwidth of the closed-loop system is limited by the effects of the control surface slew rates. This limit is at 0.57 rad.s^{-1}, but can safely be extended if necessary. It would be desirable to design controllers in the continuous domain and then simply use Euler transformations to convert the designed controllers to the digital domain. If a minimum sampling frequency 20 times faster than the bandwidth of the closed- and open-loop systems is required for an acceptable system response after conversion into the digital domain [16, p108], then the minimum sampling frequency of the controllers needs to be above 2 Hz to cater for the bandwidth of the slew limit. None of the open-loop systems has a higher bandwidth than the slew limit, so for now it can be assumed that this sampling frequency will suffice. A sample rate of 2 Hz is rather slow, however, and it is expected that the hardware on board the AUV is able to operate at higher sampling frequencies. All controller designs will be carried out in the continuous domain and later converted to digital

domain using the first-order Euler transform at a suitable sampling frequency. The effects of this will be analysed in the designs.

Speed control

No speed control is currently implemented on the AUV. The thrusters are always operated at full throttle because the thrust on the AUV is limited and the AUV needs to maintain its full speed so that the control fins remain effective. No speed controller is designed in this thesis either, since this aspect of the AUV is not considered to be crucial. As was shown in **Section 4.2**, the response of the system to thrust changes is like that of a simple first-order low-pass SISO system. Should the need arise, a speed controller could be easily designed. The thrusters also couple into the yaw effectiveness of the rudders on the AUV, so keeping the thrusters at a constant value reduces uncertainty in this aspect of the AUV. The data in **Section 2** shows that during normal operation the speed of the AUV is reasonably constant and does not necessitate a controller.

Rate control

As discussed in **Chapter 4**, angular rate feedback is recommended above attitude angle feedback for damping the natural responses of the AUV, especially on the lateral controllers. Once the natural response of the AUV is damped, then the attitude angles can be controlled. Angular rates are more representative of the fundamental dynamics of the AUV than are attitude angles, since the moments on the AUV are only integrated once to give the angular rates. Angular rates are also measured relative to the AUV body axis, whereas attitude angles are measured relative to the inertial axis system and linearised for the model. Disturbances can therefore be more effectively rejected by using rate control, without having to increase controller complexity. Better stability margins can often be attained by using SLC to first control angular rates, followed by attitude angles. When controlling attitude angles directly, the controller often needs to include forms of derivative action to achieve good stability margins. One of the new guidance methods which was developed for the AUV provides only angular rate references and is independent of the AUV's attitude angles. For this guidance method, then, attitude angle controllers are not necessary and rate controllers are imperative.

6.2 SLC controller design

The three attitude angles of the AUV will be controlled separately, since they are mostly decoupled, so the closed-loop controllers are not expected to influence each

other much. No specifications have been given for the design. The primary design focus will therefore be on system robustness. Performance of the AUV is limited by its slow translational speed and poor control surface effectiveness, so the controllers will be designed to be as fast as possible without exceeding the actuator limits. The design of all controllers was carried out initially on a root locus plot. Inverse Nichols charts were used to fine-tune the controllers and evaluate the stability margins of the final design. Although not necessary for stabilisation, integrators were used in all the controllers to remove as much plant uncertainty as possible at low frequency for outer control loops that close around the rate controllers. This makes outer-loop design simpler and is necessary for good tracking performance, especially when the inner loops are interfaced with directly by the guidance. To aid in the design process, double root locus plots were generated, which show how the plant poles are expected to move not only with proportional gain changes, but also with integrator gain changes. All controllers using integrators were designed using the standard PI controller form shown in **(6.1)**. Here, K_p is the proportional gain for the controller and K_i is the integrator gain. This controller places an open-loop pole at the origin of the complex plane, and a zero on the real axis at $-K_i$

$$G_{PI}(s) = K_p\left(1 + \frac{Ki}{s}\right) \tag{6.1}$$

Rate control loops

Pitch rate control

Both the elevator and common mode front fin control inputs can be used to control the AUV pitch. Since the control effectiveness of the AUV fins is limited, it would be beneficial to make use of all the available control actuation. To create a SISO feedback loop, a new control input, δp, must be defined, which is some linear combination of the elevator and front fin inputs. The simplest way to mix the two input signals into one would be either to add or to subtract them. The relevant minor of the standard control matrix, $\mathbf{B}_{\text{long}}$, is shown below in **(6.2)** along with the minor input matrix of $\mathbf{u}_{\text{long}}$, originally defined in **(3.86)**. The two simple mixing schemes are shown in **(6.3)** and **(6.4)** respectively. Since pitch rate is the measurement used in feedback, the best mixing scheme should give the most control over pitch rate and preferably little influence over the other states. Considering only the magnitudes of the control influences on the AUV states, it is clear that commanding the front fins and elevator together, instead of in opposition to each other, is better for the purposes of pitch control. More complicated mixing can be used; however, it was shown that the elevator is far more effective at controlling the AUV pitch than are the front fins. Scaling the relative inputs to the front fins and elevator is therefore not likely to improve the performance of the controller much without saturating one

set of actuators, which increases the non-linearity of the system. One such mixing scheme is shown in **(6.5)**, where the mixing is chosen such that there is no influence on the AUV angle of attack. However, the change in the control vector is rather small but the front fins would be caused to saturate when the elevator reaches 70% of its full-scale deflection. The elevator and front fins will therefore be operated in unison. This results in the new matrices shown in **(6.6)** and **(6.7)** replacing those of the original system for this controller design.

$$\begin{bmatrix}\dot{\alpha}\\ \dot{q}\end{bmatrix} = \begin{bmatrix}0.000556 & -0.000794\\ -0.00054 & -0.00767\end{bmatrix}\begin{bmatrix}\delta a_c\\ \delta e\end{bmatrix} \tag{6.2}$$

$$\begin{bmatrix}\dot{\alpha}\\ \dot{q}\end{bmatrix} = \begin{bmatrix}-0.00024\\ -0.00821\end{bmatrix}\begin{bmatrix}\delta p\end{bmatrix} \qquad \begin{cases}\delta a_c = \delta p\\ \delta e = \delta p\end{cases} \tag{6.3}$$

$$\begin{bmatrix}\dot{\alpha}\\ \dot{q}\end{bmatrix} = \begin{bmatrix}-0.00135\\ -0.00713\end{bmatrix}\begin{bmatrix}\delta p\end{bmatrix} \qquad \begin{cases}\delta_{a_c} = -\delta p\\ \delta_e = \delta p\end{cases} \tag{6.4}$$

$$\begin{bmatrix}\dot{\alpha}\\ \dot{q}\end{bmatrix} = \begin{bmatrix}0\\ -0.00845\end{bmatrix}\begin{bmatrix}\delta p\end{bmatrix} \qquad \begin{cases}\delta_{a_c} = 1.428 * \delta p\\ \delta_e = \delta p\end{cases} \tag{6.5}$$

$$\mathbf{B}_{\text{long}} = \begin{bmatrix}0.3 & 0\\ 0 & -0.00024\\ 0 & -0.00821\end{bmatrix} \tag{6.6}$$

$$\mathbf{u}_{\text{long}} = \begin{bmatrix}\delta t_c\\ \delta p\end{bmatrix} \tag{6.7}$$

The open-loop plant transfer function has a zero at the origin. This zero is a result of the buoyancy-induced restoring moments on the AUV. It may seem counterintuitive to add an integrator to the controller, therefore, since no steady state tracking of a constant pitch rate is possible with a constant fin deflection. Adding an integrator creates a hidden mode in the system, which results in the controller output signal running away to infinity if a constant pitch rate is commanded. However, a sustained constant pitch rate will not be commanded, since this would result in the AUV performing loops. The AUV's ability to track steady state pitch angle commands is important, though. By placing the integrator in this control loop, the design constraints on outer control loops or guidance loops are relaxed. If a zero pitch rate command is given to the pitch rate controller it can now maintain a constant fin angle, which would be required to maintain a specific pitch angle in steady state. This integrator could be placed in an attitude angle control loop to achieve the same effect; however, this is not possible if the guidance interfaces directly with these inner loops, as is the case with the guidance designs in the following chapter. The open-loop plant also has a very low frequency pole at -0.005 rad.s^{-1} on the real axis, which results in good steady state tracking if the zero at the origin is in fact cancelled. The effects of the buoyancy-induced zero at the origin are more evident in the roll control loop discussed later.

A pitch rate controller was thus designed where the pitch rate was fed back to the controller input, which outputs the same command signals to both the elevator and common mode front fin inputs. The controller has the form of a PI controller, shown in **(6.1)**, with the values for the controller gains shown in **(6.8)**. The controller proportional gain for this controller may seem quite high. This is, however, due to the fact that the states are measured in SI units, whereas the control surface deflections are measured in degrees. The same is true of the other inner-loop controller designs following this.

The final design is shown on a root locus plot in **Figure 6.1** with the final plant poles placed close to the same frequency as that of the theoretical slew pole. The closed-loop system bandwidth is slightly higher than the theoretical slew limit, but no instability relating to slew limiting has been observed in simulation. The plant zero near the same frequency makes it difficult to reduce the closed-loop bandwidth without significantly hampering the performance of the controlled plant with either a slow response or too much overshoot.

The theoretical time response of the AUV to a 0.1 rad.s^{-1} pitch rate command is shown in **Figure 6.2**. This is clearly a demanding reference to follow, since initially the control fins are commanded to exceed their limits by 40%. However, this limit should result in the AUV pitch rate increasing at a constant rate towards the reference, which should not pose a threat to the AUV's stability in the short term. This may cause instability if the AUV is required to reject ongoing pitch rate disturbances of such magnitude, but this would suggest that the AUV is operating in conditions that are outside its performance limits. The plot also shows that the slew limit is exceeded only for a short time, which suggests that this non-linearity has been sufficiently dealt with in this design.

The inverse Nichols chart shown in **Figure 6.3** was used to gauge the system's stability margins. The continuous time system design has an infinite gain margin and a good phase margin of about 80°. However, the approximate effects of digitising the controller, according to [15], at a sampling frequency of 2Hz are quite pronounced and bring the system much closer to the Nyquist point. This is in fact dangerously close when one considers that most physical systems have delay inherent in them, which produces phase lag. This, added to the lag that will occur if the actuator slew limit is encountered and other plant uncertainty, could quite easily cause the system to become unstable. Although it was not observed in this loop in simulation, the roll control loop became unstable when the sampling rate was as low as 2Hz. The effects of sampling at 10Hz are also shown in **Figure 6.3**, where the robust stability margins are still very good. This high a sample rate may not be necessary in this loop, but would be preferred if the AUV can reliably operate at that sample rate.

$$\begin{aligned} K_{p_Q} &= -200 \\ K_{i_Q} &= 3 \end{aligned} \tag{6.8}$$

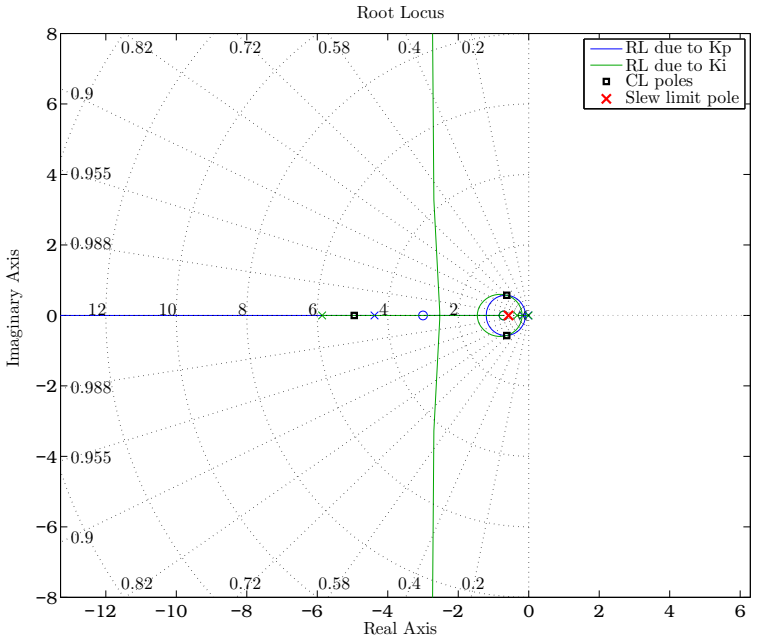

Figure 6.1: Root locus plot of pitch rate controller

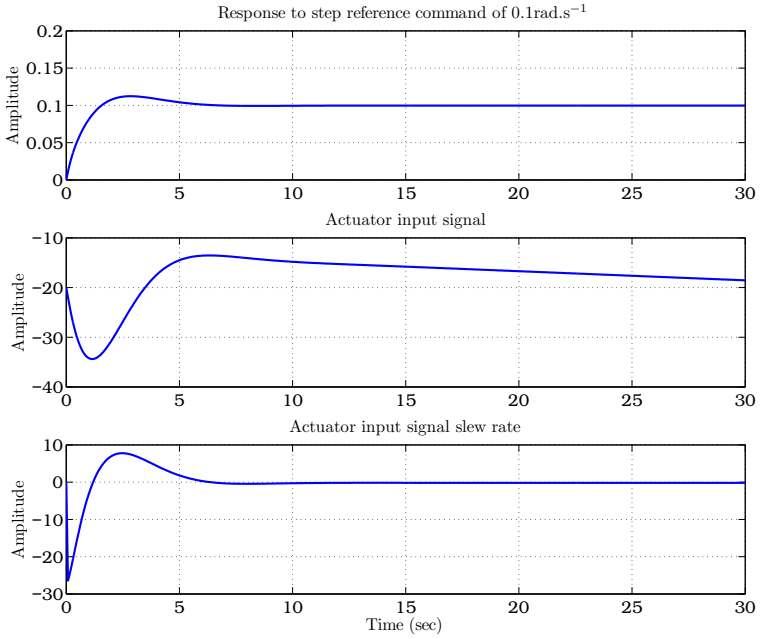

Figure 6.2: Step responses for pitch rate controller

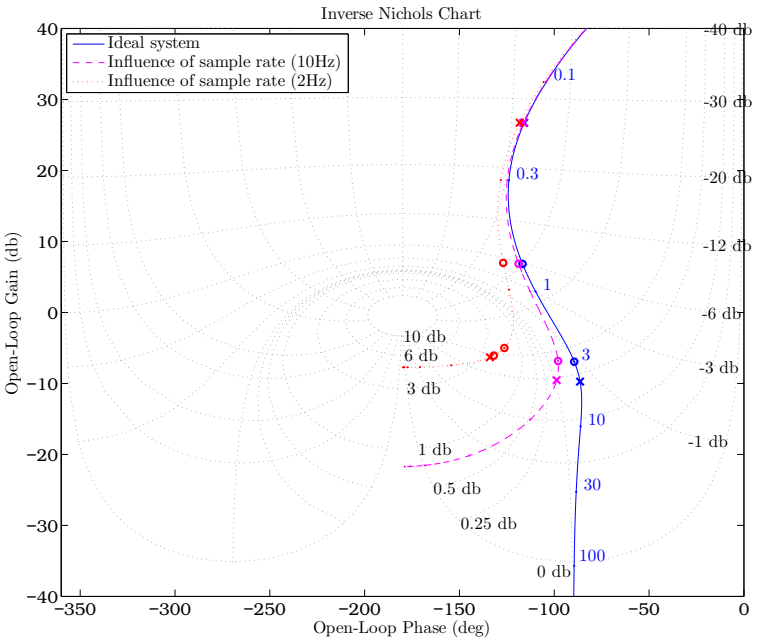

Figure 6.3: Inverse Nichols chart plot for pitch rate controller

Yaw rate control

Similar to the pitch control problem above, there are two control inputs that can be used to control the yaw of the AUV: the rudder fins and differential thrusting. As stated in **Section 4.2**, both control inputs are equally capable of controlling the yaw of the AUV. Individually, therefore, each control input at full deflection should result in practically the same AUV yaw rate. However, the differential thrust couples into the rudder effectiveness, which is multiplied by the square of the thruster outlet velocity, which is assumed to vary linearly with the thruster input signal. The nominal point for which the rudders were modelled was with full thrust on both thrusters. This is usually the level at which they are operated, to achieve maximum movement speed for the AUV. If the thrusters were used differentially, one of the thruster outlet velocities would decrease, reducing the effectiveness of the rudder in that thruster's flow. Assuming that the thrusters are at their full differential limit, that is one has full forward thrust and the other has full reverse thrust, the effects of one rudder would now be reversed, cancelling the effects of the other. It seems therefore, that no more control could be gained by using differential thrusting in conjunction with the rudders. Since differential thrusting would hamper the forward speed of the AUV it is recommended that it be ignored altogether. The only way this might be effective is if the rudders were able to be controlled individually so that each could be adjusted with the change in thruster outlet velocity. The AUV would first require better thrusters, however, so that the thrusters could be operated differentially while still being able to control

forward velocity. One advantage of the differential thrusting over the rudders is that it is a more absolute method of control, unlike the rudders which are dependent the velocity of the fluid flowing over them. But because of the reasons mentioned above, differential thrusting will be ignored for this design.

As with the pitch control loop, a PI controller was used to control the AUV yaw, with the gain values given below in **(6.9)**. The controller design is shown on the root locus plot in **Figure 6.4**. There is a real plant zero at -0.341, which makes choice of gains for this controller difficult. The zero limits the bandwidth of the dominant pole, but as the controller gain is increased, the effects of that pole are cancelled by the zero, which makes the faster complex poles more dominant in the system. These poles are beyond the desired bandwidth for keeping the fin's slew rate within specification. The zero of the controller cannot be placed too close to the low frequency pole either, and placing it at a higher frequency reduces the damping of the complex poles.

The final system for this loop is quite similar to that of the pitch control loop. The same conclusions can therefore be drawn about this loop design. The step responses shown in **Figure 6.5** suggest that the slew limit has been adequately dealt with. The inverse Nichols chart in **Figure 6.6** indicates again that the stability margins of the system are very good, but they start to diminish quickly under the effect of the digital sampling frequency of 2Hz.

$$\begin{aligned} K_{p_R} &= -80 \\ K_{i_R} &= 1 \end{aligned} \tag{6.9}$$

Roll rate control

Roll control is not implemented at all in the current control system of the AUV. This suggests that it may not be necessary and is well constrained by the buoyancy of the AUV. As seen in **Section 2**, the AUV roll is better damped than the model predicts. A roll controller will still be designed, as it will be useful in final recommended control implementation and will improve the robustness and predictability of the AUV's performance. The control input for this design is limited to the differential front fin deflection as no other actuators are capable of controlling the roll of the AUV. The model analysis in **Section 4.2**, with reference to **Figure 4.5** and **Figure 4.6**, showed that the AUV roll couples into its yaw, although the coupling is an order of magnitude lower than the effects on the AUV roll. Because the roll control of the AUV does not play a significant part in the AUV's performance, but is more for stability and to reduce coupling between the lateral and longitudinal motions of the AUV, the controller was designed such that the system was well damped.

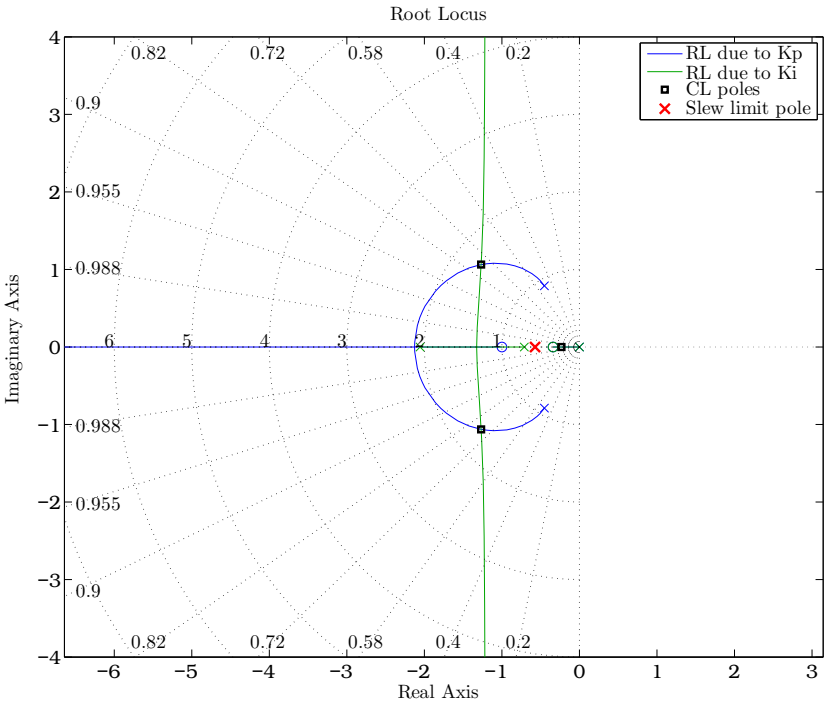

Figure 6.4: Root locus plot of yaw rate controller

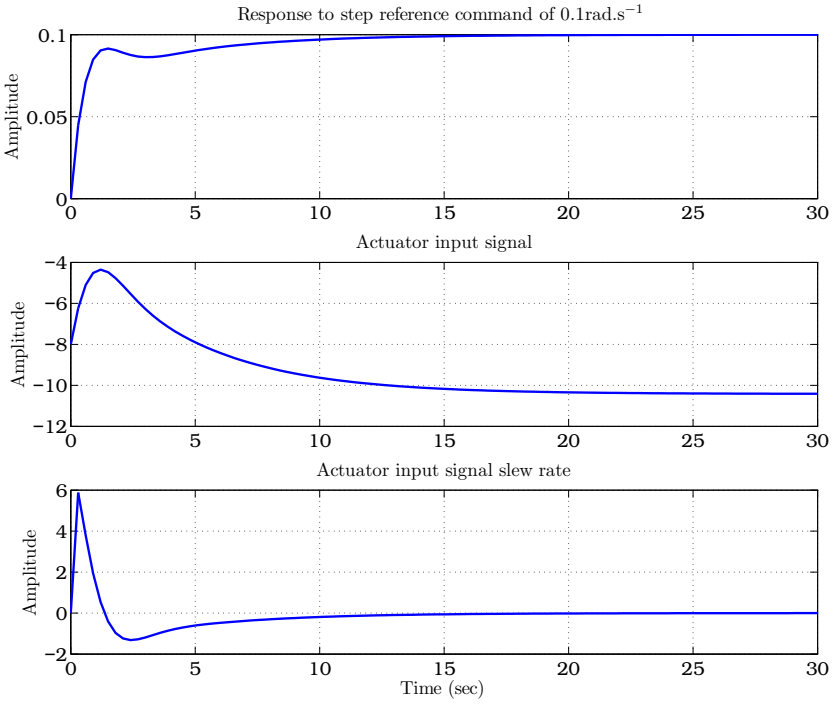

Figure 6.5: Step responses for yaw rate controller

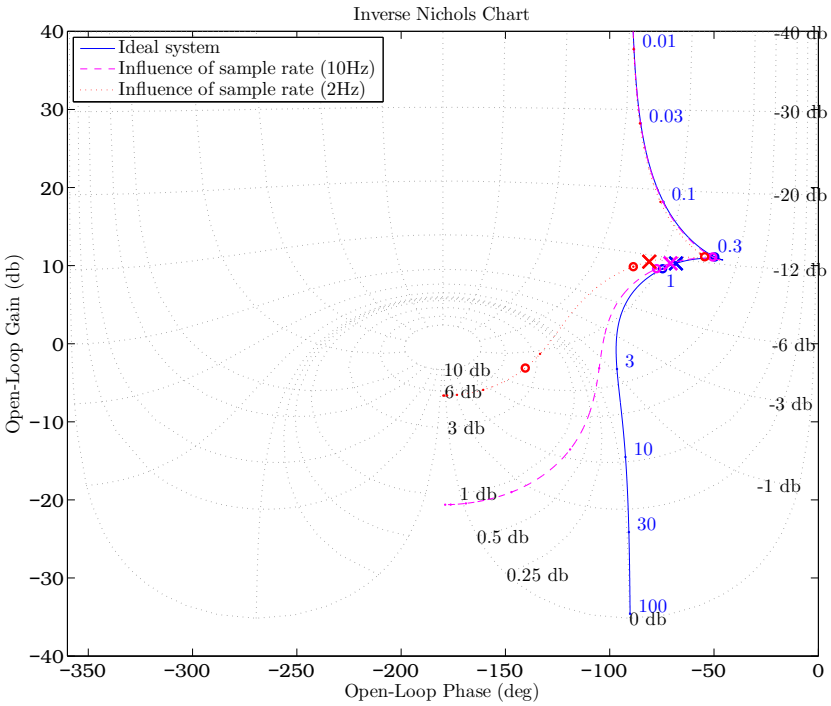

Figure 6.6: Inverse Nichols chart plot for yaw rate controller

Both of the complex conjugate poles associated with the roll rate of the AUV were placed on the real axis.

As with the pitch rate loop, there is a zero at the origin of the open-loop transfer function due to the buoyancy-related restoring moments created on the AUV. An integrator was also used in this controller, with reasoning similar to that of the pitch control loop. The closed-loop poles can be placed in similar positions without using an integrator; however, there are a number of advantages to using an integrator in this controller. Doing so effectively allows the zero at the origin to be moved anywhere along the real axis, since the controller places a new zero. This allows for more control over where the final closed-loop poles end up and effectively moves the zero, which helps ease the constraints on the outer loops. The danger of placing an integrator pole on the zero at the origin is that the control signals run away and wind up when steady state commands are given, and this is evident in the step response plot in **Figure 6.8**. However, constant roll rates will not be commanded for extended periods of time, since a constantly rolling AUV has no real practical purpose. Rolling the AUV to a specific angle will be required. To hold a specific roll angle, a constant fin offset and zero roll rate will be needed. With the integrator, this controller can command a constant fin deflection with zero input.

The results of the final controller design, with gains shown in **(6.10)**, are plotted on the root locus in **Figure 6.7** and inverse Nichols chart in **Figure 6.9**. As with the

other loop design thus far, the inverse Nichols chart shows that the sampling rate of 2Hz may cause stability problems with large plant uncertainty. A final point to note about this loop is that the plant and slew limit have very similar bandwidths, which suggests these actuators may not be adequate for achieving good performance with the AUV in terms of roll control.

$$\begin{aligned} K_{p_p} &= -60 \\ K_{i_p} &= 0.25 \end{aligned} \tag{6.10}$$

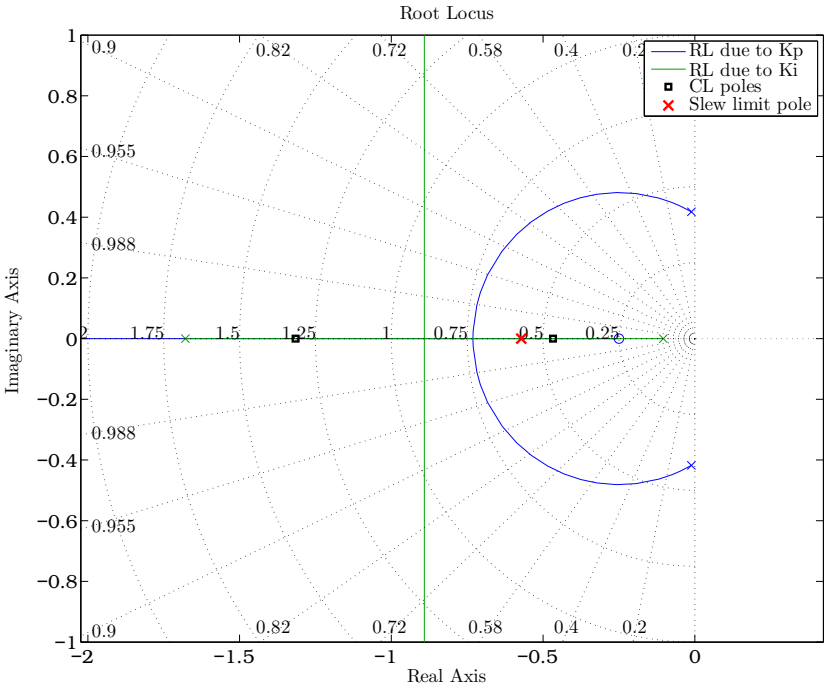

Figure 6.7: Root locus plot of roll rate controller

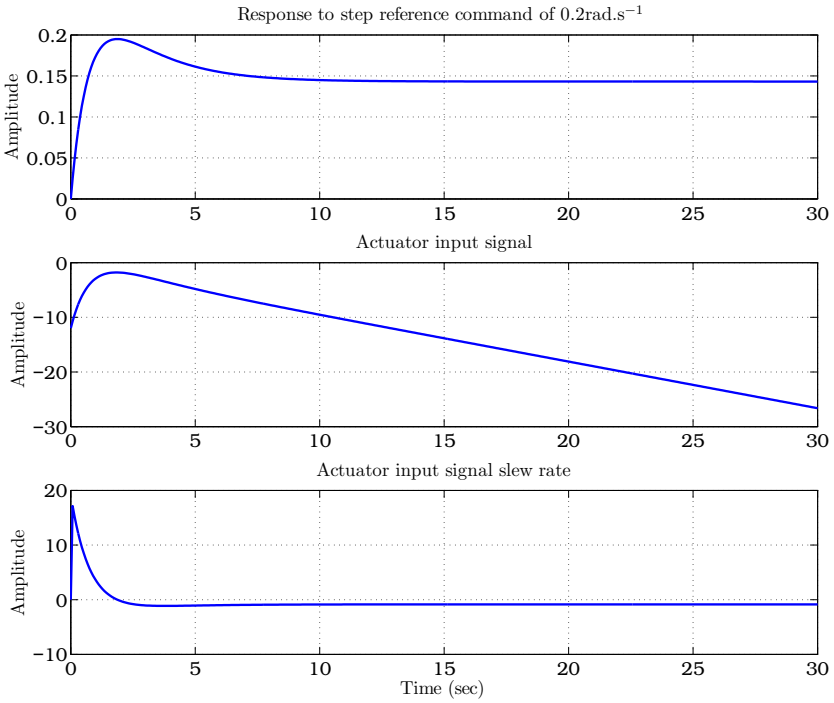

Figure 6.8: Step responses for roll rate controller

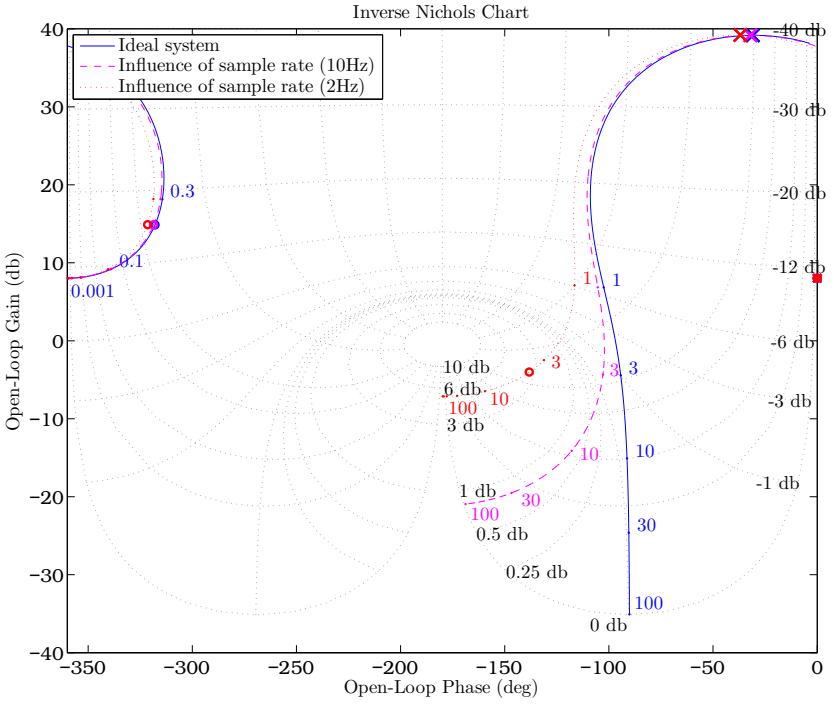

Figure 6.9: Inverse Nichols chart plot for roll rate controller

Outer loops

Attitude angle loops now need to be closed around the rate control loops that have been designed. For the most part, designing the outer-loop controllers is very straight forward. The closed-loop poles of the previous loops designs now become the open-loop poles of the outer-loop designs. The same tools and methods were used to design the outer loops as were used to design the inner loops. Because of the inner-loop designs, all the outer-loop designs used simple proportional feedback. Step response results show that this is all that is required for steady state tracking. The individual designs are not discussed, but the final feedback gains for each loop are shown below. Plots relating to these loop designs are shown in **Appendix C**.

$$\begin{aligned} \text{pitch angle feedback:} \quad & K_{p_\Theta} = 0.5 \\ \text{yaw angle feedback:} \quad & K_{p_\Psi} = 1 \\ \text{roll angle feedback:} \quad & K_{p_\Phi} = 0.5 \end{aligned}$$

These results can be compared with the IMT feedback gains. The plant transfer functions for the inner-loop controller designs have low gains, therefore the control gain from angle reference through to actuator position is given simply by the product of the inner and outer-loop gains. The integrators are ignored for this comparison since their effect at the plant bandwidth is negligible. To compare these results to the IMT-designed gains, the IMT gains must be scaled to use the same measurement units (radians) as these designs. The scaled IMT gains are given in **(6.11)** and **(6.13)**, followed respectively by the equivalent gains of this controller design in **(6.12)** and **(6.14)**. Although the IMT designs will have less gain at low frequency because they lack integrators, the high frequency gains are reasonably close to those of these designs, which suggests these controller designs will work in practice. In the pitch loop the IMT gains are 2.3 times higher and in the yaw loop they are 4 times lower; these are still within a single order of magnitude of the new designs.

$$K_{\Theta_{IMT}} = -229.2 \tag{6.11}$$
$$K_\Theta = -100 \tag{6.12}$$
$$K_{\Psi_{IMT}} = -28.6 \tag{6.13}$$
$$K_\Psi = -111.5 \tag{6.14}$$

6.3 COM controller strategy

Due to the ineffectiveness of the fin control surfaces, as well as the dependence on fluid flow over the control surfaces, an alternative theoretical control strategy is

proposed in this section. This controller strategy is based on displacing the centre of mass (COM) of the AUV relative to its centre of buoyancy (COB). Physically, the COB is fixed and based on geometry of the AUV; therefore the COM needs to be moved, relative to the AUV's geometry. This control strategy is being investigated, since it provides a means of absolute control over the pitch and roll moments imposed on the AUV. That is, the control effectiveness is not dependent on the fluid flow around the AUV and is relative to the NED axis system. The feasibility of such a control strategy will be assessed at the end of this section. This method of control can also be used in conjunction with the current control systems. The implementation of a combined control architecture is discussed following the analysis of the COB-based controller on its own.

It is important that a shift of the COM does not change other dynamics of the AUV too much. Although that is another avenue that could be explored for controlling the AUV, it is not desirable for this controller strategy analysis. Ideally, the other dynamics of the AUV need to remain constant as the COM is shifted around, with changes occurring only to the restoring moments being created by the buoyancy. Analysis thus far has shown that even small displacements, on the order of millimetres, of the COB relative to the COM generate considerable moments on the AUV. Thus, if the hydrodynamic coefficients can be shown to be practically invariant with small shifts in COM, then this control strategy may be feasible.

The rate damping dynamics of the AUV are not expected to change much with small displacements of the COM, since this is dependent mostly on the geometry of the AUV about the rotational axis. The dynamics of greatest concern are those that affect the AUV's static stability. Looking first at the AUV's longitudinal dynamics, the AUV has a centre of lift, at which the total lift force on the AUV will act. If this centre of lift is displaced from the COM, then the total lift force on the AUV will also generate moments on the AUV. Restricting this to pitching moments for now, the distance of the centre of lift from the COM would be given by **(6.15)**. During steady state travel, the lift force would be generated mostly by the AUV's angle of attack. The M_H and Z_H terms in **(6.15)** can therefore be replaced with M_α and $-L_\alpha$ respectively, which leads to an expression in terms of the non-dimensional hydrodynamic derivatives shown in **(6.16)**. In the same way, an expression for the distance of the centre of side force on the AUV can be obtained. The numerical answers for the centre of lift and centre of side force positions relative to the COM are given in **(6.17)** and **(6.18)** respectively. Although the centre of lift is in front of the COM and the centre of side force is behind the COM, both are significantly far from the COM such that displacing the COM by a few centimetres should not

noticeably change the AUV hydrodynamics.

$$l_\Theta = -\frac{M_H}{Z_H} \tag{6.15}$$

$$l_\Theta = l\frac{C_{M_\alpha}}{C_{L_\alpha}} \tag{6.16}$$

$$l_\Theta = 1.17 \tag{6.17}$$

$$l_\Psi = -0.67 \tag{6.18}$$

Modification of model

Since the existing model takes into account the displacement of the COB from the COM, this convention will be upheld for simplicity's sake. The assumption that the other AUV dynamics do not change with a shifting COM makes it mathematically equivalent to shifting the COB of the AUV. It is assumed that control of the x_{COB} and y_{COB} displacements of the AUV's COB relative to its COM are possible. Any z_{COB} component in the displacement of the COB in the negative direction (upwards) will add stability by creating restoring forces. This component of the displacement will be included in the AUV model as before. The various displacements of the COB along each axis will create moments which tend to align that axis of the AUV to the vertical inertial axis. The magnitude of the buoyancy of the AUV does not affect which way the restoring forces act, but only their effectiveness. Based on this, a positive displacement of the COB along the AUV x-axis will cause positive pitching moment and a positive displacement of the COB along the AUV y-axis will cause a negative rolling moment. It follows from **(3.21)** that the equations for the roll and pitch moments generated by displacing the COB from the COM are given respectively in **(6.19)** and **(6.20)**. These are linearised about the trim conditions to become **(6.21)** and **(6.22)**

$$K_{\text{COB}} = -y_{\text{COB}} B\cos(\Phi)\cos(\Theta) \tag{6.19}$$

$$M_{\text{COB}} = x_{\text{COB}} B\cos(\Theta) \tag{6.20}$$

$$K_{\text{COB}} = -y_{\text{COB}} B \tag{6.21}$$

$$M_{\text{COB}} = x_{\text{COB}} B \tag{6.22}$$

Most underwater vehicles are close to neutrally buoyant, making $B \approx W = mg$. The restoring forces are therefore large, even for small displacements of the COB. One problem however, revealed by **(6.19)** and **(6.20)**, is that rolling the AUV is effected by the AUV pitch angle and also tends to counteract the pitching moment on the AUV. Nevertheless, linearising these equations decouples them for small deviations about trim.

The fin actuators not in use are removed from the model and replaced by the COB shifting control inputs. If needed, all fin control surfaces could be removed. The rudder yaw action can be accomplished through differential thrusting. The aim of this section is to evaluate the possibility of using the COM shifting alternative, so the yaw control related aspects of the AUV model will be left intact. The control input matrices in the models can now be replaced by those shown in **(6.23)** and **(6.24)**.

New linear longitudinal state space model:

$$\begin{bmatrix} \dot{\bar{v}} \\ \dot{\alpha} \\ \dot{q} \\ \dot{\theta} \end{bmatrix} = \begin{bmatrix} A_{\text{long}} \end{bmatrix} \begin{bmatrix} \bar{v} \\ \alpha \\ q \\ \theta \end{bmatrix} + \begin{bmatrix} \frac{1}{m_x} \\ \frac{1}{m_z \bar{V}_0} \\ \frac{1}{I_y} \\ 1 \end{bmatrix}_D \begin{bmatrix} 2c_T & 0 \\ 0 & 0 \\ 0 & B \\ 0 & 0 \end{bmatrix} \begin{bmatrix} \delta t_c \\ \delta x_{\text{COB}} \end{bmatrix} \tag{6.23}$$

New linear lateral state space model:

$$\begin{bmatrix} \dot{\beta} \\ \dot{p} \\ \dot{r} \\ \dot{\phi} \\ \dot{\psi} \end{bmatrix} = \begin{bmatrix} A_{\text{lat}} \end{bmatrix} \begin{bmatrix} \beta \\ p \\ r \\ \phi \\ \psi \end{bmatrix} + \begin{bmatrix} \frac{1}{m_y \bar{V}_0} \\ \frac{1}{I_x} \\ \frac{1}{I_z} \\ 1 \\ 1 \end{bmatrix}_D \begin{bmatrix} 0 & Y_{\delta r} \\ -B & 0 \\ 0 & N_{\delta r} \\ 0 & 0 \\ 0 & 0 \end{bmatrix} \begin{bmatrix} \delta y_{\text{COB}} \\ \delta r \end{bmatrix} \tag{6.24}$$

Controller design

In order for these controllers to be evaluated, their performance should be the same as that of previously designed controllers. Since the AUV model itself has not changed, only the control inputs, the closed-loop system poles can be placed exactly as before with the correct controller gain choices. The same control scheme will be used as before, with PI controllers used to regulate the AUV pitch and roll rate variables. These controllers receive their commands from pitch and roll attitude angle controllers, which consist of a proportional gain term only. This is achieved through the gain choices shown below in **(6.25)** and **(6.26)**. There is a small discrepancy in the final system poles of the pitch control loops due to the influence of the fin control surfaces on the AUV angle of attack, but it can be considered negligible.

$$\begin{aligned} K_{p_{Q_{\text{COB}}}} &= K_{p_{Q_{\text{SLC}}}} \frac{M_{\delta a_d} + M_{\delta e}}{B} \\ K_{i_{Q_{\text{COB}}}} &= K_{i_{Q_{\text{SLC}}}} \\ K_{p_{\Theta_{\text{COB}}}} &= K_{p_{\Theta_{\text{SLC}}}} \end{aligned} \tag{6.25}$$

$$\begin{aligned} K_{p_{P_{COB}}} &= K_{p_{P_{SLC}}} \frac{K_{\delta a_d}}{B} \\ K_{i_{P_{COB}}} &= K_{i_{P_{SLC}}} \\ K_{p_{\Phi_{COB}}} &= K_{p_{\Phi_{SLC}}} \end{aligned} \tag{6.26}$$

Performance evaluation

Since the closed-loop poles are the same as before, theoretically the system performance will be the same. To enhance the comparison, slew limiting was also implemented for the COB-based controller by scaling the slew rate limit the same way the controller gains were scaled. Although the theoretical closed-loop poles are the same, the two control methods are expected to differ in the following ways. The performance of the COB controller should not change when the AUV speed is varied, unlike that of the fin controllers whose effectiveness decreases as the AUV speed drops. The COB-based controller performance is, however, dependent on the current AUV attitude angles, since the buoyancy forces are always in the direction of gravity. As the attitude angles of the AUV approach $\pm\pi/2 radians$, this effectiveness of this controller is expected to decrease. This is not often the case, though, and the AUV pitch and roll angles are usually controlled within $\pm\pi/6 radians$. A simulation was run to compare the performance of the two controllers when the AUV speed was decreased, with the results shown in **Figure 6.10**. The AUV was set to follow simple straight waypoints with step depth changes. The performance of the COB-based controller and the standard fin-based controller at full speed are shown in **Figure 6.10a** and **Figure 6.10b** respectively. As expected, the responses shown in these plots are quite similar. The AUV thrust was then reduced to half and the simulation re-run. The response of the system when using the COB controller is shown in **Figure 6.10c**. This response closely resembles its original response. The system response using the fin control surfaces is shown in **Figure 6.10d**. Clearly, with reduced speed the AUV fins lose their effectiveness and the AUV cannot track the desired path. These plots display the clear advantage of using such a control scheme when the AUV is expected to operate at varying speeds with constrained pitch and roll attitude angles. Although the AUV speed during operation is fairly constant, such a control scheme could be used to extend the range of motion and robustness of the AUV.

Control effort

Although theoretically effective, if the COB of the AUV cannot be controlled in reality then these results would not be useful. The control signal for the x_{COB} displacement from one of the simulation runs is shown in **Figure 6.11**. The x_{COB} displacement was constrained to be within ±2 cm. Although some large spikes

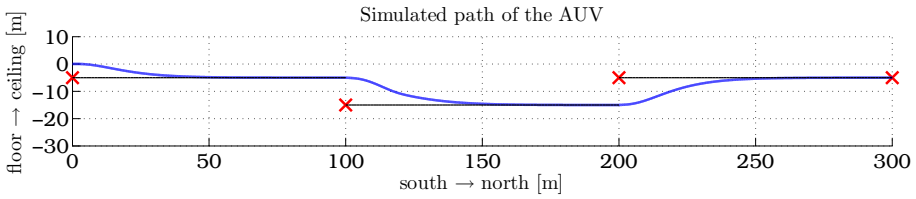

(a) COM controller at full thrust

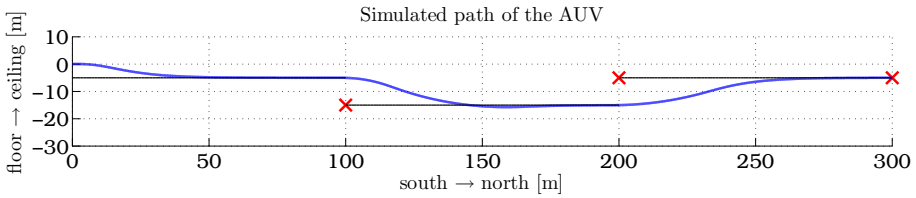

(b) Standard controller at full thrust

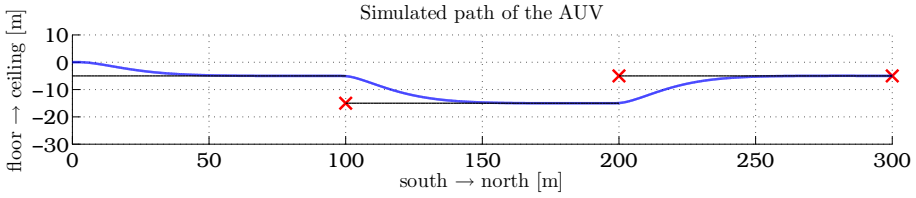

(c) COM controller at half thrust

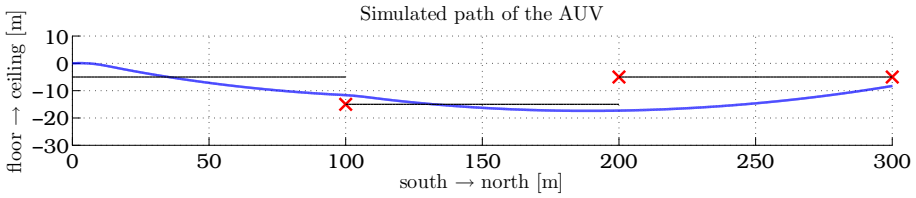

(d) Standard controller at half thrust

Figure 6.10: Simulation results for controller comparison

in the control signals do occur, most of the x_{COB} commands lie within 1cm of its nominal point, which is around 0.6 cm. To displace the COB from the COM by 1 cm, the entire mass of the AUV would need to be moved, relative to its outer geometry, by 1 cm. This may not seem feasible, but it is equivalent to moving some fraction of the AUV's mass, $\frac{1}{x}$, by x cm relative to its geometry. This shift in the relative positions of the COM and COB could be achieved, then, if the necessary actuators and space inside the AUV could be made available. Conceivably, though, the mechanics needed to achieve this could be quite bulky, especially considering that the flooded mass of the AUV is close to 850 kg.

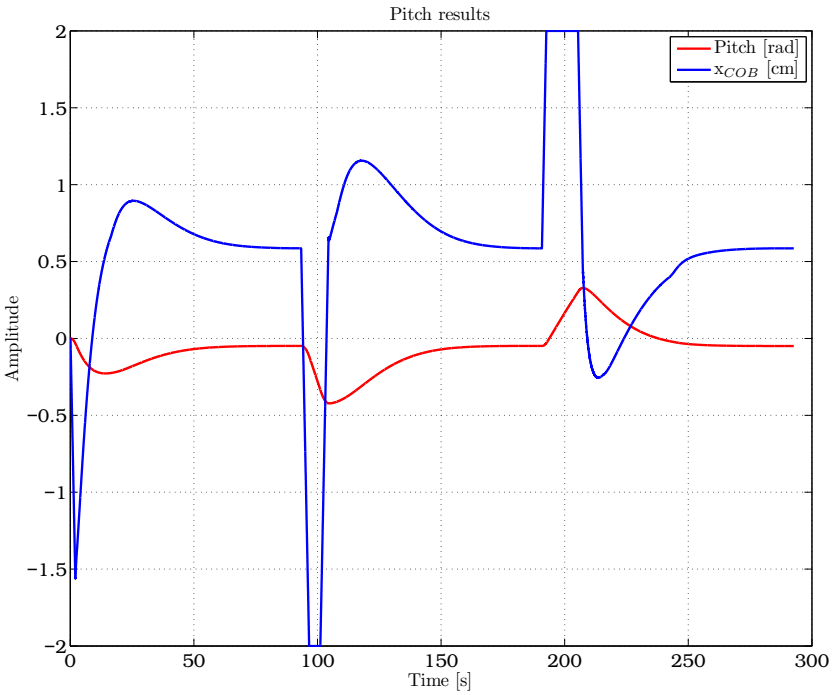

Figure 6.11: Plot showing necessary movement in the COM position

Summary comparison with previous controllers

The advantages and disadvantages of using this control method compared to using the usual fin control surfaces are listed below.

Advantages

- No fluid flow over a control surface is needed for the controller to be effective, and therefore it provides linear control for a far greater range of AUV operating speeds.
- The control is linked to the Earth's gravitational acceleration vector, and so may be very useful for recovering from instability.

Disadvantages

- Cannot be used to perform manoeuvres requiring extreme changes in orientation.
- The actuators necessary to create displacements in the AUV COM relative to its COB may be difficult to realise in practice.

- This control method becomes less feasible as AUV sizes increase, since large amounts of mass need to be shifted.

Augmented controller architecture

The COB-based controller in practice may suffer from a number of practical issues. If the COM is shifted at too fast a rate it may excite other dynamics in the AUV. Moving the COM of the AUV may be practically challenging in terms of the required actuators and power needed to achieve the shift. However, practical use could be made of this theory by using the regular fin actuators to control the high-frequency dynamics of the AUV, while using the shifting COM to cater for low-frequency dynamics and steady state offsets. In this way, the COB controllers essentially act as an auto-trim system for the AUV. This would allow the full dynamic range of the fin actuators to be used for disturbance rejection and stability control and also caters for unmodelled measurement, calibration and disturbance offsets. This trim adjustment facility would also be useful for improving the AUV's ability to dive or surface as needed.

A similar type of load-sharing, bandwidth-separated control scheme using multiple actuators is implemented in [17]. In essence, this scheme works by linking both actuator control inputs to the same controller output through separate high and low pass filters, each having the same cutoff frequency of $\omega = \frac{1}{\tau}$ as shown in **Figure 6.12**. A single new virtual actuator, δX, is therefore created which feeds both the other actuator inputs. In the case of the AUV roll control, for example, this would be realised by creating the new virtual roll actuator, $\delta roll$, which uses the differential front fin deflection for the high-frequency control and the movement of the COB along the Y^B-axis for low-frequency control, as shown in **Figure 6.13**. The gain K_n is a normalising gain which must be chosen such that both control inputs have the same influence on the system behaviour if fed with the same input signal. In the case of the AUV roll control, the value of K_n is given in **(6.27)** below. In this way, the low-frequency actuators can be easily augmented to the original SLC fin controllers simply by using the correct value for K_n and choosing a crossover frequency between the actuators of $\omega = \frac{1}{\tau}$.

$$K_n = \frac{K_{\delta a_d}}{B} \tag{6.27}$$

This controller augmentation can be applied to many other aspects of the AUV control. The differential thrust input could be used as the low-frequency augmentation for the rudders, to cater for yaw rate offsets. Ballast tanks could be used to aid AUV diving and surfacing in much the same way.

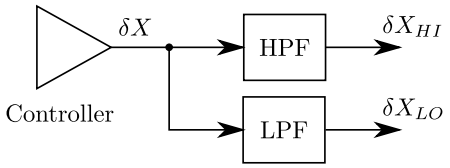

Figure 6.12: Basic load-sharing bandwidth-separated control scheme

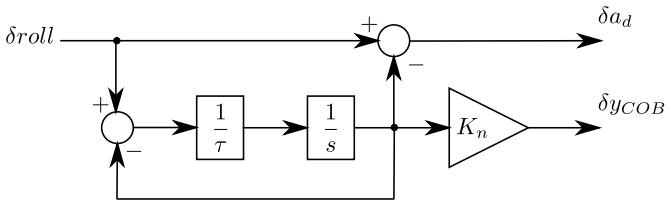

Figure 6.13: Block diagram showing practical implementation of the AUV roll control using bandwidth-separated actuator scheme

6.4 Chapter summary

Simple robust controllers for all aspects of the AUV's movement were designed in this chapter. These take the form of inner PI feedback loops, used to first control the AUV angular rates, followed by proportional controllers in outer-loops with attitude angle feedback. These controllers are intended to be given reference commands from the AUV guidance systems, which will be designed in the next chapter. Although it may be difficult to implement mechanically, it may be worth doing some research into the possibilities of movement control on an AUV by changing the position of the COM relative to the COB of the AUV. This control method is independent of the AUV travel velocity and is linked to the Earth's gravitational acceleration vector, so it could be very useful for recovery from instability as well as for general control. The most practical use of such actuation would be to augment the normal fin controllers with the COB-based controllers. This would provide the AUV with an auto-trim feature, which would solve many of the current problems affecting the AUV. These include poorly trimmed fin control surfaces, difficulty in getting the AUV to dive, and imbalances in the AUV construction and calibration. For the rest of this thesis, however, only the conventional fin-based controllers will be considered in analyses.

Chapter 7

Guidance

Analysis thus far has shown that the primary cause of the AUV's poor tracking performance is the current guidance method. This chapter covers the design of new guidance methods, which will work in conjunction with the newly designed controllers to improve the tracking ability of the AUV. For simplicity all the guidance analyses will be restricted to the $X^E Y^E$-plane, commanding only the AUV yaw states. The results can then be applied to different aspects of the AUV guidance as necessary. At the end of the chapter the complete new control and guidance system designs will be presented.

Before beginning with guidance designs, some important differences between UAV and AUV movement should be examined. Most automated vehicle control and guidance research takes place in the field of aerial vehicles. This research has provided the background for most of the work in this project; however, UAVs and AUVs differ in some fundamental ways which affect the approach taken to guidance system designs. Aerial vehicles have to generate significant lift forces to counter the gravitational forces they experience so they can remain airborne. This lift force is used to steer the UAV's direction by rolling the vehicle and performing what is known as a coordinated turn. AUVs, however, usually combat gravitational forces with their buoyancy, which is independent of their orientation in space. AUVs therefore use their fins directly to steer and can roll arbitrarily without affecting their current direction of travel in the ideal case. The directional and longitudinal guidance of the AUV can therefore be handled using the same principles for both.

The primary problem with the IMT guidance approach is that simply aiming for points in space will always produce poor results. This is especially true when the aiming point is in the distance, since the angular deviation caused by being off-course will be small. Since the desired behaviour is for the AUV to travel directly between the points, it makes sense to develop a guidance method that tracks to a specific path. The most intuitive approach to solving this problem would be

to reduce the perpendicular distance between the AUV and a line joining two waypoints, known as cross-track error guidance. This is reportedly not the best method of tracking a path, according to [18, p. 39], but will be analysed first in this chapter as a benchmark guidance design since it is in common use and very intuitive. Another method for tracking paths can be found in [18]. This algorithm was developed to track circular paths which, although not specifically needed by IMT, may provide some useful functionality in the future. Designing a tracking algorithm for circular paths may also provide some useful insight into how to track straight paths and would hopefully yield one general tracking algorithm, which could be applied to straight paths simply by assuming they are circular paths with an infinite radius. A new guidance method was thus designed in the second half of this chapter, based on the one presented in [18].

Since the waypoint definition system is simple and based only on points in three-dimensional space, it will require modification to extend the capabilities of the guidance systems. The waypoint system will be redefined in **Section 7.6**, such that paths for the AUV are defined, instead of destination points. The general aim of the guidance will remain the same, that is, to guide the AUV from a starting point to an ending point. In this way the same behaviour can be achieved, but with greater certainty of the AUV's position between waypoints. Currently, the AUV's position between waypoints is undetermined and heavily dependent on the disturbances it receives and initial conditions with which it begins tracking the waypoint.

7.1 Cross-track error guidance

This guidance method was designed as an initial improvement on the current AUV guidance. It is simple and intuitive to design and analyse, while still yielding good performance. Cross-track error guidance works by using the perpendicular error between a vehicle and its desired tracking path to generate commands for reducing that error. In its simplest case this is usually done by making the commanded attitude angle of the vehicle, relative to the path direction, proportional to the error from the path, as given in **(7.1)**, where K_x is the proportional gain. The variables e and Ψ represent the cross-track error and relative heading of the vehicle respectively, as shown in **Figure 7.1**. This is essentially the guidance method used by IMT for the AUV depth control. It is difficult to apply this method to tracking circular paths directly. An intuitive analysis of this method also reveals that it would be susceptible to measurement offset errors and disturbances, making reliable steady state tracking impossible. This can be partially solved by using integral control. Attempts at this have had little success, however, since the integrator time constants had to be made very large to avoid instability. The addition of integral control also results in the AUV overshooting the desired tracking path considerably unless it is

turned off in some way when the AUV is not near to the desired path. This method of performing cross-track error guidance is not sufficient and must be modified.

$$\Psi = K_x e \tag{7.1}$$

By using the AUV travelling direction, φ, in place of its attitude angle in relation to the desired tracking path, the performance of the cross-track error guidance can be greatly improved. The feedback structure of such a guidance scheme is shown in **Figure 7.2**. The feedback gain K_φ is expected to have a value similar to the outer-loop attitude angle feedback gain obtained in **Section 6** and should be simple to design. The gain can be replaced by a more complicated controller, but this is not necessary. The guidance gain K_x also needs to be designed, following an analysis of the guidance method. This modified version of the basic cross-track error guidance can be easily applied to tracking circular paths without steady state error after a few modifications. A feed-forward reference for the AUV yaw rate, $r_{R_{ff}}$, must be supplied, which would make the AUV track the circular path perfectly at its current speed in the ideal case. The perpendicular error from the path is measured along a projection of the circular path's radius through the current position of the AUV, and the travel direction must be commanded relative to the tangent to the circular path at the projected position of the AUV. A diagram of this situation is shown in **Figure 7.3**. The cross-track error guidance dynamics are derived in the following section.

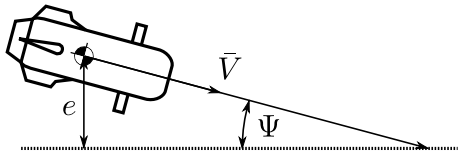

Figure 7.1: Basic cross-track error guidance situation

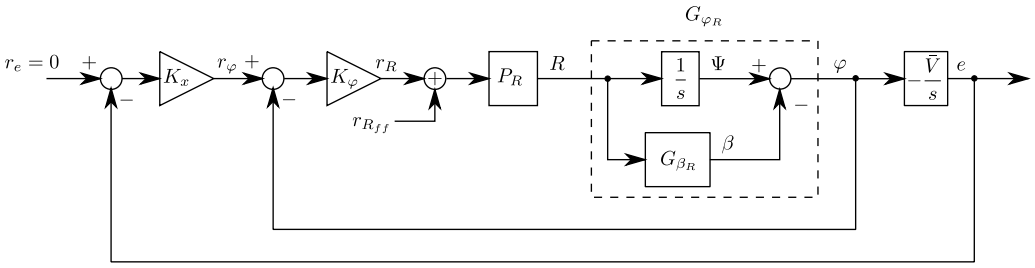

Figure 7.2: Feedback structure of the improved cross-track error guidance system

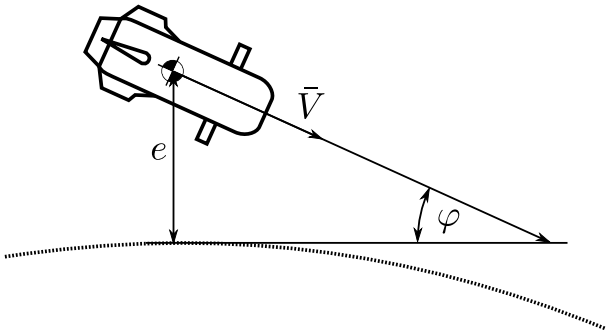

Figure 7.3: Cross-track error guidance applied to a circular path

Guidance dynamics

Assume the AUV dynamics are much faster than the guidance dynamics for this derivation. Therefore, $G_{\beta_R} = 0$ and the inner-loop plant transfer function $P_R = 1$ at all frequencies concerning the guidance. Firstly, considering the guidance dynamics when the vehicle is far from the path, the commanded relative travel direction will be large. If the magnitude of the commanded relative travel direction is greater than $\pi/2$ then it must be saturated at or below $\pi/2$ so that the vehicle does not travel backwards along the path or get stuck in looping motions when it is too far away from the desired path. Therefore, at a distance the vehicle will simply head straight towards the desired path. The dynamics at this point will be determined by the travel direction controller.

When the vehicle is close enough to the tracking path such that the travel direction command is not saturated, the system dynamics can be determined from the linearised feedback structure shown in **Figure 7.2**. The transfer function from reference to cross-track error is given in **(7.2)**. When compared to the standard second-order low-pass transfer function form shown in **(7.3)**, expressions for the natural frequency, ω_n, and damping factor, ξ, of the AUV's response can be obtained in terms of the cross-track error guidance gains as in **(7.4)** and **(7.5)**. The guidance gains can now be designed to achieve a specific plant convergence response.

$$G_e = \frac{1}{\frac{s^2}{K_\varphi K_x \bar{V}} + \frac{s}{K_x \bar{V}} + 1} \tag{7.2}$$

$$G_2 = \frac{1}{s^2 \frac{1}{\omega_n^2} + s\frac{2\xi}{\omega_n} + 1} \tag{7.3}$$

$$\omega_n = \sqrt{K_x K_\varphi \bar{V}} \tag{7.4}$$

$$\xi = \frac{1}{2}\sqrt{\frac{K_\varphi}{K_x \bar{V}}} \tag{7.5}$$

7.2 Chase guidance

In an attempt to improve upon the cross-track error guidance designed above, a new guidance method was designed based on the guidance method put forward in [18]. The approach to this design is different from that of the cross-track error guidance. This guidance seeks to use an alternative measured quantity to produce guidance commands, instead of the actual error from the path. The guidance method in [18] operates by *looking ahead* to some point on the desired tracking path, and commanding a lateral acceleration for the vehicle based on the angular difference between its current direction of travel and the direction of the point on the tracking path. The point is chosen as the point on the desired tracking path that is always a specific distance away from the vehicle. This method of guidance could be used here, but some problems were identified with this method. The equations for finding the point on the path involve solving for the intersection of a circle with the desired tracking path.

- Each solution yields two answers, one of which is in the reverse direction along the path.
- If the vehicle is too far from the path, then no solution is found.
- The equations for finding the intersection points of two circles (as will be the case when tracking a circular path) require a lot of calculation effort, which may not be feasible on processors used for simple guidance.
- This becomes even worse when the guidance is not constrained to a single two-dimensional plane and requires solving for the intersections of the path with a sphere.

A slight modification was made in order to reduce the calculation complexity required to execute this guidance. The derivation begins with the idea of tracking circular paths and works towards the solution.

Derivation of the chase guidance method

Analysis of circular path

Before designing a new guidance algorithm, the characteristics of a vehicle tracking a circular path will be analysed. This analysis begins with a vehicle on a circular path, assumed to be in steady state, tracking the path without error, as in **Figure 7.4**. If the circular path has a radius, ρ, and the vehicle is travelling at a some velocity $\mathbf{V}$, the following are known.

- The velocity of the vehicle will always be tangential to the path.
- The vehicle velocity will change with an angular rate, $\omega = \mathbf{V}/\rho$.
- The vehicle experiences a centripetal acceleration, $a_\perp = \mathbf{V}^2/\rho = \omega^2\rho$.

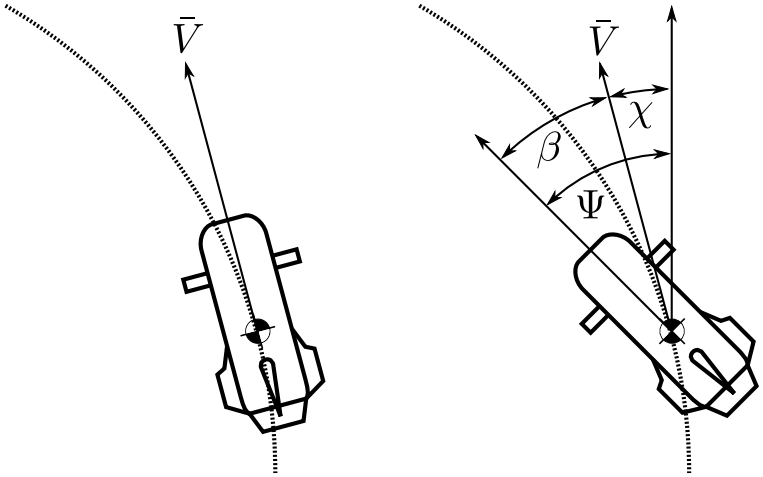

Figure 7.4: AUV tracking a circular path

Initially it may be assumed that the vehicle's heading and velocity vectors are aligned, as they are on the left of **Figure 7.4**. However, the hydrodynamics of the vehicle hardly ever allow this to be the case, especially in the case of the AUV with fins at the back of its geometry. The case is usually more like the diagram on the right of **Figure 7.4** (β exaggerated for clarity). Here one can see that the vehicle has a non-zero angle of sideslip, β, which would hamper the performance of any attitude-based guidance system. The vehicle's acceleration in general can be described by **(7.6)**. For the derivation of an acceleration-based guidance method a definition for $a_\perp$ is needed. For the sake of simplicity, assume all motion is confined to the horizontal $X^E Y^E$-plane and that vehicle is travelling at constant speed $\bar{V}_0$. The rest of the derivation follows from [19]. The total acceleration of the AUV will be given by **(7.6)**. The components of the AUV's velocity in body axes are given by **(7.7)** to **(7.9)**. These are substituted into **(7.6)** to give **(7.10)**.

$$a = \frac{\mathrm{d}\mathbf{V}}{\mathrm{d}t} = \frac{\mathrm{d}V_N}{\mathrm{d}t}i + \frac{\mathrm{d}V_E}{\mathrm{d}t}j + \frac{\mathrm{d}V_D}{\mathrm{d}t}k \tag{7.6}$$

$$V_N = \bar{V}\cos(\chi) \tag{7.7}$$

$$V_E = \bar{V}\sin(\chi) \tag{7.8}$$

$$V_D = 0 \tag{7.9}$$

$$a = -\bar{V}\sin(\chi)\frac{\mathrm{d}\chi}{\mathrm{d}t}i + \bar{V}\cos(\chi)\frac{\mathrm{d}\chi}{\mathrm{d}t}j \tag{7.10}$$

The vehicle acceleration can be separated into two orthogonal components, with reference to the vehicle's direction of travel, as in **(7.11)**. The unit vector in direction of **V** is $u_{\|} = \cos(\chi)i + \sin(\chi)j$; and perpendicular to **V** is $u_{\perp} = -\sin(\chi)i + \cos(\chi)j$. This allows the calculation of each of the components of the AUV's acceleration, resulting in **(7.12)** and **(7.13)**. But $\chi = \Psi + \beta$ (Ψ in **Figure 7.4** is negative). Thus the final result for tangential acceleration in terms of the preferred state variables is given in **(7.14)**

$$\begin{aligned} a &= a_{\|} + a_{\perp} && (7.11)\\ &= a \cdot u_{\|} + a \cdot u_{\perp} \\ a_{\|} &= 0 && (7.12)\\ a_{\perp} &= \bar{V}\sin^2(\chi)\frac{d\chi}{dt} + \bar{V}\cos^2(\chi)\frac{d\chi}{dt} \\ &= \bar{V}\frac{d\chi}{dt} && (7.13)\\ a_{\perp} &= \bar{V}\left(R + \frac{d\beta}{dt}\right) && (7.14) \end{aligned}$$

This equation holds for all orientations of the vehicle since R and β are independent of the Euler orientation angles. Since in steady state a vehicle tracking a circle will have a constant β angle, $\frac{d\beta}{dt}$ will be zero. The AUV can thus be expected to track a circle with no steady state error, simply by commanding a specific angular rate, ω, as given by **(7.15)**, which conveniently turns out to be the kinematic point mass angular velocity equation. This should work even in the presence of ocean currents, which can be expected to change only the value of the constant AUV β angle. This simplifies controller design greatly, and eliminates attitude angle feedback loops from the final control and guidance system.

$$\omega = \frac{\bar{V}}{\rho} \qquad (7.15)$$

Guidance law design

A guidance algorithm based on *looking ahead* to some point further along our desired path to guide the AUV movement can now be designed. The derivation begins by referring to **Figure 7.5**, with the AUV tracking the path. The variable d is the *distance* that is chosen to look ahead on the path. Using geometry an expression for η can be obtained in **(7.16)**.

$$\begin{aligned} \xi &= \frac{d}{\rho} \\ \chi &= \frac{\pi - \xi}{2} \\ \eta &= \frac{\pi}{2} - \chi = \frac{\xi}{2} = \frac{d}{2\rho} && (7.16) \end{aligned}$$

Since the yaw rate given in **(7.15)** is required to track the circle with no steady state error, using **(7.16)** and substituting into **(7.15)** for ρ gives **(7.17)**. An equation for the guidance law is therefore developed in **(7.18)**, where the guidance gain, K_c, is as given in **(7.19)**. With the angles defined as they are in **Figure 7.5** η is positive, but a negative ω would be required to track the path; thus a negative sign is introduced at **(7.17)**.

$$\omega = -\frac{2\bar{V}\eta}{d} \tag{7.17}$$

$$\omega = K_c\eta \tag{7.18}$$

$$K_c = -\frac{2\bar{V}}{d} \tag{7.19}$$

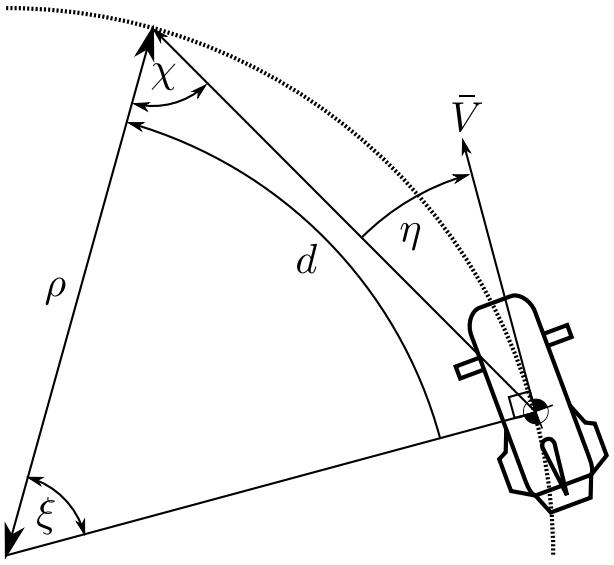

Figure 7.5: Geometry of circular path tracking

This guidance law makes intuitive sense in that, if the AUV were to stray off course, heading outside of the circle, the commanded yaw rate would increase and it should turn back towards the path. Likewise, if it were to move inside the circle, the commanded yaw rate would decrease and it should return to the path. Note also that the guidance is controlled solely by choice of the look-ahead distance, d. It should therefore apply to a straight line path as well as to circular paths. The naming of this guidance method follows from the guidance mechanism, where the AUV is always *chasing* some point that moves along the guidance path. In order to apply this guidance method in practice, the dynamics it introduces into the system must first be analysed.

Practical application of the guidance law

The guidance law can now be applied in practice as follows. Referring to **Figure 7.6**, the AUV's position in the plane of the circular path is projected radially onto the circular path. This gives its effective position along the path travelled so far. The look-ahead distance is then added from this position to find the position of the aiming point, A, of the algorithm. A line is then joined from the AUV to the aiming point and the angle between that and the current direction of travel is used in **(7.18)** to determine the commanded angular rate for the AUV. The angle, η, is signed and so will command the correctly signed rate needed to steer the AUV towards the desired path, irrespective of which side of the path it is on. This can be applied to any of the other attitude rates of the AUV in a similar way, by selecting an appropriate plane of reference for the motion and commanding the necessary angular rates.

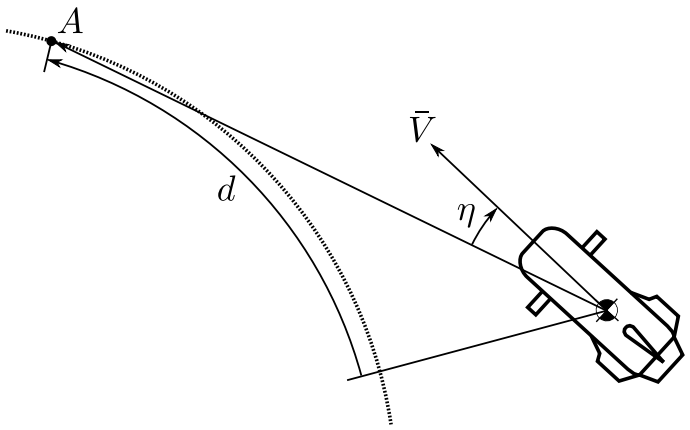

Figure 7.6: Geometry of guidance law applied practically

Guidance law analysis

Knowing the guidance dynamics is important for assessing the effectiveness of this guidance law, as well as for correct implementation of it. For now it shall be assumed that the controlled plant is much faster than the guidance dynamics and effectively has infinite bandwidth; that is, the commanded angular rate is achieved immediately and results in the velocity vector direction of the AUV changing with the commanded rate. The derivation refers to **Figure 7.7**, with the end goal being to define the dynamics of the path tracking error, e. The derivation is carried out on the case where the desired path is a straight line, as this simplifies the equations and decreases the number of assumptions that would otherwise have to be made.

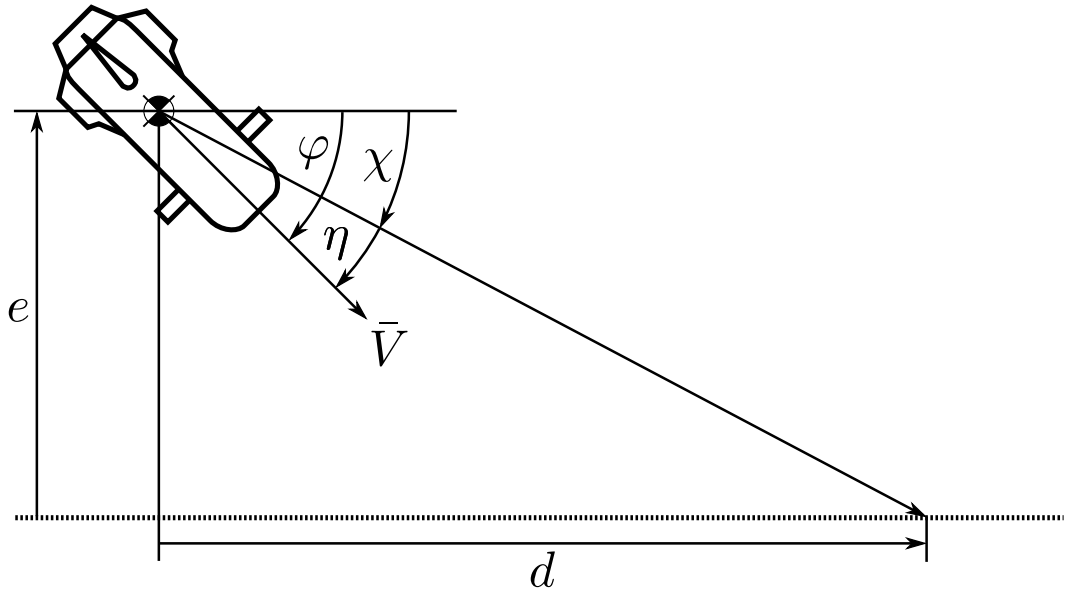

Figure 7.7: Geometry for deriving guidance dynamics

All the angles (φ, η, χ) in **Figure 7.7** are positive as defined; equations **(7.20)**, **(7.21)** and **(7.22)** are obtained purely from geometry.

$$\frac{\mathrm{d}e}{\mathrm{d}t} = -\bar{V}\sin(\varphi) \tag{7.20}$$

$$\varphi = \eta + \chi \tag{7.21}$$

$$\chi = \arctan\left(\frac{e}{d}\right) \tag{7.22}$$

First, consider the dynamics when the vehicle is approaching the path from a distance, when $e \gg d$, where the magnitude of η is expected to be small. Therefore, $\varphi \approx \pi/2$ and is changing only slowly, which results in **(7.23)** from **(7.20)**. From a distance, therefore, the error to the path simply decreases at a similar rate to the velocity magnitude of the AUV. The error dynamics at this point are described by **(7.24)**, which places a pole at the origin of the complex plane.

$$\frac{\mathrm{d}e}{\mathrm{d}t} \approx -\bar{V} \tag{7.23}$$

$$e \approx -\frac{\bar{V}}{s} \tag{7.24}$$

The dynamics close to the tracking path are of greater concern since this is the region in which the AUV is expected to be operating the majority of the time and will most likely impose the highest bandwidth requirements on the control systems. At this point, $e \ll d$ and φ is expected to be small. The original equations **(7.20)** and **(7.22)** now become **(7.25)** and **(7.26)**. Substituting **(7.26)** into **(7.21)** results in an equation

describing η in terms of φ and e in **(7.27)**.

$$\frac{\mathrm{d}e}{\mathrm{d}t} = -\bar{V}\varphi \tag{7.25}$$

$$\chi = \frac{e}{d} \tag{7.26}$$

$$\eta = \varphi - \frac{e}{d} \tag{7.27}$$

A linearised feedback structure for this guidance algorithm can now be created, as seen in **Figure 7.8**. Since the AUV dynamics were assumed to be much faster than the guidance dynamics at the beginning of this derivation, $G_{\beta_R} = 0$ and the inner-loop plant transfer function $P_R = 1$ at all frequencies concerning the guidance. Using block diagram reduction, the closed-loop transfer function from reference to output for the tracking error e is obtained in **(7.28)**. Substituting in for K_c from **(7.19)** and equating the right-hand side **(7.28)** to the standard second-order low-pass filter transfer function in **(7.3)** reveals convenient values for the natural frequency, ω_n, and the damping factor, ξ, of the error dynamics, as given in **(7.29)** and **(7.30)** respectively. These dynamics were confirmed with a simplified numerical simulation, the results of which are shown in **Figure 7.9**. This simulation does not include the dynamics of the AUV and thus gives the ideal tracking path that would be achieved with this guidance method. When the AUV is still far from the path, it heads almost directly towards it. When it is near to the path, it was observed to oscillate about the path. Based on the relative magnitudes of consecutive oscillation peaks and the oscillation period, both the damping factor and natural frequency of the guidance poles were found to be correct. The circle tracking abilities of the guidance method without AUV dynamics were also simulated and are plotted in **Figure 7.10** an **Figure 7.11**.

$$G_e = \frac{1}{s^2\frac{-d}{\bar{V}K_c} + s\frac{d}{\bar{V}} + 1} \tag{7.28}$$

$$\omega_n = \sqrt{2}\frac{\bar{V}}{d} \tag{7.29}$$

$$\xi = \frac{1}{\sqrt{2}} \tag{7.30}$$

7.3 Comparison of guidance methods

The comparison between the redesigned chase guidance and the one presented in [18] is considered first. The dynamics results in [18] and in this chapter show that the two methods are essentially equivalent when the vehicle concerned is close to the tracking path. Both exhibit the same natural frequency and damping factor in relation to the guidance gains chosen. The difference between the two methods is

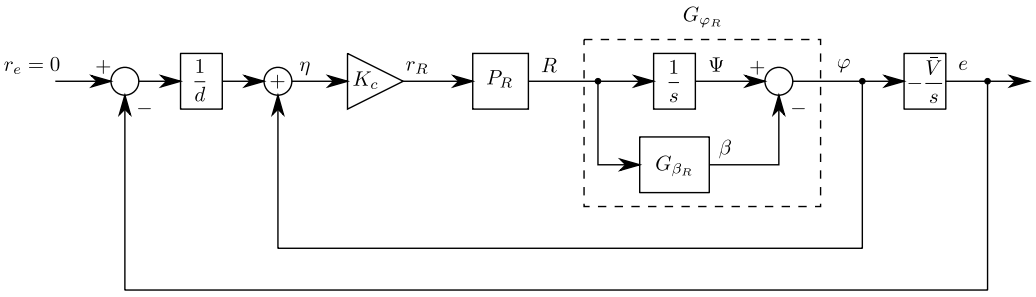

Figure 7.8: Linear feedback structure of the chase guidance

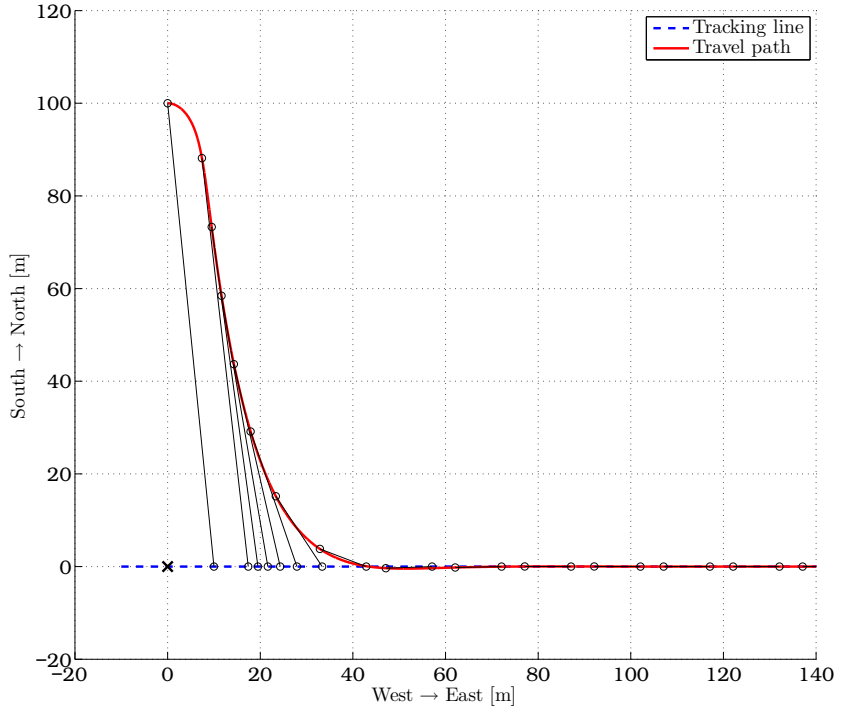

Figure 7.9: Simulated straight line tracking path of an ideal AUV using chase guidance

apparent only when the vehicle is converging to the path from a distance. From a distance, the original method commands the vehicle directly towards the path, as the cross-track error guidance would, whereas the redesigned chase guidance commands a angled approach path which tends to 90° when the vehicle is infinitely far from the path. The redesigned chase guidance requires simpler calculations to execute the guidance. Instead of solving for circle and sphere intersections with paths in three-dimensional space, the redesigned chase guidance calculations can be accomplished using simple vector operations.

The feedback structure in **Figure 7.8** reveals how similar the chase and cross-track

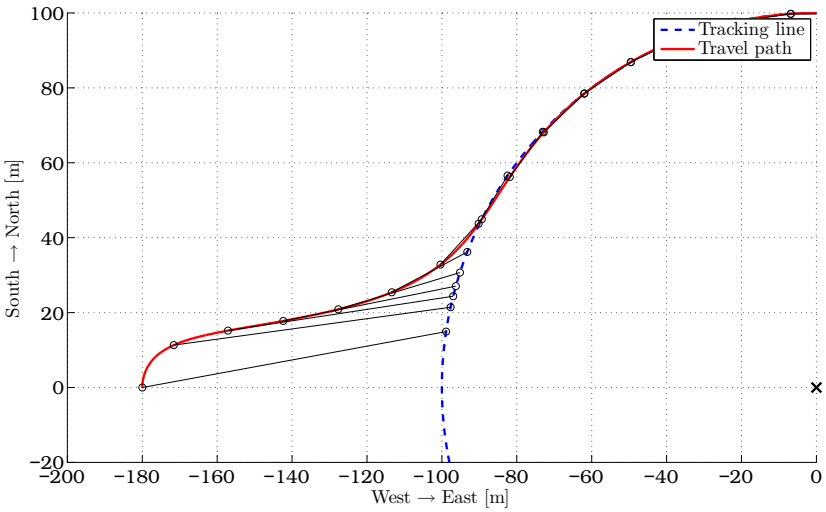

Figure 7.10: Simulated circular tracking path of an ideal AUV using chase guidance

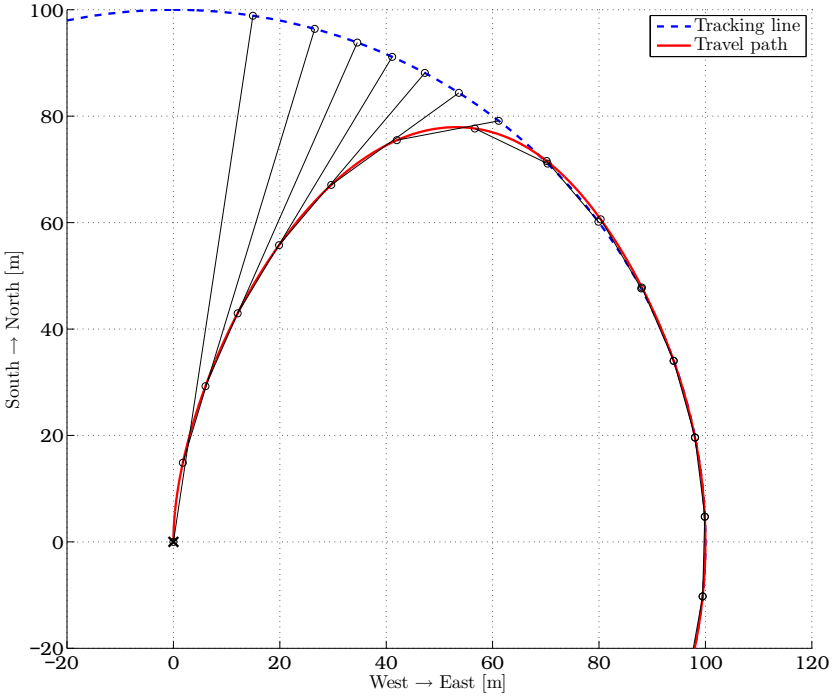

Figure 7.11: Simulated circular tracking path of an ideal AUV using chase guidance

error guidance methods are. When the AUV is close to the tracking path and the guidance linearisations apply, they are almost the same. By setting the respective guidance gains equal to one another, as shown in **(7.31)** and **(7.32)**, the guidance responses can be compared directly. The cross-track error guidance has a slightly more aggressive response, which produces more overshoot in the response but has better tracking characteristics in the presence of disturbances. The differences are

small, though, and the two methods can be considered equally effective. The cross-track error guidance, however, is more traditional and simpler to implement. It is also slightly more flexible in that the gains can be adjusted to achieve different response characteristics, unlike the chase guidance which always produces a guidance response with complex poles at a damping factor of $1/\sqrt{2}$. For all guidance implementations, the maximum frequency of the final complex poles is limited by the poles of the inner-loop plant. The guidance poles must be slow enough such that they do not interact with the inner-loop poles and cause oscillation or instability. These designs are most easily performed by trial and error using simulation results as a basis.

$$K_x = \frac{1}{d} \tag{7.31}$$

$$K_\varphi = K_c \tag{7.32}$$

It seems that, of all the guidance methods, cross-track error guidance is the simplest and most effective method. This may be due to dynamics of the AUV that are slightly different to those of standard UAVs, which allow the use of direct rate control for steering, as opposed to the roll-to-turn mechanism. Since the guidance methods designed in this chapter only give reference commands for the AUV angular rates, the outer-loop control designs in the previous chapter are redundant. The attitude angle controllers would be necessary only for simple forms of guidance such as the elementary cross-track error guidance mentioned in the beginning of this chapter.

7.4 Practical considerations

Disturbance rejection

All output disturbances on the AUV are expected to come from the water surrounding the AUV. Based on [20], [21], [22] and [23], most ocean waves occur at frequencies ranging from about 1 rad.s^{-1} down to 0.01 rad.s^{-1}. This covers the extent of the plant bandwidth. Since the AUV travels below the surface of the water, the disturbances that could come from ocean waves are not expected to influence the AUV. The data from IMT, shown in **Section 2**, also does not display any evidence of such disturbances. As was mentioned in that section, the most likely cause of tracking errors for the AUV will be constant ocean currents, which push the AUV off its desired path. For the AUV to track perfectly under these conditions, some component of its velocity vector needs to counteract the constant current. Both of the guidance methods designed in this thesis perform perfectly in this regard when tracking straight lines, since they command angular rates to achieve a desired travel direction. Thus, once the AUV has converged to the path, the guidance commands zero angular rate and the AUV travels along the path, possibly with some offset

attitude angle so that the thrust can counter the disturbance current. When tracking circular paths, however, a constant current disturbance is essentially transformed into a disturbance at the same frequency with which the AUV completes single full traversals of the circular path; that is $\omega = \frac{\bar{V}}{\rho}$. When tracking circular paths in the presence of a constant current disturbance, both guidance method responses result in tracking errors. The disturbance rejection capabilities of the AUV are now determined mostly by the disturbance rejection capabilities of the inner-loop rate controllers. These errors are reasonably small, however. To gauge the AUV's performance in this regard a simulation with circular paths of various radii was run, with a constant disturbance current magnitude of 0.3m.s^{-1}. The simulation results are shown below in **Table 7.1**. The chase guidance performs slightly worse than the cross-track error guidance in this regard. The resulting tracking paths were circles of the correct radius, displaced from the circular path by the maximum error amount, perpendicular to the disturbance direction. The direction of the displacement is due to the AUV hydrodynamics and would be in the opposite direction if the circular path were to be tracked in the opposite direction. These tracking errors can be considered reasonable for the majority of AUV operations.

Table 7.1: Maximum tracking errors for various circular path radii (0.3m.s^{-1} constant current disturbance)

Radius [m]	100	50	30	20	15
Chase: Error [m]	0.25	0.45	0.71	0.95	1.45
Xtrack: Error [m]	0.20	0.39	0.61	0.83	1.15

Measurement error robustness

The state measurements that affect the guidance are primarily the AUV velocity and angular rate measurements. The inner-loop controllers depend on angular rate measurements and the guidance depends on velocity measurements to calculate the velocity direction and magnitude. Fortunately the AUV uses good sensors which provide practically perfect measurements for these AUV states. Although the position measurements may drift over time, they cannot be compensated for in any way by the control of guidance.

Impact of plant limitations

Naturally, the guidance gains cannot simply be increased indefinitely without causing instability or other undesirable behaviour. The two main plant limitations of

concern here are the plant bandwidth and angular rate saturation.

Assume that the AUV can track angular rate commands perfectly, with the only limitation on its tracking ability being a maximum angular rate. With reference to the feedback structures in **Figure** 7.2 and **Figure** 7.8, the reference angular rate (neglecting any feed-forward reference) will therefore be entirely determined by the rate of change of the reference travel direction and the gain K_φ or K_c as the case may be. The rate of change of the reference travel direction is dependent on the other guidance gains and the rate of change of the cross-track error to the path, which cannot exceed the AUV velocity. The maximum angular rate reference will then be given simply by the product of the guidance gains and the AUV velocity, which must not exceed the angular rate capabilities of the AUV. However, the square root of the product of the guidance gains and the AUV velocity determines the natural frequency of the guided tracking response of the AUV, which should not exceed the minimum bandwidth of the inner-loop controlled plant. This gives the two inequalities shown in **(7.33)** and **(7.34)** below, where $R_{\max}$ is the maximum achievable angular rate of the AUV and $\omega_{\min}$ is the minimum bandwidth of the inner-loop plant. In the case of the AUV, the limits are given in **(7.35)** and **(7.36)** below. The primary limitation of the AUV is therefore its maximum angular rate. This derivation considers only the lateral control of the AUV; however, the same principles would apply to other aspects of the AUV's motion in the same way. Substituting into **(7.35)** with the value in **(7.33)** and the chase guidance gains, which are linked and use only one free parameter, a basic estimate for the minimum value of the chase distance, d, can be obtained as in **(7.37)**. This estimate was found to be too small, however, with a more reasonable value being two to three times higher. Simulations were used to determine that this is largely due to the β dynamics of the AUV, which were assumed to be negligible for this derivation.

$$K_x K_\varphi \bar{V} < R_{\max} \tag{7.33}$$

$$K_x K_\varphi \bar{V} < (\omega_{\min})^2 \tag{7.34}$$

$$R_{\max} = \frac{\bar{V}_0}{\rho_{\min}} \approx 0.13 \tag{7.35}$$

$$(\omega_{\min})^2 \approx 0.25 \tag{7.36}$$

$$d > 5 \tag{7.37}$$

Computational efficiency

The main motivation for redesigning the guidance method found in [18] was to reduce the calculation load needed to perform the guidance. This was achieved by changing the geometry of the problem slightly, which allowed the required calculations to be simplified. The basic steps involved in each evaluation of the guidance are shown below.

1. Calculate velocity magnitude and unit vector.
2. Calculate guidance gain K_c.
3. Find aiming point on the tracking line.
4. Calculate the unit vector pointing from the AUV to the aiming point.
5. Resolve vectors into the plane of interest for the control concerned.
6. Calculate error angle η.
7. Apply guidance gain.

Most of the above steps can be performed using simple vector operations, such as dot and cross products, which use only additions and multiplications. Only four inverse trigonometric functions were used for the implementation of the entire guidance system for all the aspects of control for the AUV, over and above the ones common to all guidance implementations. There are some other calculations that occur at waypoint transitions, but these are common to any guidance implementation. The trigonometric functions would usually consume the most calculation time on microprocessors. This implementation was tested on the AUV, which only used about ten% of its full calculation capacity at any one time. The cross-track error guidance requires even less calculation than the chase guidance.

7.5 Summary of guidance methods

The guidance methods designed in this chapter are both expected to perform better than the current guidance implementation on the AUV. Although the design approaches for each guidance method were very different, the end results, including performance, are very similar for both. The cross-track error guidance uses the perpendicular distance between the AUV and the desired tracking path to calculate controller commands for tracking to the path. The guidance law in **(7.38)** is used to generate a reference travel direction, which is used to command the AUV angular rate through **(7.39)**.

$$r_\varphi = K_x e \tag{7.38}$$

$$r_R = K_\varphi (r_\varphi - \varphi) \tag{7.39}$$

The chase guidance method uses the principle of looking ahead to some chase point along the path and generating controller commands based on the AUV travel direction in comparison to the direction of the chase point on the path. It does so

by generating an angular rate command for the AUV directly through the guidance law in **(7.40)**

$$r_R = \frac{2\bar{V}}{d}\eta \tag{7.40}$$

The chase guidance improves on the calculation load required to execute the guidance method found in [18]. Using the new guidance methods, the AUV can be commanded to track straight line paths with zero steady state error, even in the presence of constant ocean currents. These guidance methods can also command the AUV to track circular paths with reasonable accuracy.

7.6 Waypoint definitions

The new guidance requires a new method of defining waypoints to make use of circular path tracking. The new definition must also be general enough such that both circular and straight line path segments can be followed. As with the chase guidance derivation, the circular case will be covered first and then applied to the straight line case. Instead of defining waypoints, the desired behaviour of the AUV is now governed by specific paths, or way-segments. These will still be referred to as waypoints, preceded by the qualifiers *circular* and *straight line* as the case may be. An arbitrary circular waypoint is shown in **Figure 7.12a**. This circular waypoint may have any orientation in three-dimensional space. The circle on which the waypoint lies can be succinctly described by two unit vectors, a centre point and a scalar radius. The scalar, ρ, represents the radius length of the circular waypoint. The two vectors, $V1$ and $V2$, are perpendicular to one another and both lie in the plane of the circle. Any arbitrary point on the circular path can then be described by **(7.41)**, where θ is the angle created between that point and point P_1. Vector V_1 points to P_1 on the circle, which is defined as the starting point for the path. Vector V_2 is defined as pointing towards a point which is $\pi/2$ radians along the circular path from P_1 in the direction of travel. The path then extends to point P_2 through angle ϑ, which marks the end of the waypoint. This angle is measured from zero and can be defined beyond a single revolution.

$$P = \rho\left(V_1\cos(\theta) + V_2\sin(\theta)\right) + C \tag{7.41}$$

Each waypoint is passed to the guidance system as an eleven-element array. The array consists of the following components, in order:

- three-element unit vector $V_{1_{xyz}}$
- three-element unit vector $V_{2_{xyz}}$
- three-element centre coordinate C_{xyz}

- Scalar circle radius ρ
- Scalar angular displacement ϑ

The angular displacement ϑ is given a negative sign when the circle is to be followed in a counterclockwise direction when viewed from above.

A straight line segment can be described more easily than can a circle, so the eleven-element array can be filled with whatever information would be most useful to the guidance calculations. As such, when the desired path is a straight line, as in **Figure 7.12b**, the array consists of the following

- three-element starting point $P1_{xyz}$
- three-element ending point $P2_{xyz}$
- three-element unit vector from P_1 to P_2, V_{xyz}
- Scalar less than 1
- Scalar displacement x

The tenth element of the array is used to inform the guidance that this is a straight line waypoint. Some of the information in this array is redundant, but the amount of data is small; therefore this definition is retained for simplicity. In the case of both circular and straight line waypoints, the AUV is considered to have reached its destination once it has travelled past the desired displacement value in the array. This method of updating the waypoints avoids the problem of the AUV circling the final waypoint indefinitely because it is unable to enter a region close enough to the final waypoint. This situation is usually completely avoided in any case by tracking paths and not just points.

7.7 Complete control and guidance system implementations

The designs discussed in previous chapters can now be combined into complete systems capable of commanding meaningful behaviour from the AUV. A number of possible final implementations are presented in the next section, with the focus on one recommended implementation. These various designs were compared in simulation to establish the advantages and disadvantages of each. In particular, the differences between the current implementation and the recommended one are highlighted.

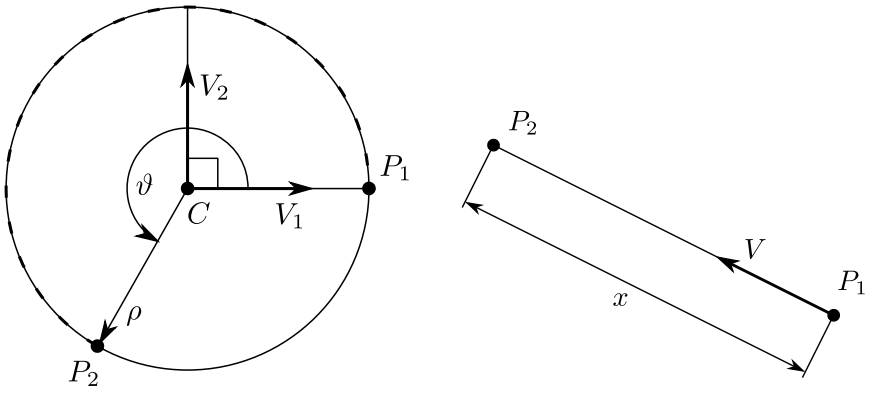

(a) Circular waypoint (b) Straight line waypoint

Figure 7.12: New waypoint geometric definitions

Recommended implementation

The design of the recommended guidance and control system is covered in this section. This system is both robust and flexible. Using the new waypoint system, a number of interesting path combinations can be constructed. The simulation results in the next chapter show this implementation to have excellent tracking, even when the commanded tracking paths have aggressive bank angles. Either of the new guidance designs could be used for this implementation. The chase guidance was used for this implementation in simulation.

Roll control

The roll control of the AUV is performed by providing a reference roll angle to the roll attitude angle controller, which commands the innermost control loop that regulates the roll rate of the AUV. The reference roll angle is set such that the Z^B-axis of the AUV is parallel to the normal vector of the plane of the current waypoint. For a circular waypoint, this would be the plane in which the circular path lies. For a straight line waypoint, this would be the plane that results in zero AUV roll when the AUV is tracking the line perfectly without disturbance. Commanding the AUV roll angle in this way means that the other aspects of the AUV's motion are decoupled during tracking. For example, when the AUV is tracking a circular waypoint which is tilted it does not need to track changing references for pitch and yaw rates, but is essentially commanded as it would be for a circular waypoint lying in a perfectly horizontal plane. If this is performed correctly, all pitch commands should control only the perpendicular displacement of the AUV from the plane of waypoint and all yaw commands should control only the displacement of the AUV in planes of motion with the same orientation as that of the plane of the waypoint.

This is possible with AUV guidance because of lack of a lift vector required by the AUV to avoid sinking, as opposed to UAV guidance designs. An example of this is given in **Figure 7.13**, where the AUV is approaching the straight line waypoint from a distance. As the AUV gets closer to the line, the yaw controller will begin to point the front of the AUV towards P_2. When this happens the roll angle of the AUV will tend to zero, and the pitch angle will tend to align itself with the line joining P_1 and P_2.

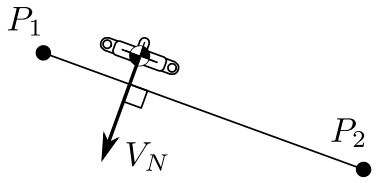

Figure 7.13: AUV alignment with waypoint plane

Pitching control

Following the successful implementation of the roll controller described above, the pitch control of the AUV is now relative to the plane of the waypoint. The pitch control is used to reduce the perpendicular distance between the AUV's current position and the plane of the waypoint. A modified form of the chase guidance method is used to command the pitch rate control loop. The aim point for the chase guidance is not located on the tracking path, but is always located in the plane of the waypoint, directly ahead of the projected position of the AUV onto the waypoint plane. Thus, the pitch control influences only the AUV's perpendicular distance from the waypoint plane. The pitch control of the AUV must be constrained, however, or else it will couple into the roll and yaw aspects of the AUV's motion, essentially creating disturbances for the other control loops. Once the AUV is travelling in the plane of the waypoint, however, this will not pose a problem. The chase distance for the guidance was redesigned for the pitch control, using the same design procedure as in **Section 7.2**, with the chase distance being set at 22m. Naturally, this can be easily performed using cross-track error guidance as well.

Yaw control

The yaw control of the AUV is now used only to steer the AUV parallel to the plane of the waypoint. This is done using the chase guidance algorithm, as it was described in **Section 7.2**, with a chase distance of 15m. The guidance provides reference commands to the yaw rate control loop.

Other designs

A number of other guidance designs were implemented for comparison purposes in simulation and for physical testing. None of the other designs has circular waypoint tracking abilities, so comparisons took place with straight line waypoints only.

Basic cross-track error guidance

A full design using the basic cross-track error guidance was implemented in simulation for comparison with the recommended implementation. This design was simpler than the recommended one, however, with the AUV roll angle always referenced to zero. For most situations, the difference is unnoticeable and this design is essentially the same as the main design, except that it uses the basic cross-track error guidance method for both the pitch and yaw control. Due to the nature of this guidance method, the guidance provides attitude angle references to the pitch and yaw angle outer control loops, which each command inner rate control loops. This design was tested to demonstrate the poor performance of attitude angle based guidance methods, especially in the presence of disturbances.

IMT comparative design

A modified version of the recommended implementation was developed, where the waypoints are modified during operation to mimic the behaviour of the IMT control system. Initially all waypoints are redefined such that the depth-based guidance of the IMT would be emulated, instead of smooth linear transitions between waypoints at different depths. In order to emulate the IMT yaw guidance method of heading directly towards the next waypoint, new straight line waypoints are created on-the-fly. An example of this situation is shown in **Figure 7.14**. Assuming the AUV enters the straight line waypoint ($P_1 \rightarrow P_2$), as shown, its usual path when guided by the original system would be as indicated by the dashed line. To mimic this behaviour, this design creates the new waypoint ($P_n \rightarrow P_2$) shown in red, as it faces P_2, which then becomes its new tracking path. Without disturbances, this design should have a very similar response to the current IMT design. However, under the influence of disturbance currents, this new design should maintain the same tracking path that would be created in the absence of disturbances, whereas the original IMT guidance will have a different tracking path. This design presents a more reliable practical implementation for simply aiming for points, which is the goal of the IMT guidance.

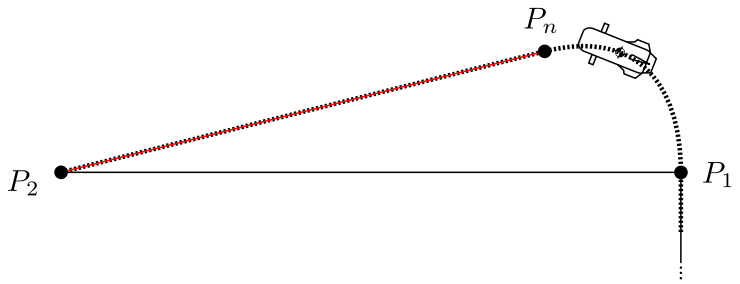

Figure 7.14: On-the-fly waypoint modification for IMT comparative guidance design

7.8 Chapter summary

In the first half of this chapter, two new guidance methods were designed which are both capable of tracking line paths with zero steady state error in the presence of constant current disturbances. These new guidance designs also make it possible to command the AUV along a circular path with good tracking ability. This necessitated a redesign of the waypoint system used by the AUV to one which is defined in terms of paths rather than points. The paths can be either straight line or circular paths. The last section in this chapter covered the implementation of the full control and guidance system which could be used to command the AUV along desired paths. The various final implementations will be compared, along with the current system, in the simulation chapter which is to follow.

Chapter 8

Simulation

Simulation formed the basis for most of the testing and analysis of the control system designs, since use of the physical AUV was constrained by weather conditions and AUV availability. The original simulation environment was developed in SIMULINK as part of the work performed in [1]. This simulation environment was updated and added to in this project so that the new features could be tested. The basics of the simulation environment are reviewed in this chapter, followed by simulation results. A number of different control and guidance configurations were tested and are compared in this chapter to demonstrate the capabilities of each.

8.1 Overview of the simulation

The basic elements of the simulation, as obtained from work performed in [1], are shown in **Figure 8.1**. The block on the right is a full six degrees of freedom equation block that calculates the rigid body motions of the AUV based on force and moment inputs and a number of constant parameters such as the AUV mass and inertial tensor. The block on the left handles all the mathematics specific to the AUV model, that is, the thruster, buoyancy, gravity, actuator and hydrodynamic aspects of the AUV. These are all contained within a single subsystem in the main simulation, in the block labelled AUV, as seen in **Figure 8.2**. The main simulation can accept user input through a joystick interface. In addition to any graphs and plots that SIMULINK can generate, the output of the simulation can be seen in a graphical front-end, which shows a three-dimensional graphical view of the current state of the simulation. This extension to the simulation was also created as part of the work done in [1]. This is extremely useful for interactive simulations and for getting an intuitive feel of how the AUV behaves in simulation. A small function was coded to synchronise the simulation time-scale with the computer timer, to give a near realtime simulation rate when needed. The guidance and controller blocks, which

contain the various AUV control and guidance implementations, are also pictured in **Figure 8.2**.

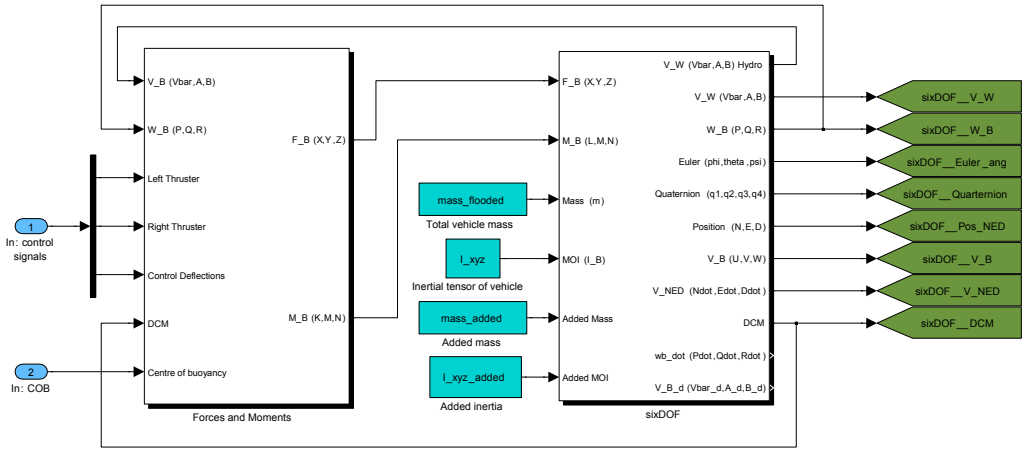

Figure 8.1: The original simulation section created in [1]

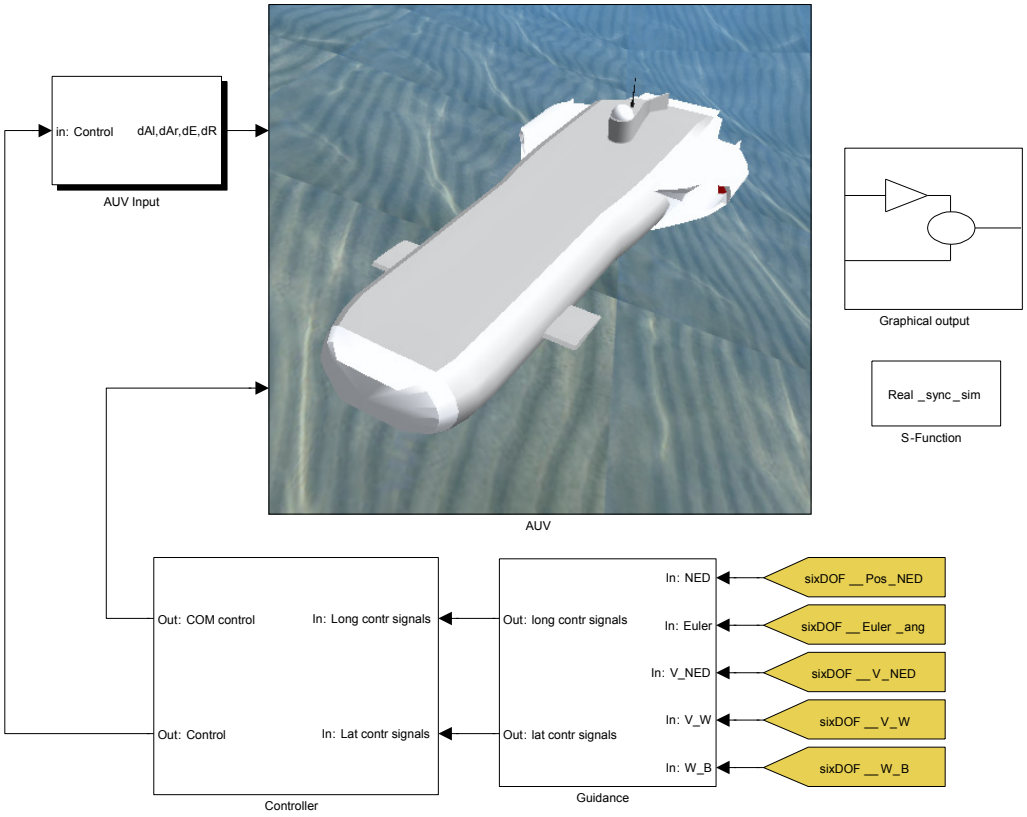

Figure 8.2: The top level of the SIMULINK simulation

8.2 Additions to the simulation

A number of additions to the simulation environment were necessary to include the new control designs into the simulation. These additions are summarised below.

- AUV input non-linearities, fin actuator quantisation and fin actuator slew rate limits
- Continuous time controllers
- Digital controllers and guidance systems
- Serial port interfaces for the input and output of the AUV software and HIL capability.

Controller implementations

In the initial phase of controller testing, the controllers were implemented as continuous time controllers using standard SIMULINK blocks. The controllers were later implemented in digital form. In order to avoid inconsistencies and unnecessary time consumption associated with recoding controllers, the controllers were coded into a standard dynamic link library (DLL) using C code. This library could then be loaded by SIMULINK for use directly in the simulation and also into the Delphi code on the AUV. Simple wrapper functions were all that was needed to interface with the DLL in both cases. General PI controller functions were coded that would automatically implement the Euler transformed digital controllers, given values for the proportional gain, integral gain, sample time and saturation value for the integrator wind-up protection which was also coded into the function. Due to the complicated nature of the guidance, this was implemented only in code, and not in SIMULINK itself.

AUV software interface

The controller designs were initially tested in simulation, with the end goal of physical implementation in mind. To this end, not only the controller designs, but also the software that runs on the AUV itself, was incorporated into the simulation. A virtual environment was created for the AUV software such that it could be tested in simulation and transferred directly onto the physical vehicle for sea trials. This was achieved by creating virtual serial port interfaces with SIMULINK, to mimic the physical serial ports to which the software would usually connect. The AUV software communicates with all its peripherals using serial ports. Although it interfaces with numerous devices, only two are of concern for its incorporation

into the simulation environment. All the actuators on the AUV are controlled by a single control board, which interfaces to the AUV software on a single serial port. This board controls the fin actuators as well as the thrusters on the AUV. All the sensor data for the AUV is handled by the IMU, which also communicates with the software on a single serial port. Virtual serial port pairs were then created which could be used to connect the software to SIMULINK. One of the ports in each pair must have the same port name as the corresponding port on the AUV to which the AUV software connects. C-coded S-functions were then created which allow SIMULINK to connect to the corresponding virtual serial ports to communicate with the AUV software. The S-function code also needs to emulate the IMU and control board communication protocols.

Following the successful implementation of this, these virtual ports can be replaced with physical serial ports to connect the actual AUV to the simulation. The AUV hardware can then be run in a hardware-in-the-loop (HIL) simulation, where the simulation environment *fakes* the sensor inputs to the AUV. The AUV hardware will then send the actuator commands to the simulation, which can then simulate the behaviour of the AUV. HIL provides a very useful testing and validation tool for new designs and removes part of the risk involved in testing new designs in physical trials.

The software on the AUV is usually controlled remotely from a ground station, via a wireless connection. The AUV software also interfaces with the wireless communication board using serial ports. The ground station is used, among other things, to initialise the tracking mode and start the guidance. This, too, was later emulated and added to SIMULINK using another virtual serial port pair, so that the AUV software would start automatically with the simulation. This is not crucial for incorporating the AUV software into the simulation environment, though.

The block diagram in **Figure 8.3** shows the basic interconnections in the final simulation environment. The control input for the AUV can be switched between manual control, SIMULINK implemented control and HIL control.

8.3 Simulation results

To compare the different control and guidance implementations, the same set of waypoints was run using different implementations under different conditions. This set of waypoints was used to gauge the lateral tracking abilities of the various guidance methods and thus all waypoints were defined to lie in the same horizontal plane. First an undisturbed trial was simulated, followed by trials with 0.3m.s^{-1} constant currents flowing from east to west and then from south to north. In each of the following figures, the results of a specific implementation under these three

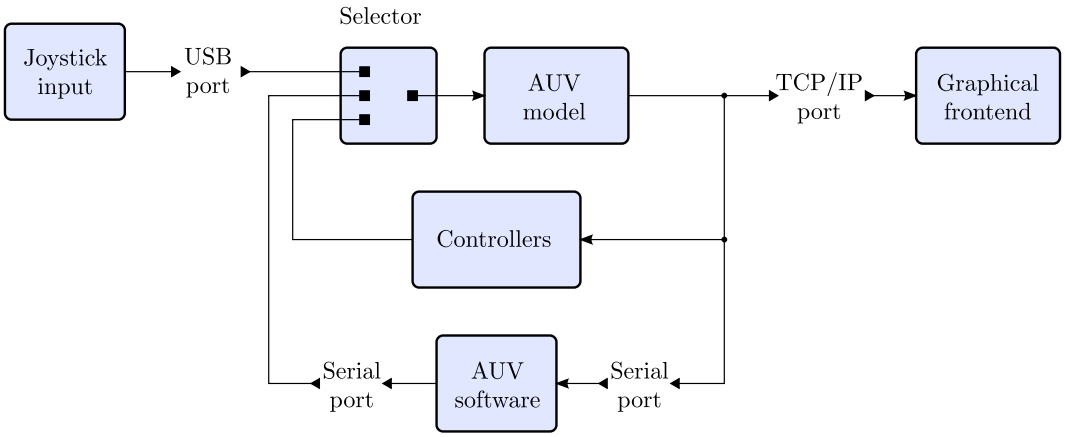

Figure 8.3: Simulation interconnections

different conditions are shown from top to bottom. All figures have the same legend, as shown in **Figure 8.4**.

The first set of plots, shown in **Figure 8.5**, shows the path taken by the AUV as guided by the current IMT guidance implementation. The effects of the disturbance currents are quite pronounced and significantly change the path taken by the AUV. The AUV is seen to often miss the centre of the waypoints by a few metres and has a noticeably curved travel path between certain waypoints.

The second set of plots, shown in **Figure 8.6**, shows the path taken by the AUV as guided by the recommended implementation. The tracking results are much more consistent than in **Figure 8.5**. The biggest differences in tracking path occur when the controller is essentially open-loop, due to actuator saturation. This is most evident in the transitions between waypoints.

The third set of plots, shown in **Figure 8.7**, shows the path taken by the AUV as guided by the IMT comparative implementation, which is a modification of the recommended one. This implementation is slightly more aggressive than IMT's one, with visible overshoot after each turn as it tracks to the newly created guidance line. This, however, results in less overshoot at the end of each waypoint section. Otherwise, the response is very similar to the one the AUV would usually have. As with the recommended implementation, the tracking results are much more consistent than in **Figure 8.5**, with the inconsistencies appearing in the turns at the beginning of waypoint sections. This is the most efficient tracking path in terms of time and energy usage, since the AUV is always heading directly for the end points of the tracking path sections.

The fourth set of plots, shown in **Figure 8.8**, shows the path taken by the AUV as guided by the basic cross-track error based implementation. These results are similar to those of the recommended implementation. As predicted, the disturbance currents result in tracking offsets when using this implementation. Based on the

plots, the maximum tracking error displayed is 2.2 m. This is close to the predicted 2.38 m, obtained from the linear approximation formula for the offset error in **(8.1)**.

$$\begin{aligned} e &\approx \frac{V_C}{\bar{V} K_{x_{p_\Psi}}} \\ &= \frac{0.3}{(1.4)(0.09)} = 2.38 \end{aligned} \tag{8.1}$$

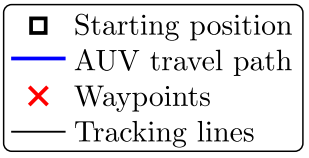

Figure 8.4: Simulation results legend

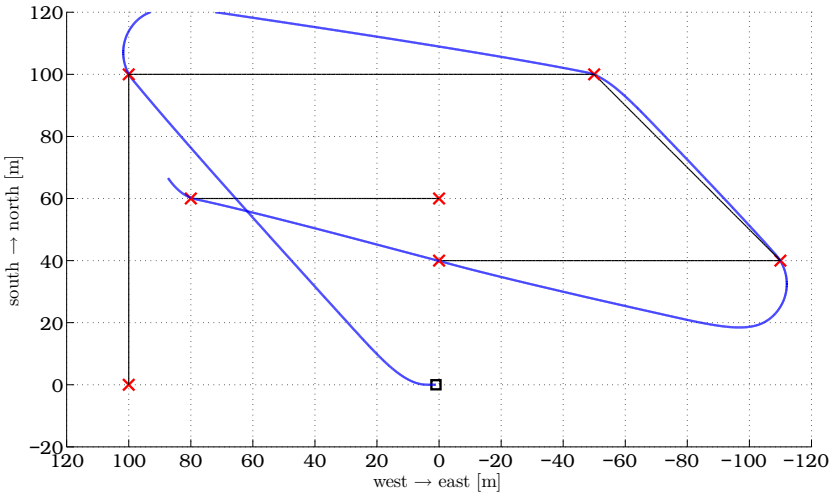

(a) Undisturbed

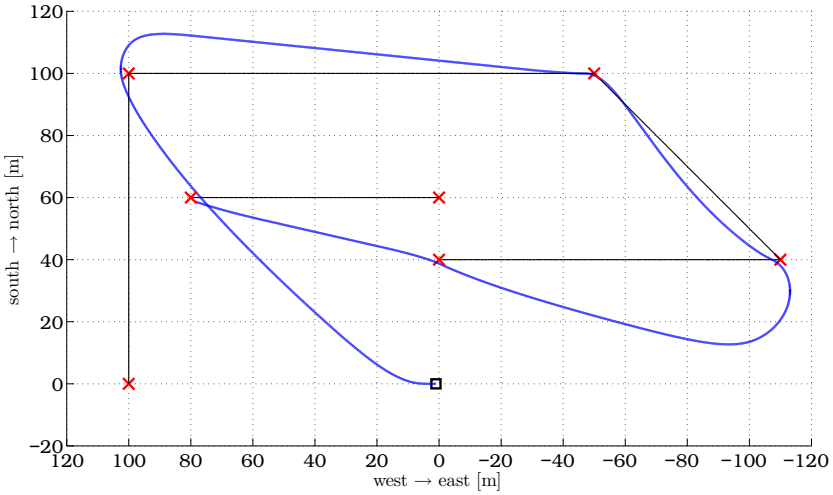

(b) East to West 0.3m.s^{-1} disturbance current

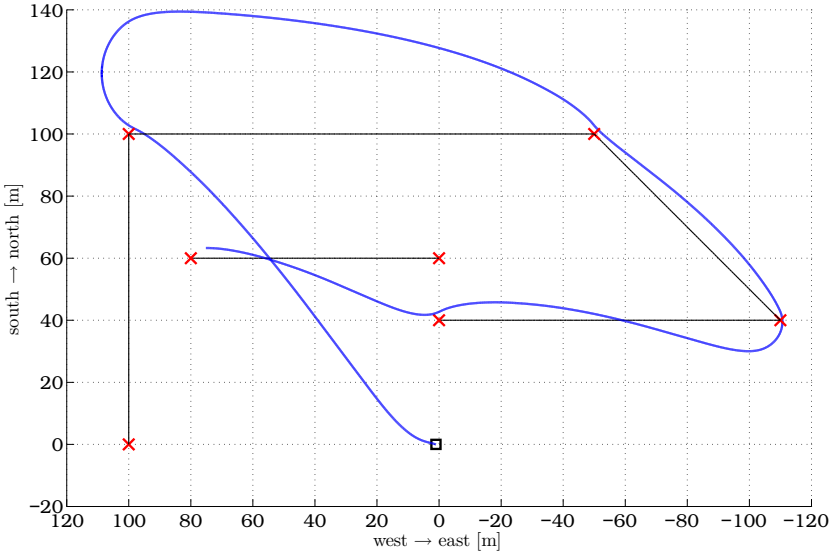

(c) South to North 0.3m.s^{-1} disturbance current

Figure 8.5: Guidance comparison simulation results (top view): current IMT guidance

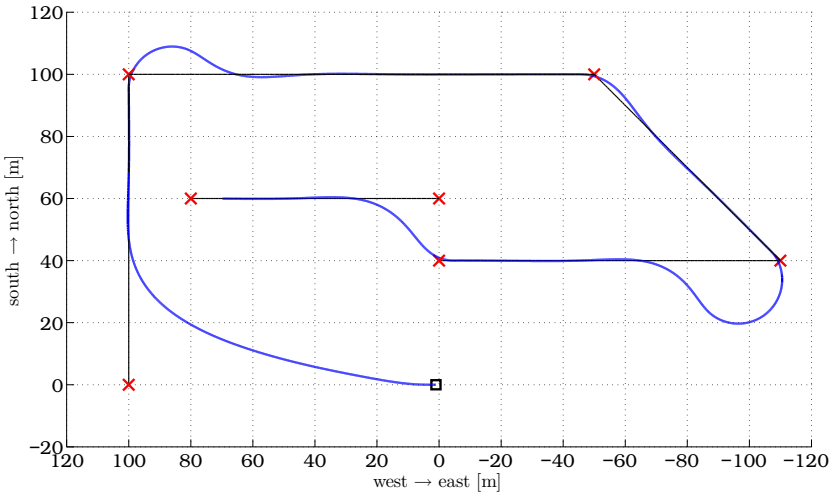

(a) Undisturbed

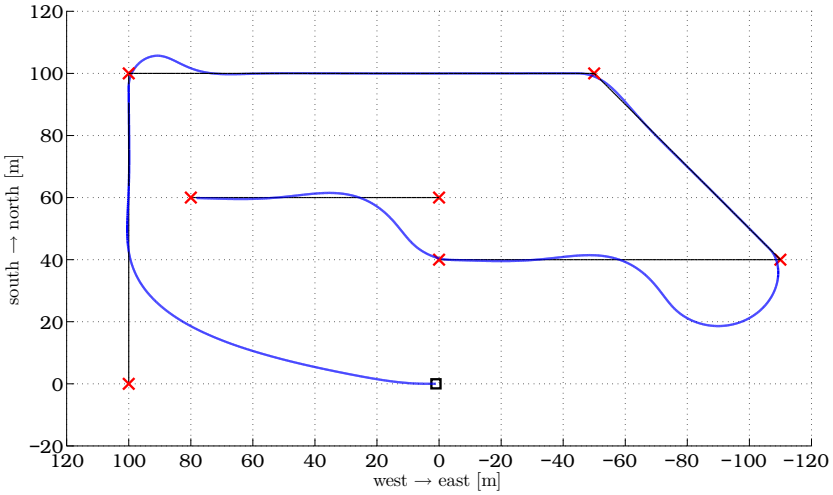

(b) East to West 0.3m.s^{-1} disturbance current

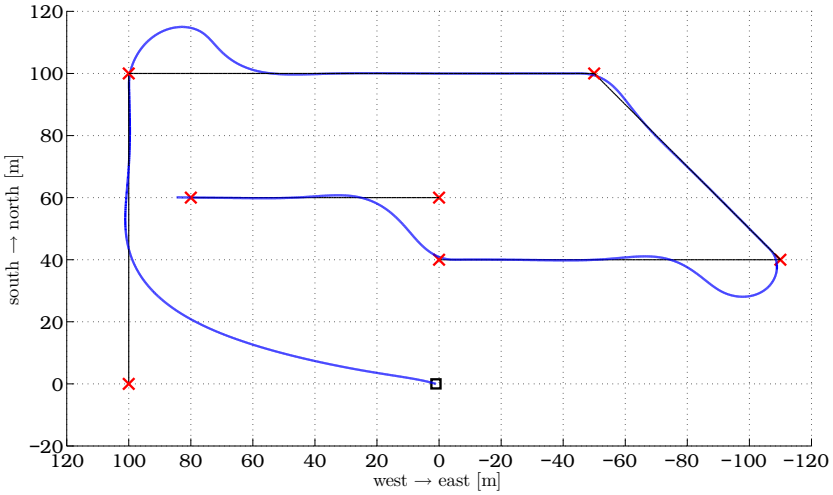

(c) South to North 0.3m.s^{-1} disturbance current

Figure 8.6: Guidance comparison simulation results (top view): chase guidance

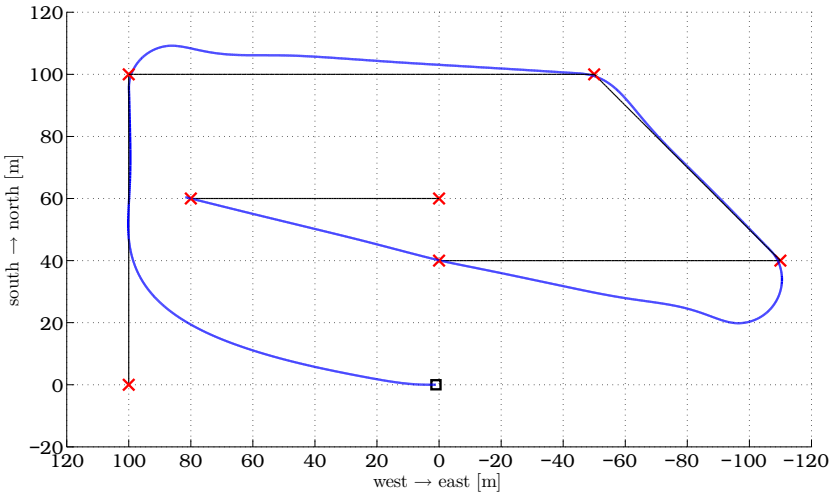

(a) Undisturbed

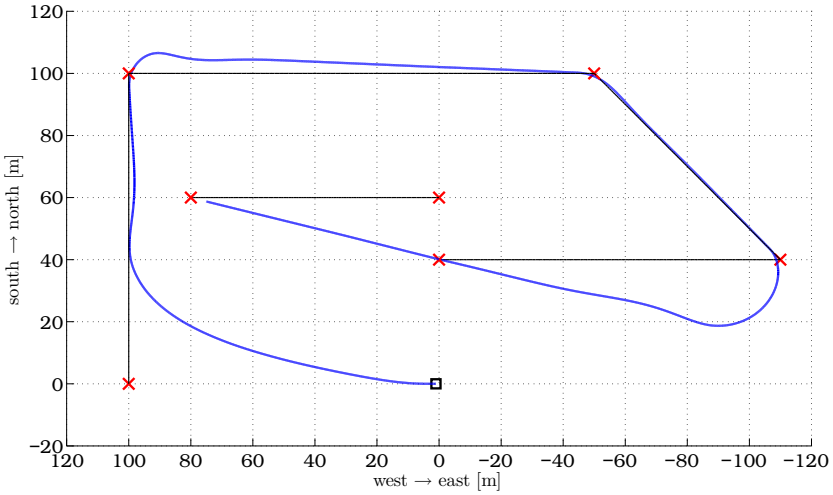

(b) East to West 0.3m.s^{-1} disturbance current

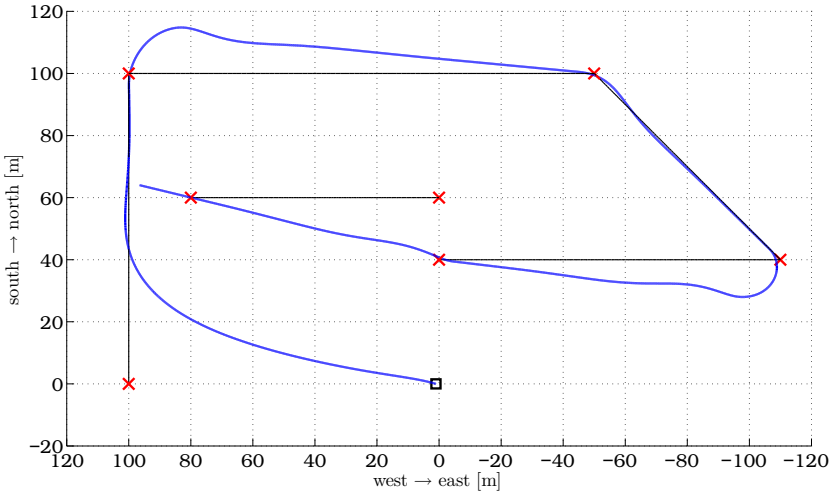

(c) South to North 0.3m.s^{-1} disturbance current

Figure 8.7: Guidance comparison simulation results (top view): IMT comparative guidance

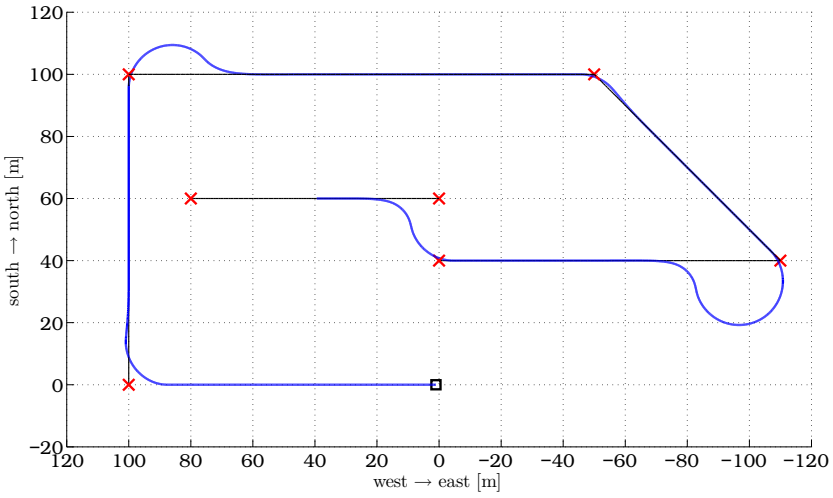

(a) Undisturbed

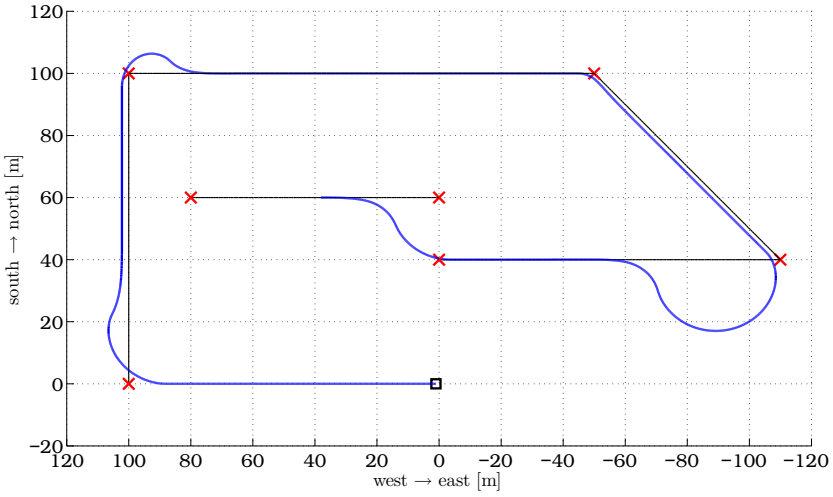

(b) East to West 0.3m.s^{-1} disturbance current

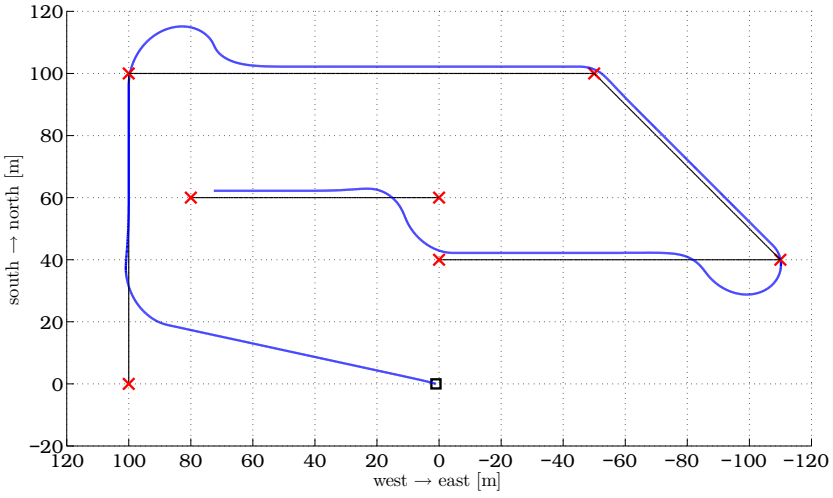

(c) South to North 0.3m.s^{-1} disturbance current

Figure 8.8: Guidance comparison simulation results (top view): cross-track guidance (proportional only)

In order to display the capabilities of the recommend implementation, a set of complicated, aggressive waypoints was set up and the AUV tracking path simulated. The course consists of the following:

- Straight line → banked large $\frac{3}{4}$ circle → banked tight $\frac{3}{4}$ circle → straight line
- Detached parallel straight line at different depth → medium $\frac{1}{2}$ circle
- Detached sloping straight line to end

This set of waypoints and the simulated AUV travel path are shown in orthographic layout in **Figure 8.9**. The first section demonstrates the circle tracking abilities of the AUV and transitions between smooth connected waypoints. The transitions between waypoints are almost completely seamless, with very little noticeable deviation from the tracking path. The circular waypoints are banked at 30° and present little problem to the guidance.

The second section demonstrates transitions between unconnected waypoints and convergence to the tracking path when the AUV is not already near the path. In this case, the transition demands a depth and full direction change from the AUV.

The final straight line waypoint demonstrates convergence to a path from a distance, with the focus on the plane-based dynamics of the AUV. This transition highlights how the guidance is based on the plane of the waypoint, with the AUV seemingly always on the path when viewed from south to north. This path also demonstrates clearly how the guidance is path based and not point based. The starting point of the line could have been extended along the line to any point west of the end point and the path of the AUV would not have changed.

The same set of waypoints was simulated again, but with a 0.3m.s^{-1} constant current disturbance flowing from west to east. The travel path of the AUV is mostly unchanged. The disturbance has the largest impact on the AUV travel path during very aggressive manoeuvres. This is most noticeable when trying to track the banked tight circular path. The other circular paths are also not tracked perfectly, since they essentially change the constant current disturbance into a variable one. However, this tracking error is only 0.7 m at most.

8.4 Chapter summary

The simulation results in this chapter demonstrate clearly the disturbance rejection and tracking abilities of the new control and guidance design over those of the current system implemented on the AUV. The new guidance system's capabilities in tracking a wide variety of different path sequences, transitions and types was also demonstrated.

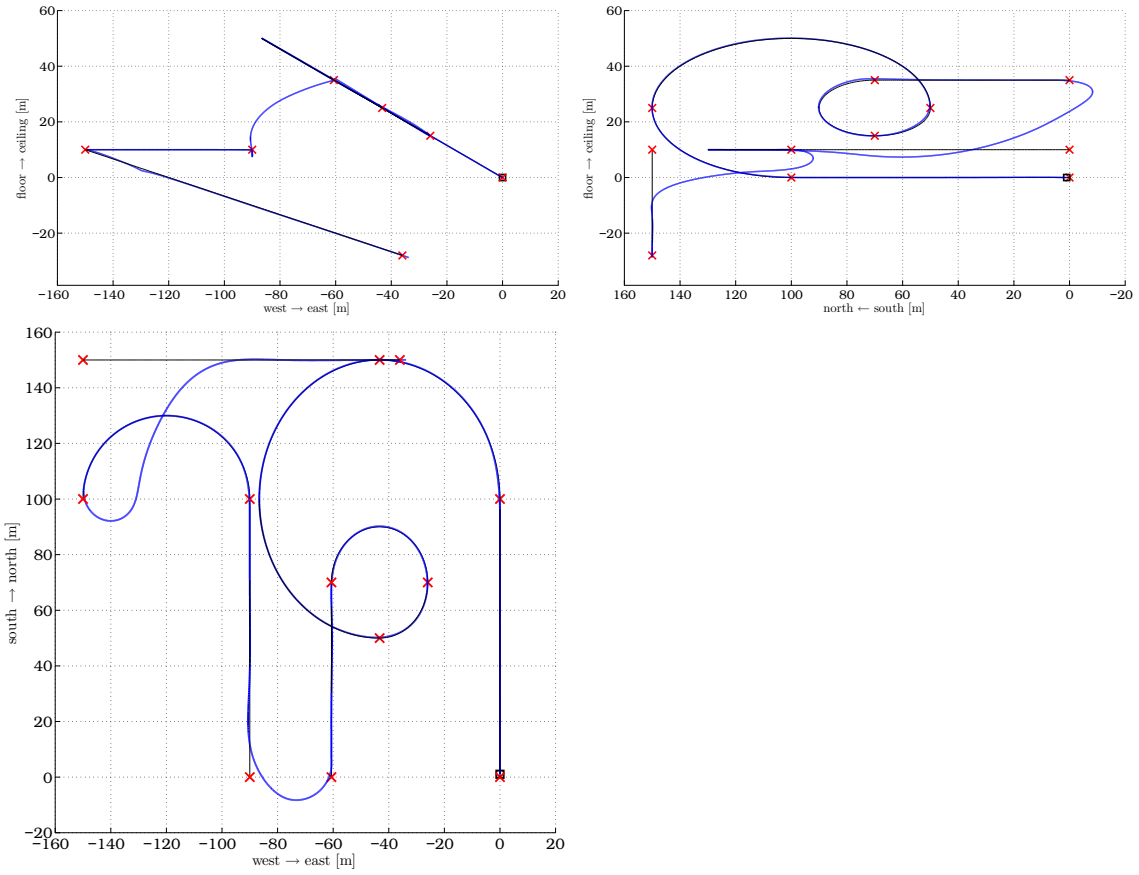

Figure 8.9: Orthographic views of simulated travel path of the AUV“

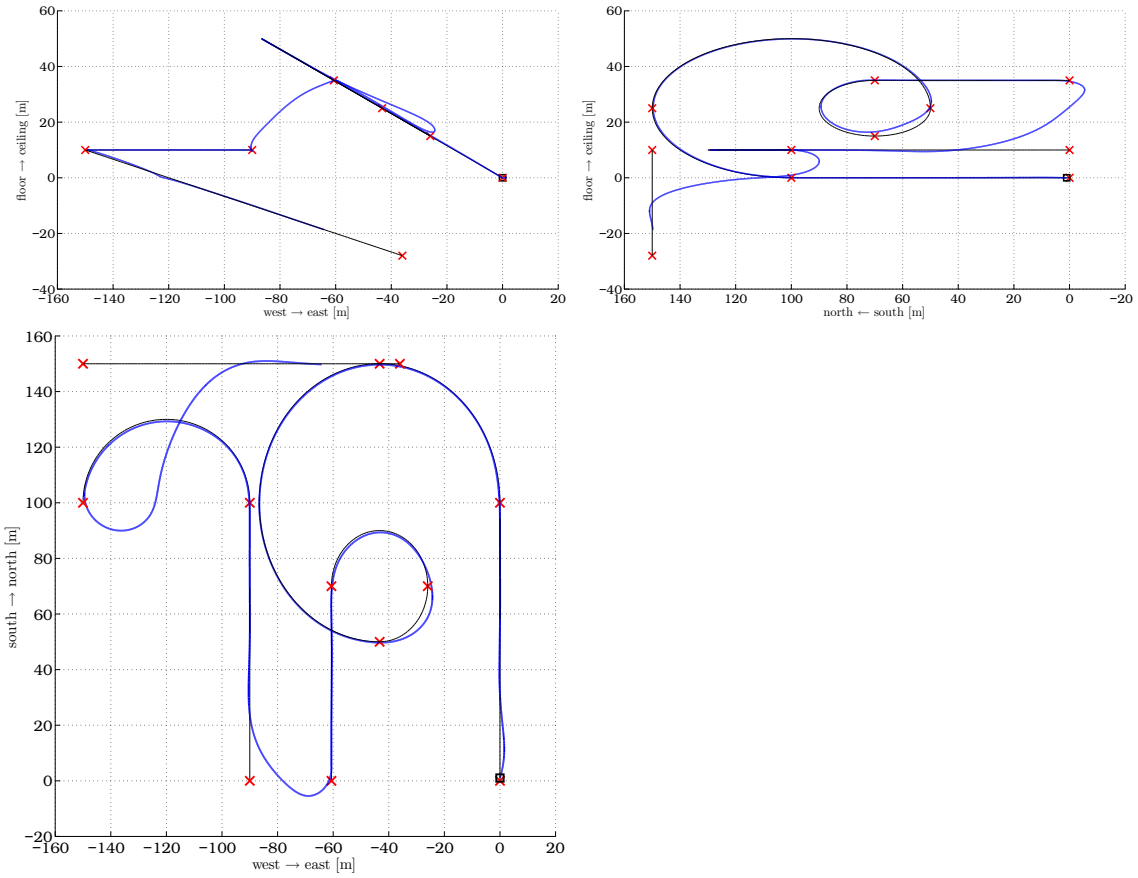

Figure 8.10: Orthographic views of simulated travel path of the AUV with disturbance

Chapter 9

Physical Testing

In order to verify the work detailed in this thesis a practical implementation of the new control and guidance systems was created, with the intention of testing it in sea trials. This chapter summarises the changes and additions made to the AUV in order to run the new designs in practice, and discusses the results from the sea trials that were performed.

9.1 Changes to AUV software

A number of problems were identified in the original Delphi code for the AUV software. The corrections and additions to the software are detailed in **Appendix B** and discussed briefly in this section. The serial port names had to be changed to be compatible with recent versions of the Microsoft Windows operating system. This was necessary for testing the software in simulation before using it on the physical AUV. The north and east position measurements were interchanged in the AUV software. This was not immediately evident and caused no problems in the original code, because the measurements were mistakenly used incorrectly, which cancelled the effects of the measurement being interchanged. The most critical error with the AUV software resulted in inconsistent measurement sample times. This is clearly seen in **Figure 2.5** which appears in **Chapter 2**. The problem was caused by the algorithm used to decoded the data string received from the IMU. The data string is headed by a particular byte value. If this byte was present later in the data string, the algorithm would discard that data string, causing that measurement sample to be skipped. This was fixed by correcting the decoding algorithm. The IMU is used to set the controller sample rate by setting how often the IMU sends its measurement data to the AUV software. The fin actuator updates used to be timed independently of the controller, but these were also changed to update with the controller calculations. Besides these corrections, the necessary code for loading

and incorporating the control and guidance functions from the DLL into the AUV software was added. It is also noted here that the rudder fin convention on the AUV is opposite to that of the model, so the controller output needs to be inverted before the command is sent to the AUV.

9.2 Test results

Three basic sets of test waypoints were prepared for the first day of testing. The first test consisted of a single straight line waypoint of constant depth of 5 m, with a mission timeout set for 3 minutes. The mission timeout is a safety mechanism, implemented by IMT, which cuts all the AUV controls after the timer has expired. The AUV then simply floats up to the surface. The primary goal of this initial test was to determine if the control system was stable.

The second set of test waypoints was again a straight line travel path, but with two 5 m step changes in the path depth. The first step change increased the path depth from 5 m to 10 m. The second step change decreased the depth back to 5 m. The aim of this test was to evaluate the performance of the longitudinal control of the AUV.

The final set of test waypoints for initial testing consisted of four straight line segments at constant depth, in a zigzag pattern with 90° turns, the aim of which was to evaluate the performance of the lateral controllers on the AUV.

The first test was run, with poor results. Only the relevant points are discussed here. Data regarding the longitudinal motion of the AUV is plotted in **Figure 9.1**. It is clear from depth data that the AUV hit the sea floor about 70 seconds into the test. This is evident from the sudden halt in depth change, and from the downwards velocity plot, which quickly jumps to zero. Once it had started pitching down, the AUV could not recover until it hit the sea floor. The reason for this is that the AUV is not trimmed correctly. In order to get the AUV to dive below the water surface it is ballasted such that its nose dips into the water. This results in an elevator trim position that is very near its lower limit. This was observed in the previous test results from IMT, as shown in **Figure 2.3** in **Section 2**. In this test, the elevator simply saturated and the AUV was unable to pitch up again. After hitting the sea floor, the AUV managed to recover and tracked the specified depth of 5 m for a short while before the mission timeout occurred. During this time, the elevator trim was also observed to be near the lower limit of its full actuation range.

In an attempt to improve these test results, the AUV was set to limit its pitch to within ±0.1rad. The test was run again, with the same poor results. It would probably be necessary to implement a pitch rate limit on the AUV in order to avoid this unrecoverable pitch condition. However, good performance can never

be expected from the AUV unless its trim is corrected such that the elevator can be operated without saturating.

Other useful results obtained from this test regard the velocity magnitude of the AUV. It was assumed previously that no speed control was necessary and that the AUV speed was fairly constant at about 1.3m.s^{-1}. A plot of the AUV speed during the test is shown in **Figure 9.2**. The plot shows that the AUV reaches a top speed of 2.2m.s^{-1}, which is almost double the value that is expected and used for modelling. The AUV most likely reached this speed because it was aided by the upwards buoyancy forces as it headed towards the water surface after hitting the sea floor. The AUV did not appear to suffer any extra overshoot or instability in its responses as it tracked to the desired depth of 5 m, though. This suggests that the controllers are robust enough to cope with this increase in speed. This is especially important, since the AUV will shortly be upgraded with new, more powerful thrusters.

No other useful data was gathered from the day of testing. Following that, the AUV has been unavailable for further tests as it is being upgraded by IMT. One of the upgrades is a much-needed boost to the thrust power of the AUV.

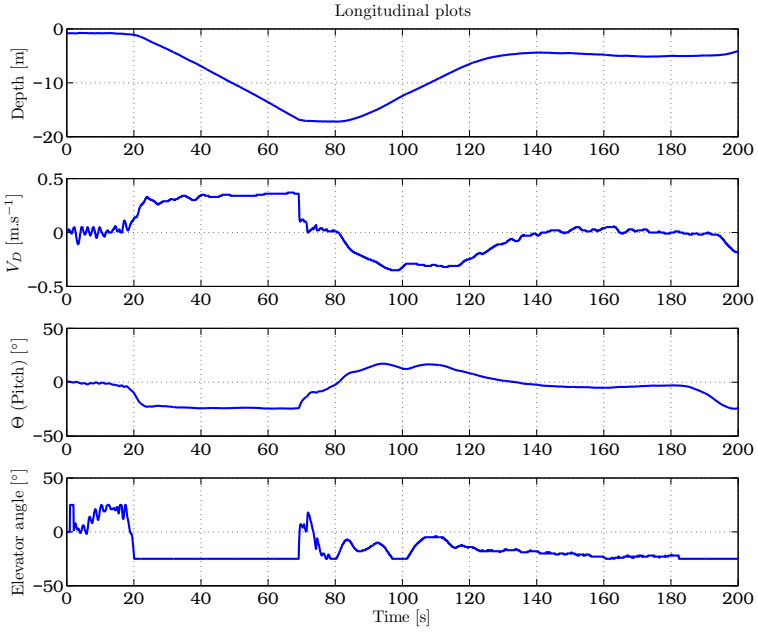

Figure 9.1: Test results: longitudinal data plots

9.3 Chapter summary

It is clear from the test results that before any other developments on the AUV can occur, the physical build needs to be improved. These improvements are possible

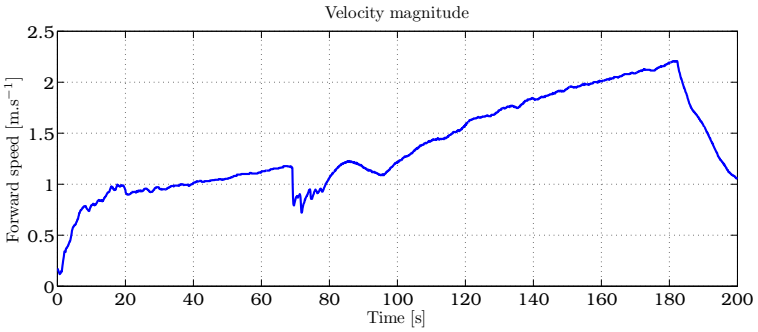

Figure 9.2: Test results: velocity magnitude

in a number of areas. Most importantly, if the current hardware is to remain intact then the AUV must be correctly trimmed so that all control surfaces have maximum possible dynamic actuation range. The control surfaces themselves could be made more effective by either increasing their sizes or placing them behind the thrusters to increase the fluid flow over them. In light of the data shown in **Figure 9.2** and the upgrading of the AUV thrusters, it may be necessary to implement speed control on the AUV. A positive outcome of the tests is that the longitudinal controls and guidance performed as expected when the elevator was not saturated.

Chapter 10

Conclusions and Recommendations

This thesis presented the work performed in designing new movement control and guidance systems for the IMT AUV. This work included the following. Existing test data from trial runs with the AUV was analysed. This analysis was used to gain insight into the behaviour of the AUV in both controlled and uncontrolled responses. This information was used in the assessment of the existing AUV control and guidance systems as well as for validating and updating the mathematical model of the AUV. The existing control and guidance systems on the AUV were analysed to quantify their performance and later compared to the upgraded designs created in this thesis. The mathematical model used for control design was partially validated and updated, based on work presented in [1]. Following this, new control and guidance systems were designed to improve the movement performance of the AUV. The new designs increase the tracking performance, stability, robustness and flexibility of the AUV movement. The existing designs as well as numerous theoretical designs were compared in simulation to gauge the expected performance of each. Finally, some practical tests were performed with the AUV using the new designs.

Analysis of the test data revealed that the AUV is poorly trimmed. The nominal control surface positions as well as the AUV attitude in the water have steady state offsets which limit the controllability of the AUV and increase the likelihood that it could become unstable. A problem with an unreliable measurement sampling time was also revealed. This was corrected by a simple change in the AUV software.

The mathematical model for the AUV, presented in [1], was linearised and simplified for control design purposes. Some of the model parameters were adjusted or recalculated based on the analysis of the existing IMT test data. Some important

modifications were made regarding the buoyancy and roll-related aspects of the mathematical model.

The existing control and guidance systems leave the AUV vulnerable to disturbances and the offset errors mentioned above. The primary weakness comes from the guidance system. The point-based guidance does not regulate the AUV's movement well when it is not near to the next target waypoint. This was rectified by a complete redesign of the control and guidance systems. The control systems were changed from proportional controllers using attitude angle feedback to proportional and integral controllers using angular rate feedback. The guidance systems which provide the controller commands were modified to track paths between waypoints instead of aiming for single points. This was shown in simulation to be very effective at making the AUV movement more predictable and reliable.

In the control design in **Chapter 6**, a theoretical augmentation to the current controllers was suggested. This augmentation considered the possibility of control using a relative shift in the centre of mass and centre of buoyancy positions of the AUV. This ability could be used to create an auto-trimming controller, which would ensure that the AUV is always trimmed correctly, even in varying environmental or other operating conditions. This would then afford the full dynamic range of actuation to the standard fin control surfaces, improving the general performance of these control surfaces. This would also cater for the problems in trim from which the AUV currently suffers.

The practical tests on the AUV were not very successful. This was mostly due to the poor trim of the AUV. The AUV essentially became unstable as it could not recover due to actuator saturation. The trim of the AUV must definitely be corrected to afford the control surfaces their full dynamic range of actuation.

Appendix A

Hydrodynamic and control derivative data

Plots of the hydrodynamic and control derivative data.

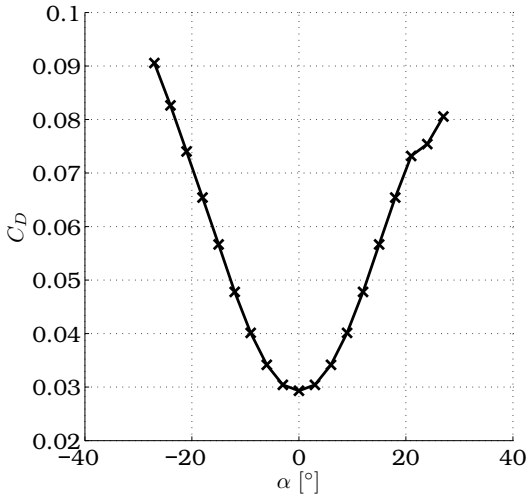

Figure A.1: Dimensionless hydrodynamic derivatives of the drag force

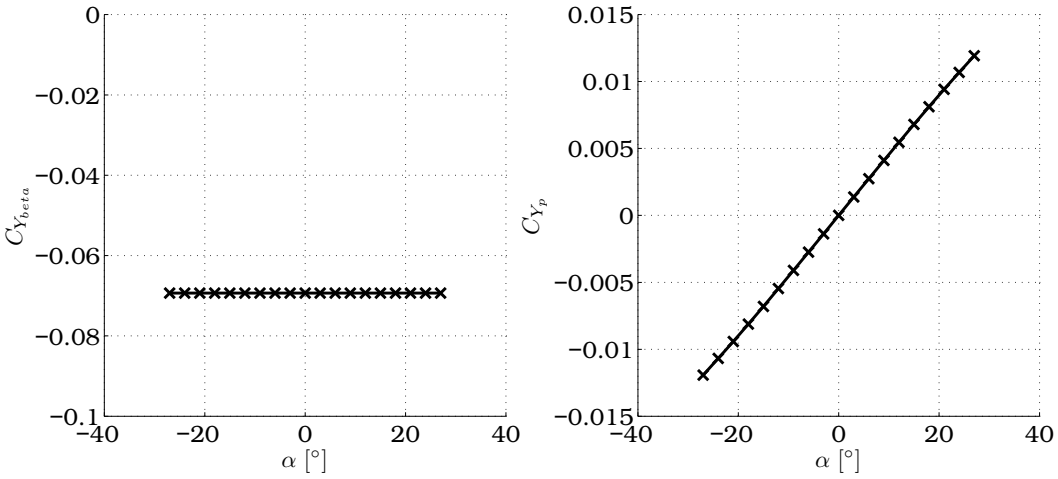

Figure A.2: Dimensionless hydrodynamic derivatives of the side force

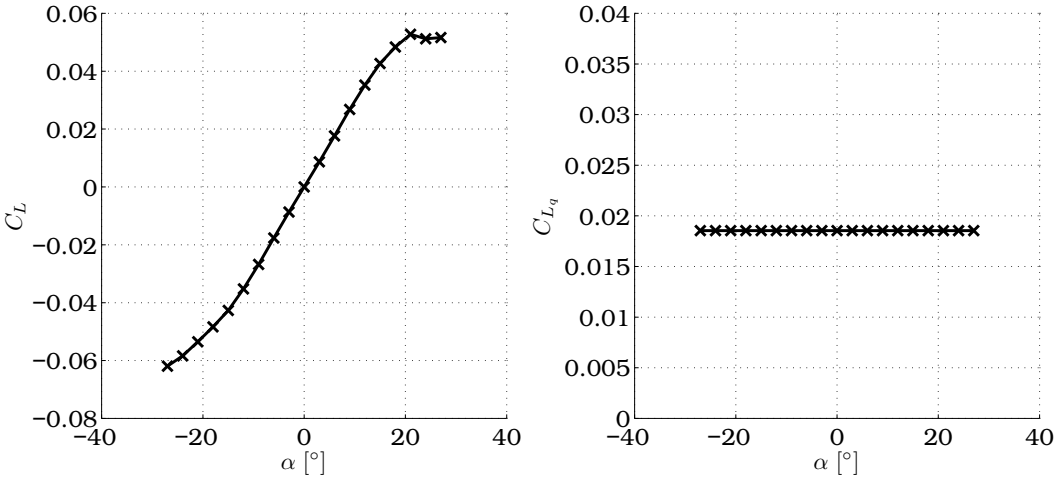

Figure A.3: Dimensionless hydrodynamic derivatives of the lift force

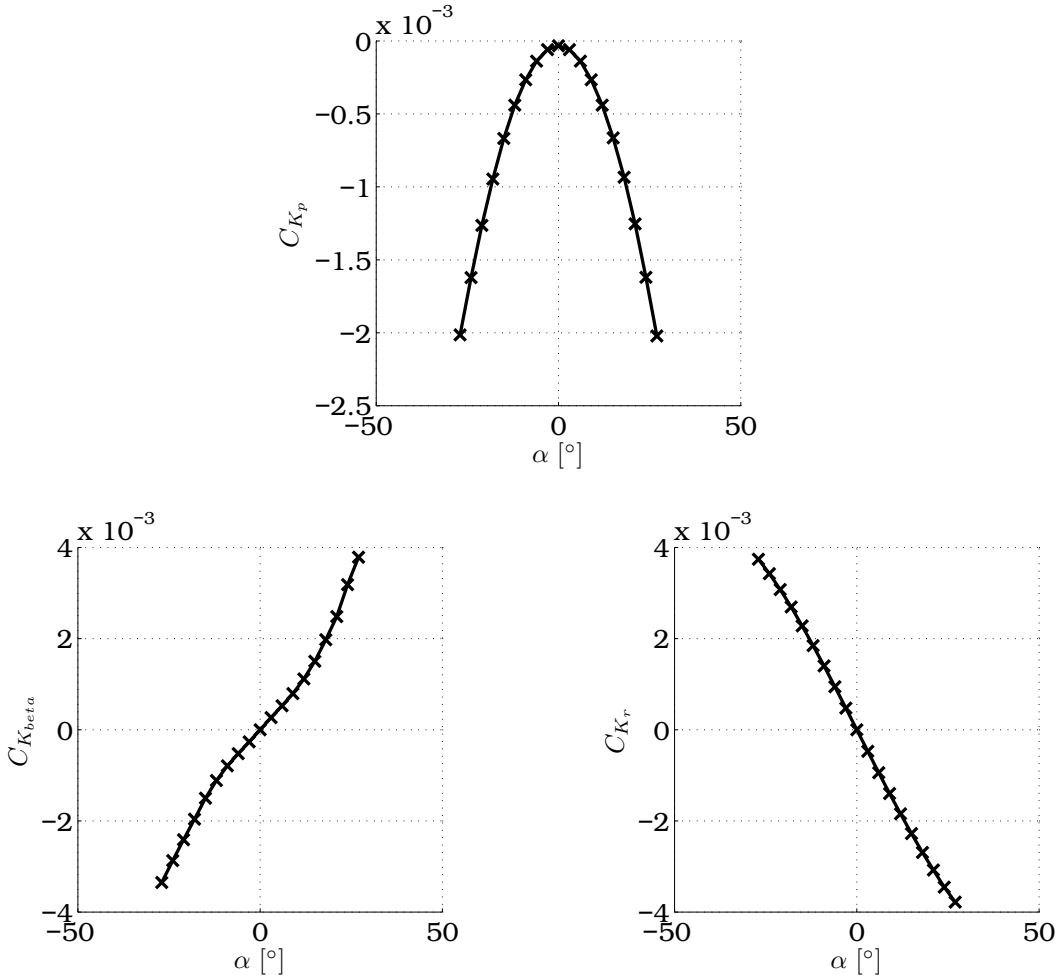

Figure A.4: Dimensionless hydrodynamic derivatives of the roll moment

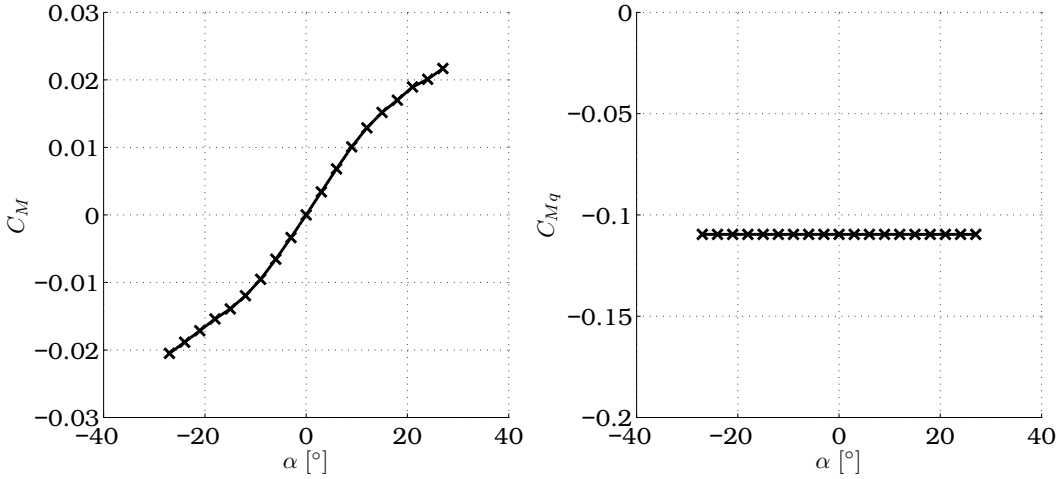

Figure A.5: Dimensionless hydrodynamic derivatives of the pitch moment

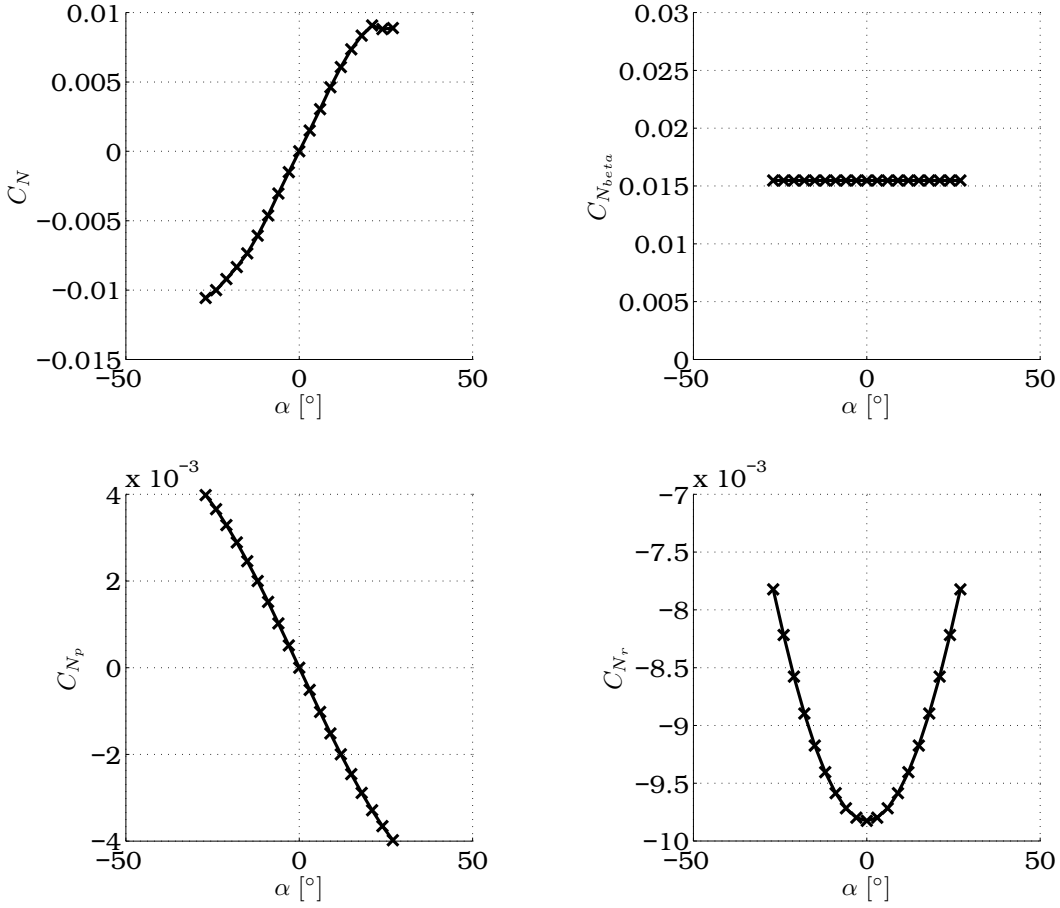

Figure A.6: Dimensionless hydrodynamic derivatives of the pitch moment

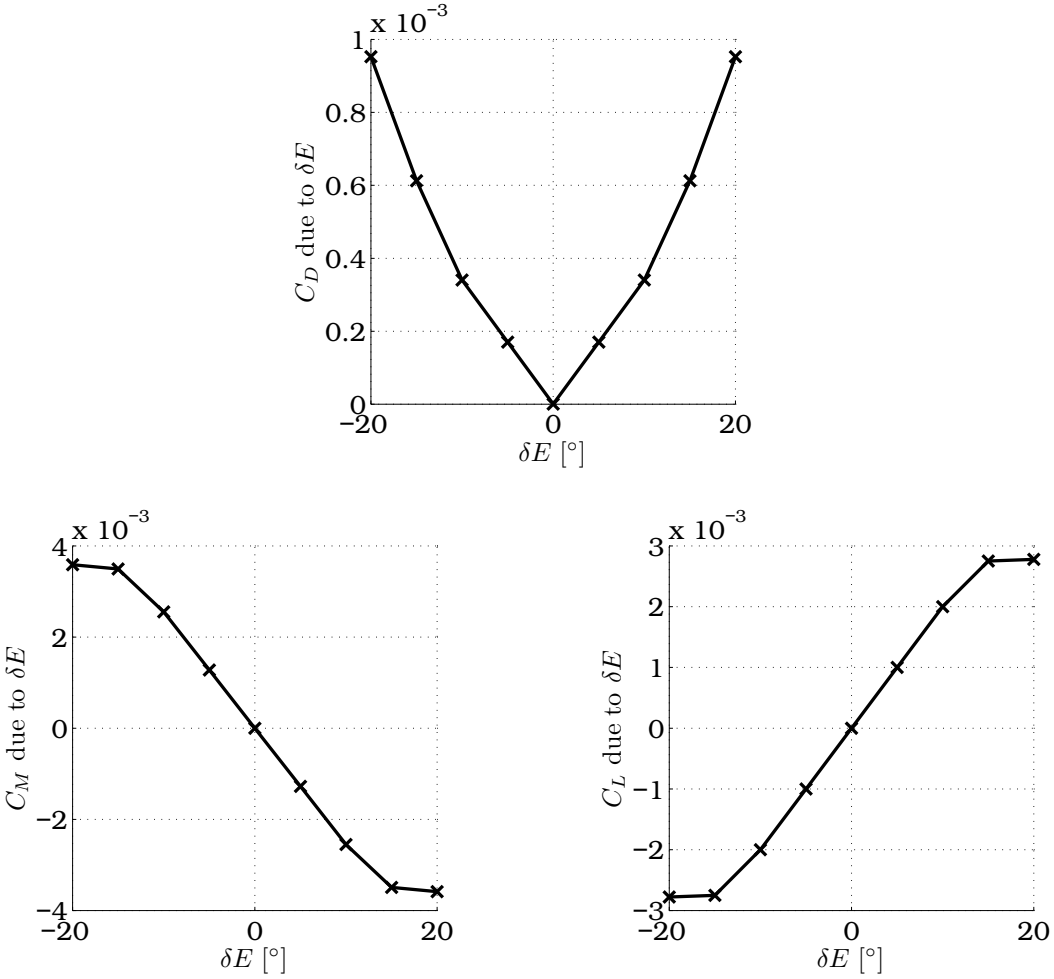

Figure A.7: Dimensionless derivatives related to the elevator

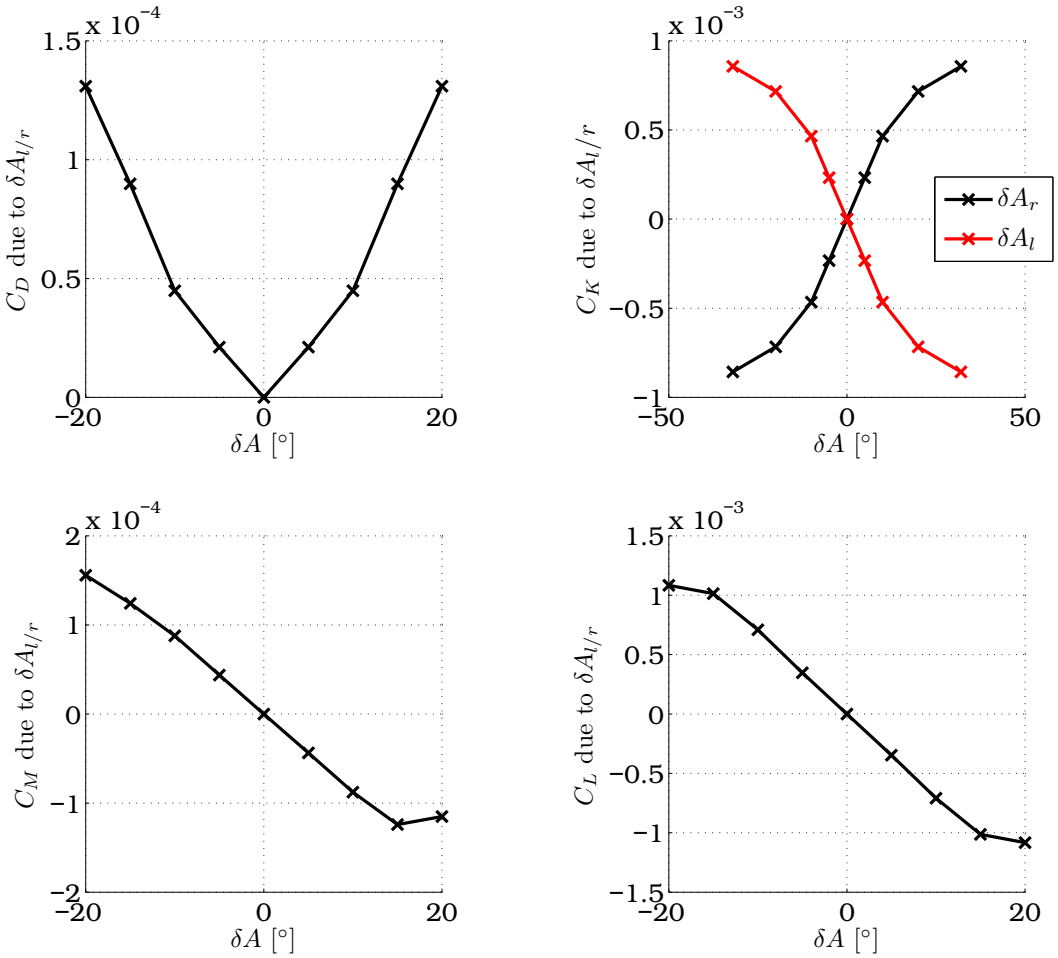

Figure A.8: Dimensionless derivatives related to the front fins

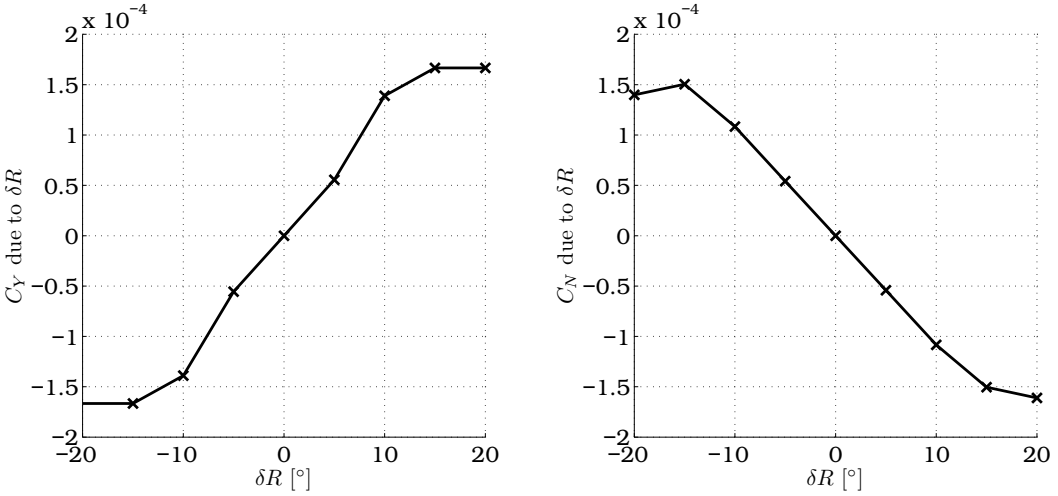

Figure A.9: Dimensionless derivatives related to the rudder

Appendix B

Detailed Corrections and Additions to AUV software

B.1 Corrections to original code

Serial port names

All the serial port names were prepended with "\\.\". For instance, "COM12" would become "\\.\COM12". This was done for compatibility when running the software on versions of Microsoft Windows more recent than Microsoft Windows 98. Later versions of Microsoft Windows cannot recognise serial ports with numbers higher than 9 unless this change is made.

North and east measurements

In the code, the measurements from the IMU for the current AUV north and east position were read into the incorrect variables in the Delphi code. This was rectified by making the following changes.

in file: UtmConvUnit.pas (unit UtmConvUnit)
The line reading:

```
procedure Calculate_UTM (var InputLat, InputLon, Easting, Northing : double);
```

change to:

```
procedure Calculate_UTM (var InputLat, InputLon, Northing, Easting : double);
```

in file: Controller.pas (unit Controller)
in: Procedure NE_Control;
The line reading:

```
AuvControllerCommands.Heading := arctan2(Xw-Xc,Yw-Yc)*180/PI;
```

change to:

```
AuvControllerCommands.Heading := arctan2(Yw-Yc, Xw-Xc)*180/PI;
```

The latitude and longitude values for the waypoints in the file "C:\waypoints\default.wpt" also need to be swapped around following the above changes.

Sample time corrections

The irregular sample times that were shown in **Figure 2.5** in **Chapter 2** were corrected by changing the code that reads in the data bytes from the IMU. Each string of data from the IMU is headed by single byte with the value of 113 (the character 'q'). After this byte is received, the subsequent bytes are accumulated in a buffer until the full length string of 42 characters is received. This is then decoded to retrieve the measurement data from the IMU. If the header character was received in the string, the original code would clear the buffer and accumulate the incoming bytes again. This would result in incomplete data strings, which were not decoded. This would result in an error, which would prevent the control system from running on that particular measurement sample. The code was then modified to clear the input buffer only once 42 or more characters have been received. The sample period is now stable and is controlled by the IMU.

The modifications were made in the file: "CommsUnit.pas" (unit CommsUnit) in: Procedure TCommsF.PhinsData_PortRxChar.

B.2 Additions

With the original code now corrected, the following changes were made to incorporate the new guidance and controllers into the AUV software. All the controller and guidance code is located in a DLL and needs to be loaded into the Delphi code.

in file: MainUnit.pas (unit MainUnit)
in: variable declarations

The necessary function pointers and variables needed by the DLL must be declared.

```
// DLL loading stuff:
  // function pointers:
    Contr_SLC_q_E:         function(e, T: single): single; cdecl;
    Contr_SLC_r_R:         function(e, T: single): single; cdecl;
```

```
    Contr_SLC_p_Ad:        function(e, T: single): single; cdecl;
    Contr_SLC_phi_Ad:      function(e, T: single): single; cdecl;
    Perform_Guidance:      function(use_guidance: word; out_ref_long,
      out_ref_lat, out_temp: floatP): smallint; cdecl;
    Load_Input_Data:       procedure(in_NED, in_Euler, in_V_NED, in_V_W,
      in_W_B: floatP); cdecl;
    Initialise_Guidance:   procedure(use_guidance: byte; in_waypoints: floatP;
      in_num_way: byte; in_rabbit_dist: single); cdecl;
    Add_Waypoint:          procedure(num_of_way, total_ways: word;
      NED1, NED2: floatP); cdecl;
    TIC:                   procedure(); cdecl;
    TOC:                   function(disp: byte): longword; cdecl;
    clrln:                 procedure(); cdecl;
    Init_Contr:            procedure(); cdecl;

  hInst_ControllerDLL:  HMODULE;

  cnt: word;
  NED1: array[1..3] of single;
  NED2: array[1..3] of single;
```

---

in file: MainUnit.pas (unit MainUnit)
in: Procedure TMainInterfaceF.FormCreate

The DLL and the controller functions are loaded.
The guidance is initialised and the waypoints loaded.

```
// Load DLLs with C code for controllers:
  hInst_ControllerDLL   := LoadLibrary('ControllerDLL.dll');
  if (hInst_ControllerDLL = 0) then
  begin
    MainInterfaceF.Label15.Caption := 'DLL load FAILED :(';
    Exit;
  end;

  Contr_SLC_q_E :=        GetProcAddress(hInst_ControllerDLL, 'Contr_SLC_q_E');
  Contr_SLC_r_R :=        GetProcAddress(hInst_ControllerDLL, 'Contr_SLC_r_R');
  Contr_SLC_p_Ad :=       GetProcAddress(hInst_ControllerDLL, 'Contr_SLC_p_Ad');
  Contr_SLC_phi_Ad :=     GetProcAddress(hInst_ControllerDLL, 'Contr_SLC_phi_Ad');
  Perform_Guidance:=      GetProcAddress(hInst_ControllerDLL, 'Perform_Guidance');
  Load_Input_Data:=       GetProcAddress(hInst_ControllerDLL, 'Load_Input_Data');
  Initialise_Guidance:=   GetProcAddress(hInst_ControllerDLL, 'Initialise_Guidance');
  Add_Waypoint:=          GetProcAddress(hInst_ControllerDLL, 'Add_Waypoint');
  TIC:=                   GetProcAddress(hInst_ControllerDLL, 'TIC');
  TOC:=                   GetProcAddress(hInst_ControllerDLL, 'TOC');
  clrln:=                 GetProcAddress(hInst_ControllerDLL, 'clrln');
  Init_Contr:=            GetProcAddress(hInst_ControllerDLL, 'Init_Contr');

  if assigned(Add_Waypoint) then
    begin
```

```
    MainInterfaceF.Label15.Caption := 'Assigning...';
    for cnt := 1 to (WayPts.Nway-1) do
    begin
      NED1[1] := WayPts.Ways[cnt].Xway;
      NED1[2] := WayPts.Ways[cnt].Yway;
      NED1[3] := WayPts.Ways[cnt].Dive_depth;
      NED2[1] := WayPts.Ways[cnt+1].Xway;
      NED2[2] := WayPts.Ways[cnt+1].Yway;
      NED2[3] := WayPts.Ways[cnt+1].Dive_depth;
      P1      := @NED1[1];
      P2      := @NED2[1];
      Add_Waypoint(WayPts.Nway-1, cnt, P1, P2);
    end;
  end;

  if assigned(Initialise_Guidance) then
  begin
    MainInterfaceF.Label15.Caption := 'Initialising guidance...';
    Initialise_Guidance(3, P1, 0, 15.0);
  end;

  if assigned(Init_Contr) then Init_Contr;
```

---

in: Procedure TMainInterfaceF.FormClose

The DLL is unloaded.

```
  // unload DLLs used:
    FreeLibrary(hInst_ControllerDLL);
```

Procedure TMainInterfaceF.ActuatorsTimerTimer is no longer used to update the actuators during a run. They are updated with every controller sample.

in file: Controller.pas (unit Controller)
in: Procedure Dynamic_Control;

This procedure was modified to call Procedure New_Controller instead of running the standard IMT controllers.

```
Procedure Dynamic_Control;
var
  temp : string;
  new_control: byte;
begin
  new_control    := 1;
```

```
  if (ControllerEnable.Dynamic_control) then
  begin
    if (new_control = 1) then
    begin
      Controller.NE_Control;
      New_Controller;
    end
    else
    begin
      if ControllerEnable.NE      then Controller.NE_Control;
      if ControllerEnable.Depth   then Controller.Depth_Control;
      if ControllerEnable.Speed   then Controller.Speed_Control;
      if ControllerEnable.Pitch   then Controller.Pitch_Control;
      if ControllerEnable.Heading then Controller.Heading_Control;
      if ControllerEnable.Roll    then Controller.Roll_Control;
    end;
  end;
  DataStorageUnit.SaveData;
end;
```

The following were added:

Procedure New_Controller;

```
procedure New_Controller;
const
  SAMPLE_RATE: single = 0.1;
var
  temp:        single;
  NED:         array[1..3] of single;
  Euler:       array[1..3] of single;
  V_NED:       array[1..3] of single;
  V_W:         array[1..3] of single;
  W_B:         array[1..3] of single;
  yOut0:       array[1..4] of single;
  yOut1:       array[1..5] of single;
  yOut2:       array[1..3] of single;
  temp_E:      single;
  temp_Ad:     single;
  temp_R:      single;
  P1, P2, P3, P4, P5: floatP;
begin
  clrln;

  // Retrieve s-function inputs:
    NED[1]         := (AuvCurrentState.PositionNED.North);
    NED[2]         := (AuvCurrentState.PositionNED.East);
    NED[3]         := (AuvCurrentState.PositionNED.Down);

    Euler[1]       := (AuvCurrentState.Orientation.Roll*pi/180);
    Euler[2]       := (AuvCurrentState.Orientation.Pitch*pi/180);
    Euler[3]       := (AuvCurrentState.Orientation.Heading*pi/180);
```

```
    V_NED[1]       := (AuvCurrentState.Velocity.North);
    V_NED[2]       := (AuvCurrentState.Velocity.East);
    V_NED[3]       := (AuvCurrentState.Velocity.Down);

    V_W[1]         := (1);
    V_W[2]         := (0);
    V_W[3]         := (0);

    W_B[1]         := (AuvCurrentState.Rates.Roll*pi/180);
    W_B[2]         := (AuvCurrentState.Rates.Pitch*pi/180);
    W_B[3]         := (AuvCurrentState.Rates.Heading*pi/180);

    P1             := @NED[1];
    P2             := @Euler[1];
    P3             := @V_NED[1];
    P4             := @V_W[1];
    P5             := @W_B[1];

  if assigned(Load_Input_Data) then Load_Input_Data(P1, P2, P3, P4, P5);

  P1             := @yOut0[1];
  P2             := @yOut1[1];
  P3             := @yOut2[1];
  if assigned(Perform_Guidance) then
    NavigationUnit.waypointCounter := Perform_Guidance(4, P1, P2, P3);

  if (NavigationUnit.waypointCounter = -1) then
  begin
    NavigationUnit.guidanceMode := SURFACE;
    exit;
  end;

  temp                       := Contr_SLC_phi_Ad(yOut1[4], SAMPLE_RATE);
  Controller.AuvControllerCommands.Pitch := temp;
  FinPosition.ElevatorAngle  := round(Contr_SLC_q_E(yOut0[3], SAMPLE_RATE));
  FinPosition.PortAngle      := round(Contr_SLC_p_Ad((yOut1[2]+temp), SAMPLE_RATE));
  FinPosition.StbdAngle      := -FinPosition.PortAngle + FinPosition.ElevatorAngle;
  FinPosition.PortAngle      := FinPosition.PortAngle + FinPosition.ElevatorAngle;
  FinPosition.RudderAngle    := -round(Contr_SLC_r_R(yOut1[3], SAMPLE_RATE));

  Controller.AuvControllerCommands.Pitch   :=  yOut1[3];
  Update_actuators;
end;
```

Procedure Update_actuators;

```
Procedure Update_actuators;
begin
  Move_Elevator;
  sleep(10);
  Move_Rudder;
  sleep(10);
  Move_PortFin;
  sleep(10);
  Move_StbdFin;
  SetMotorPower(thrusterPower.Port,thrusterPower.Starboard);
end;
```

Appendix C

Plots for outer-loop control

C.1 Pitch angle control plots

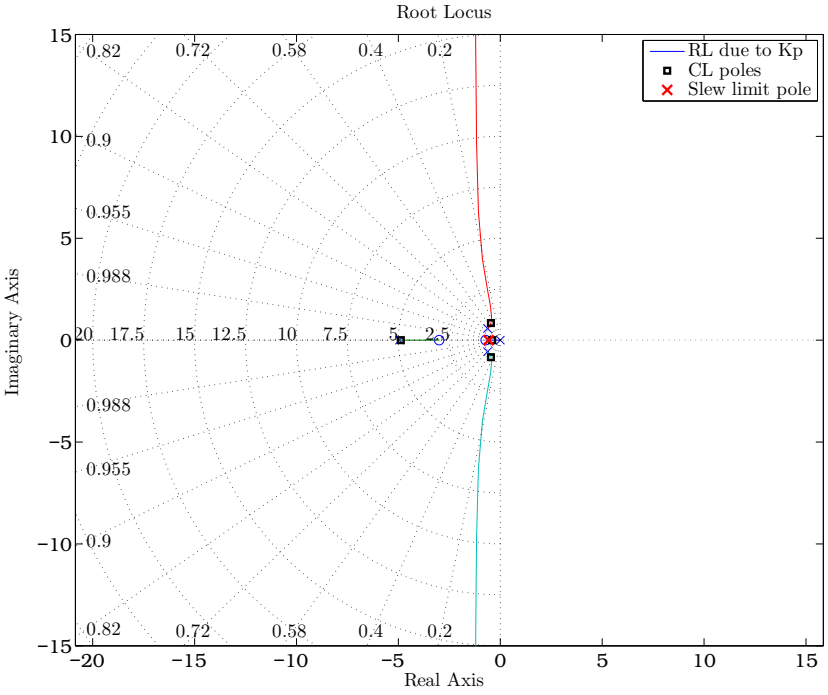

Figure C.1: Pitch angle outer control loop: root locus plot

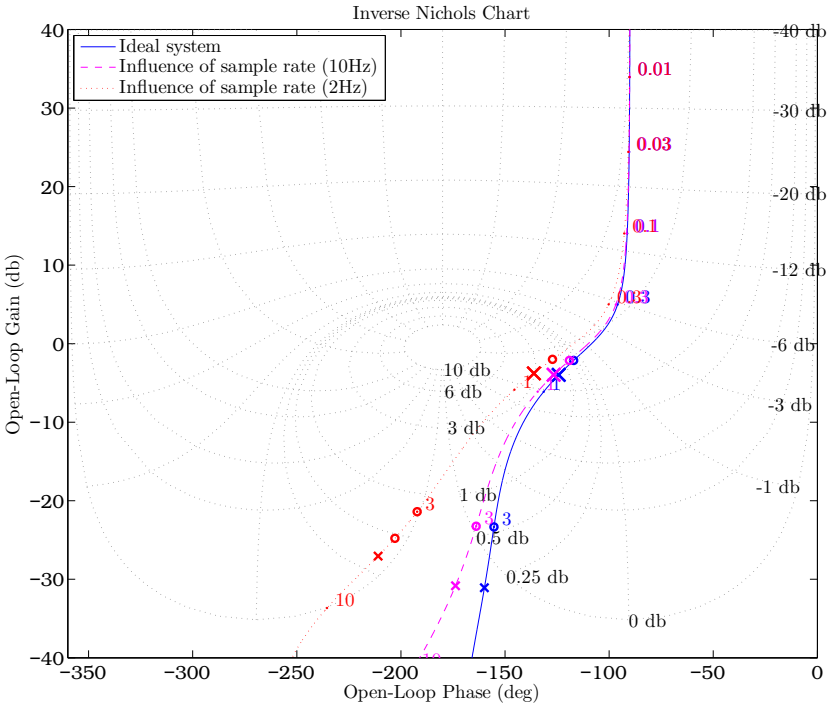

Figure C.2: Pitch angle outer control loop: inverse Nichols chart

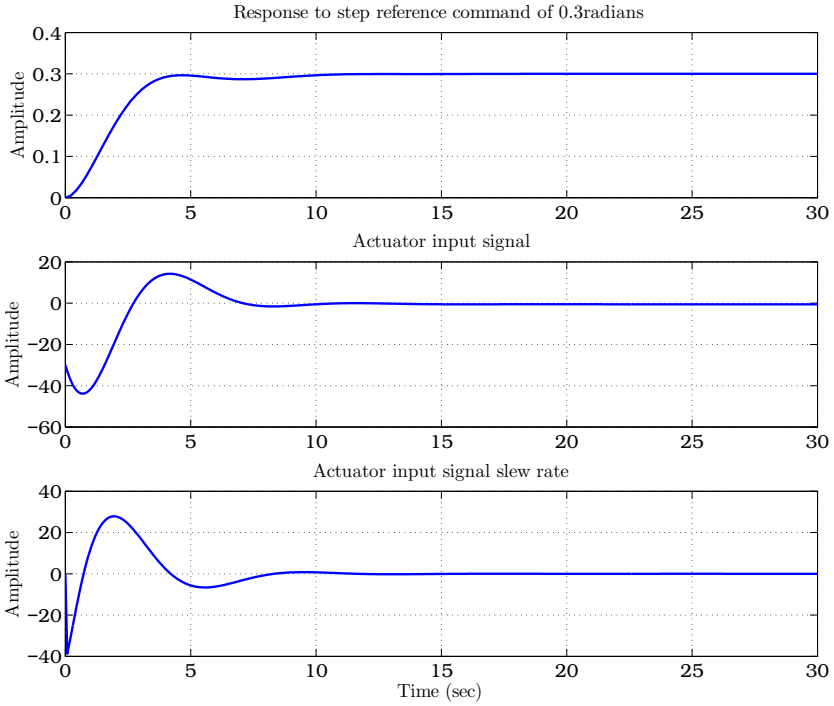

Figure C.3: Pitch angle outer control loop: closed-loop step response

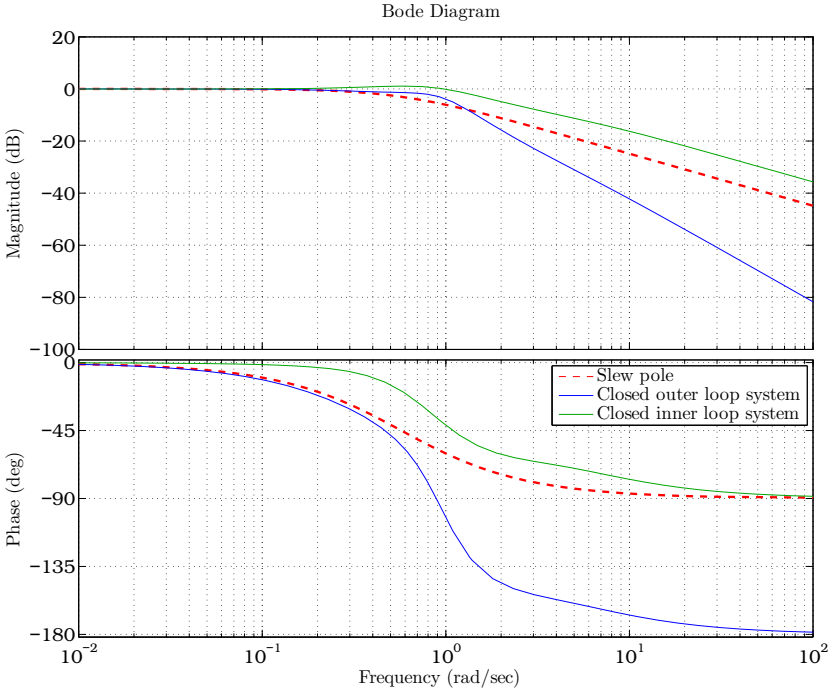

Figure C.4: Pitch angle outer control loop: closed-loop Bode plot

C.2 Roll angle control plots

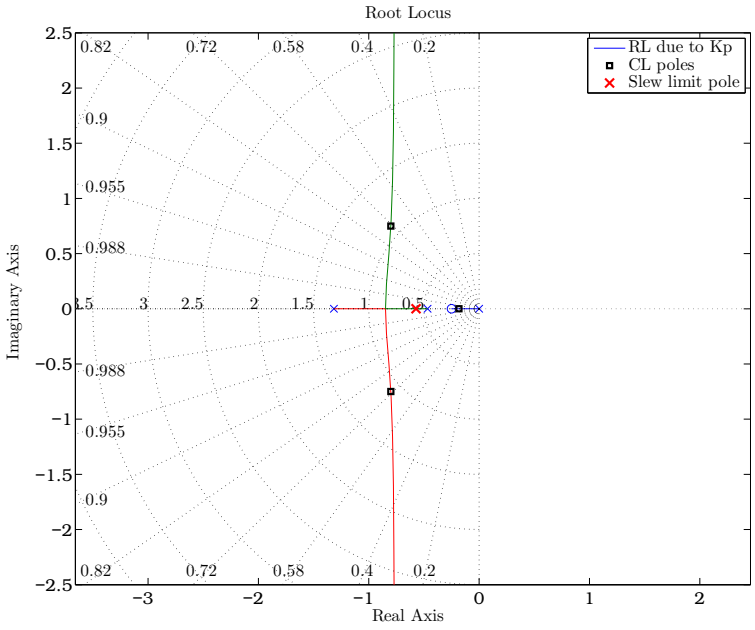

Figure C.5: Roll angle outer control loop: root locus plot

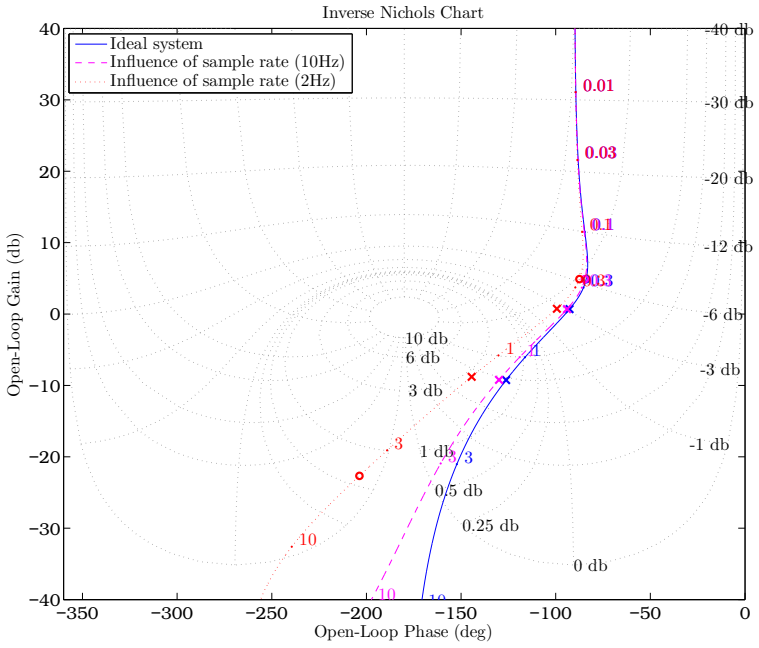

Figure C.6: Roll angle outer control loop: inverse Nichols chart

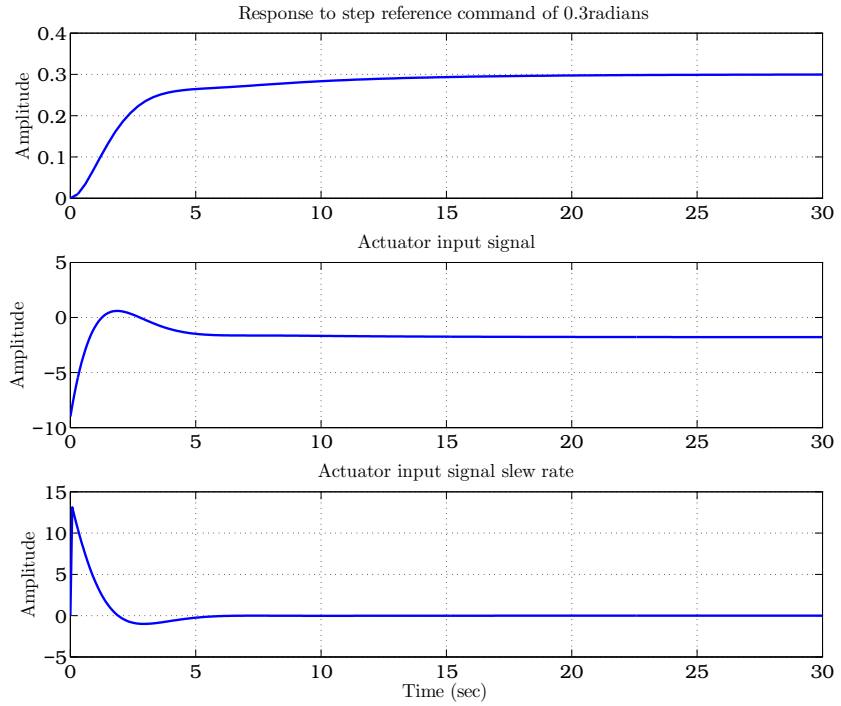

Figure C.7: Roll angle outer control loop: closed-loop step response

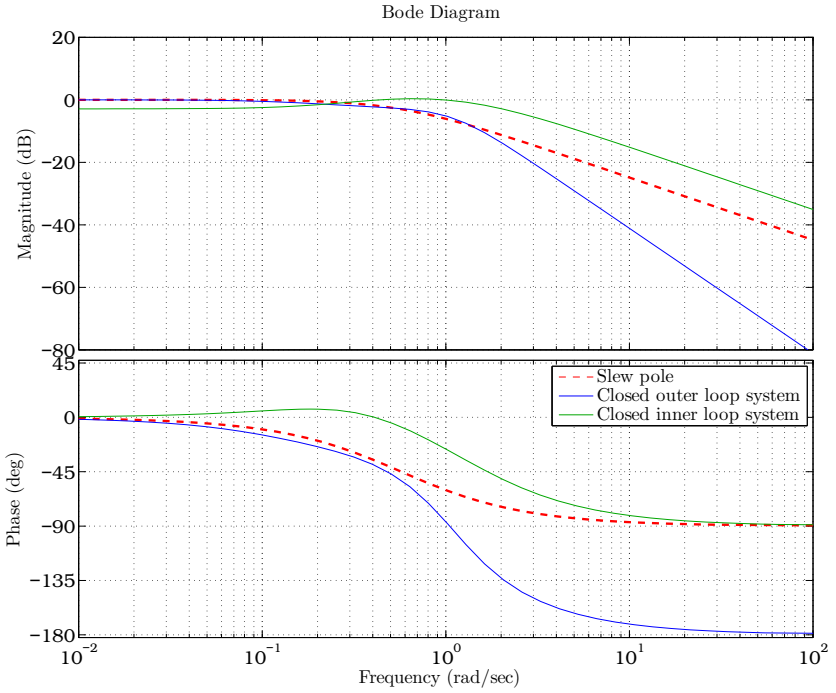

Figure C.8: Roll angle outer control loop: closed-loop Bode plot

C.3 Yaw angle control plots

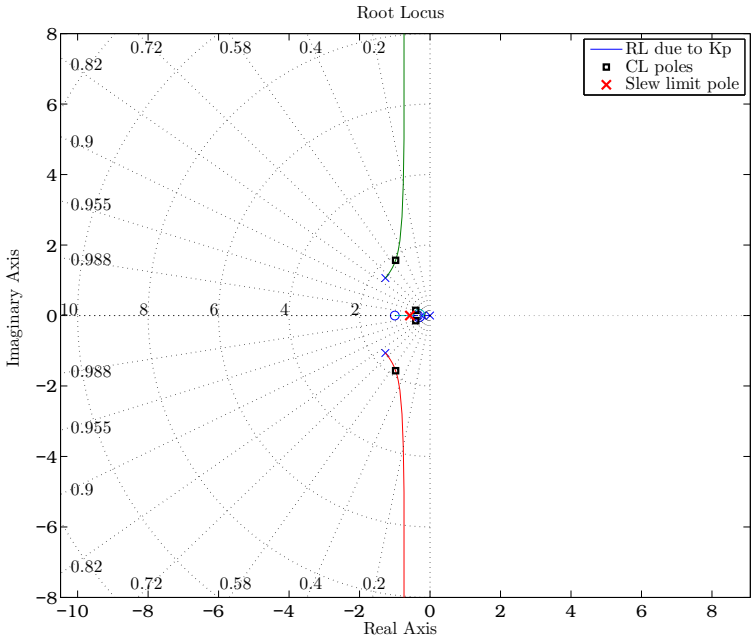

Figure C.9: Yaw angle outer control loop: root locus plot

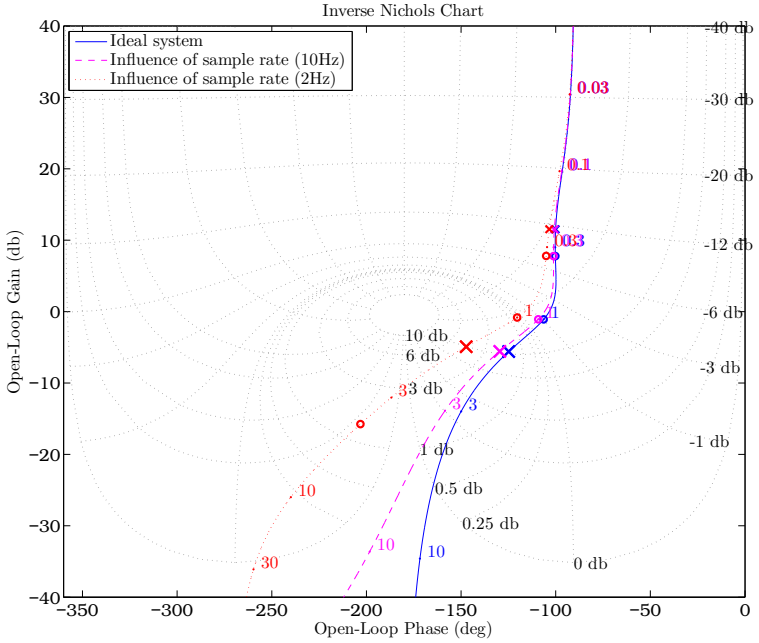

Figure C.10: Yaw angle outer control loop: inverse Nichols chart

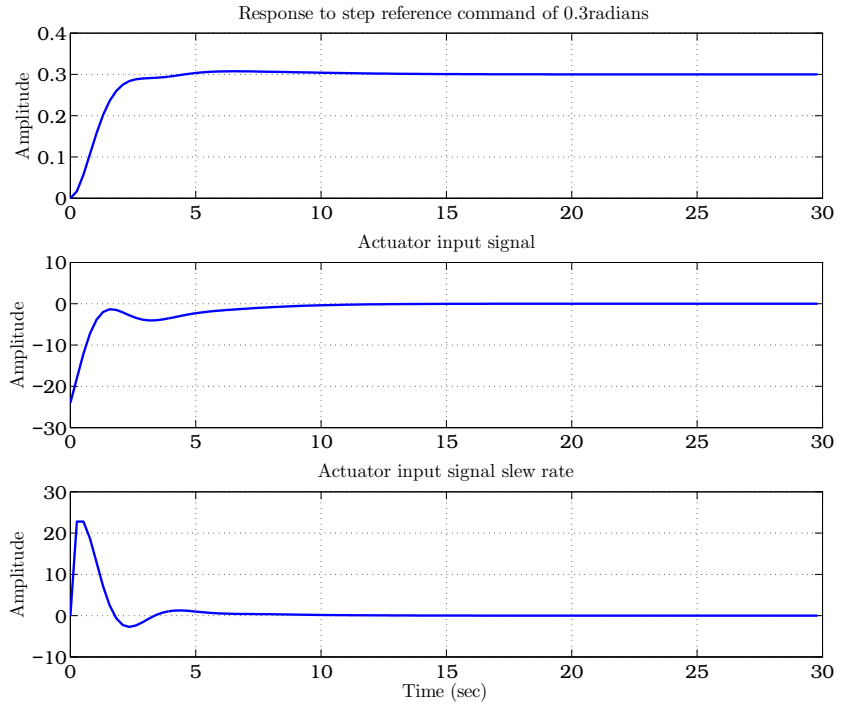

Figure C.11: Yaw angle outer control loop: closed-loop step response

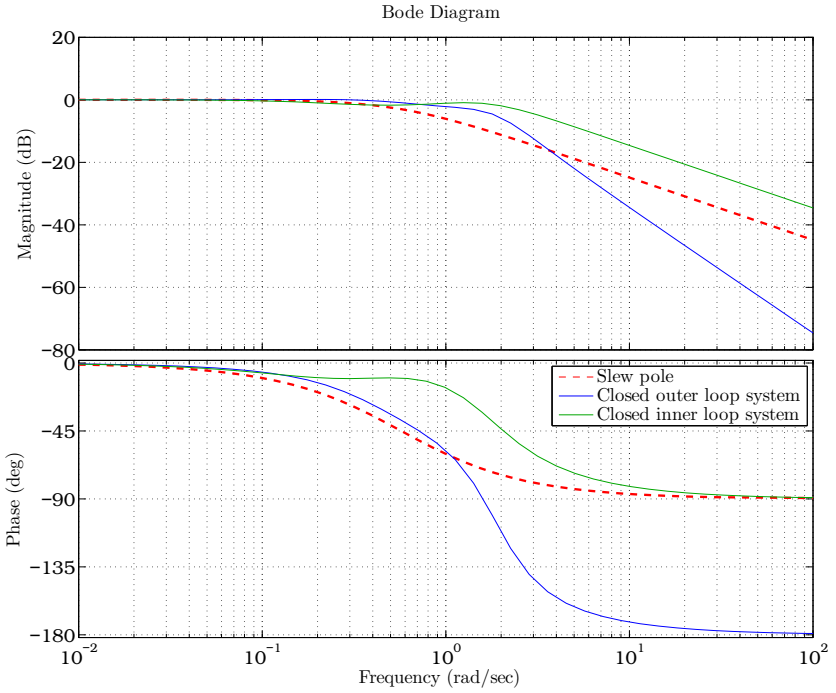

Figure C.12: Yaw angle outer control loop: closed-loop Bode plot

List of References

[1] Busch, R.: *Modelling and Simulation of an Autonomous Underwater Vehicle*. Master's thesis, Electrical & Electronic Engineering, University of Stellenbosch, April 2009.

[2] http://www.seaeye.com/falcon.html. Accessed 2009.

[3] Phins documentation.

[4] Yuh, J.: Design and control of autonomous underwater robots: A survey. *Autonomous Robots*, vol. 8, pp. 7–24, 2000.

[5] Yamamoto, I.: Research and development of past, present, and future AUV technologies, 2006. Japan Agency for Marine-Earth Science and Technology (JAMSTEC).

[6] Cruz, N. and Matos, A.: The MARES AUV, a modular autonomous robot for environment sampling, 2006. Faculty of Engineering at the University of Porto.

[7] Fryxell, D., Oliveira, P., Pascoal, A., Silvestre, C. and Kaminer, I.: Navigation, guidance and control of AUVs: an aplication to the Marius vehicle. *Control Engineering Practice*, vol. 4, pp. 401–409, 1996.

[8] Issac, M.T., Adams, S., He, M., Bose, N. and Christopher D. Williams, R.B.: Manoeuvring experiments using the MUN explorer AUV, 2006.

[9] Hyakudome, T., Aoki, T., Maeda, T., Murashima, T., Tsukioka, S., Nakajoh, H., Ida, T. and Ichikawa, T.: Buoyancy control for deep and long cruising range AUV. *Proceedings of The Twelfth International Offshore and Polar Engineering Conference*, pp. 325–329, 2002.

[10] http://auvac.org/. Accessed 2009.

[11] Desa, E.: The small AUV Maya: Initial field results, 2006. National Institute of Oceanography, Goa, India.

[12] Wang, S., Zhang, H., Hou, W. and Liang, J.: Control and navigation of the variable buoyancy AUV for underwater landing and takeoff. *International Journal of Control*, vol. 80, pp. 1018–1026, July 2007.

[13] Fish, F.E., Lauder, G.V., Mittal, R., Techet, A.H., Triantafyllou, M.S., Walker, J.A. and Webb, P.W.: Conceptual design for the construction of a biorobotic auv based on biological hydrodynamics, June 2003.

[14] Cook, M.: *Flight Dynamics Principles*. 2nd edn. Elsevier Ltd., 2007.

[15] Eitelberg, E.: *Control Engineering*. NOYB Press, 2006.

[16] Gopal, M.: *Digital Control and State Variable Methods*. 2nd edn. McGraw Hill, 2004.

[17] Peddle, I.K., Jones, T. and Treurnicht, J.: Practical near hover flight control of a ducted fan (slade). *Control Engineering Practice 17*, pp. 48–58, 2009.

[18] Park, S.: *Avionics and Control System Development for Mid-Air Rendezvous of Two Unmanned Aerial Vehicles*. Ph.D. thesis, Massachusetts Institute of Technology, February 2004.

[19] Peddle, I.: *Acceleration Based Manoeuvre Flight Control System for Unmanned Aerial Vehicles*. Ph.D. thesis, Electrical & Electronic Engineering, University of Stellenbosch, December 2008.

[20] Laing, A.: A computer model for forecasting ocean wave parameters at specific sites around the the New Zealand coast. *New Zealand Journal of Marine and Freshwater Research*, vol. 19, pp. 517–533, 1985.

[21] Torsethaugen, K. and Haver, S.: Metocean project; simplified double peak spectral model for ocean waves, 2004.

[22] Tabeshpour, M., Golafshani, A. and Seif, M.: Comprehensive study on the results of tension leg platform responses in random sea. *Journal of Zhejiang University*, vol. A, pp. 1305–1317, 2006.

[23] van der Meer, C.: *Ocean waves of maximal amplitude*. Master's thesis, Department of Applied Mathematics, University of Twente, March 2006.